THE UNIVERSITY OF TOKYO

Clusters & Hierarchies

強相関フェルミ超流動:
BCS-BECクロスオーバーを中心に

Hiroyuki Tajima

(The University of Tokyo)

Self-introduction -Hiroyuki Tajima-

Ph.D. (March 2017)
Thesis "*Thermodynamic properties of an ultracold Fermi gas in the BCS-BEC crossover region*"

https://www.keio.ac.jp/ja/

Prof. Yoji Ohashi

April 2017~September 2019
JSPS postdoctoral researcher (PD),
Quantum Hadron Physics Laboratory,
RIKEN Nishina Center,

http://www.riken.jp/

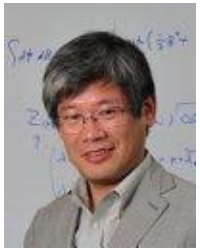

Prof. Tetsuo Hatsuda

October 2019~March 2021
Specially Appointed Assistant Professor for the project of "Clustering as a window on the hierarchical structure of quantum systems",
Kochi University.

http://www.kochi-u.ac.jp/gakubu/rigaku/

Prof. Kei Iida

Self-introduction -Hiroyuki Tajima-

<u>April 2021~present</u>
Assistant professor in Prof. Haozhao Liang group, Nuclear Theory, Department of Physics, School of Science, The University of Tokyo, Japan

Prof. Haozhao Liang

https://www.u-tokyo.ac.jp/en/index.html

1/4/2021

17/5/2021

Outline

- Cold atoms and BCS-BEC crossover
- Strong pairing fluctuations
- Unitary Fermi gas and neutron matter
- Role of the multi-band configuration
- Beyond pairing effect
- Summary

Outline

- Cold atoms and BCS-BEC crossover
- Strong pairing fluctuations
- Unitary Fermi gas and neutron matter
- Role of the multi-band configuration
- Beyond pairing effect
- Summary

What is a cold atomic gas?

Dilute gas of atoms (e.g., Li, K, Rb,…) at ultracold temperature in the chamber

Highly controllable system: quantum statistics (boson/fermion), dimensions, interactions,…

From Ultracold Quantum Gas Lab in Osaka Metro. Univ.

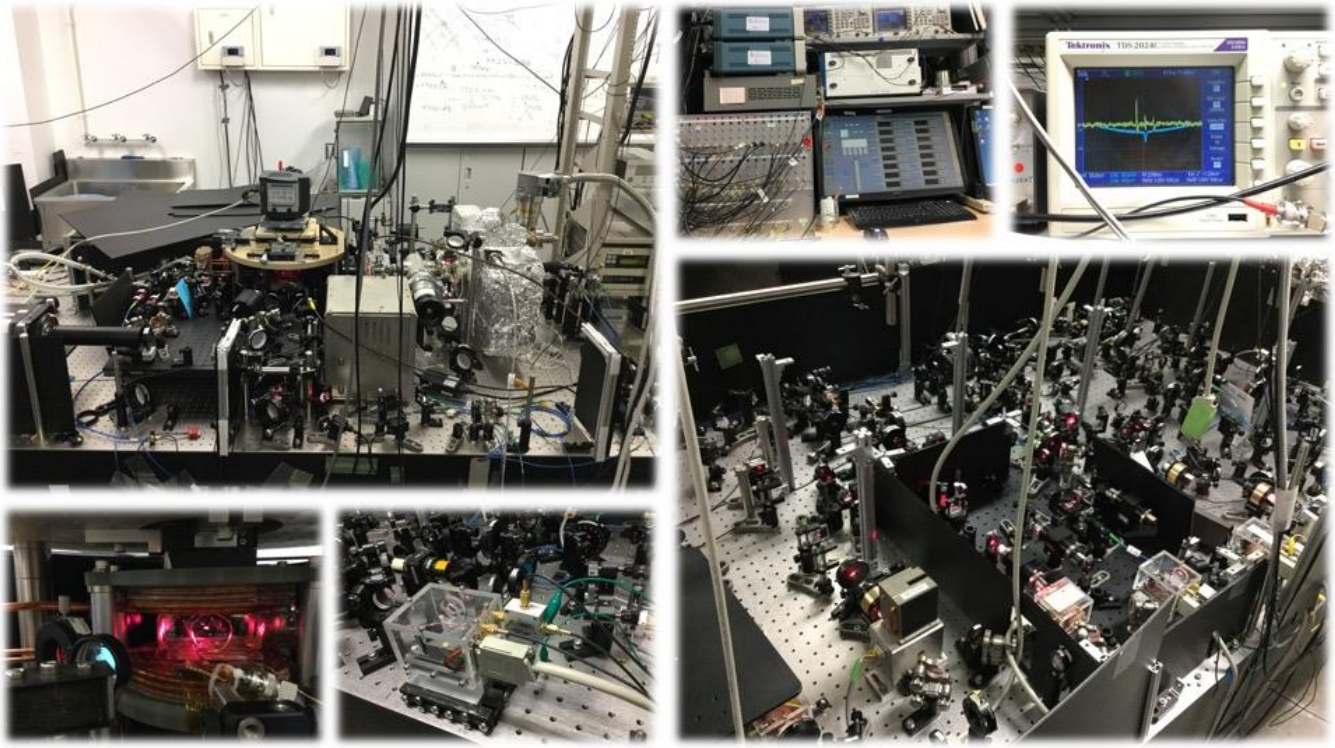

http://www.sci.osaka-cu.ac.jp/phys/laser/research_Li.html

Solid Lithium

Oven

$T \gtrsim 600\mathrm{K}$

Laser Cooling

Credits: NASA/iGoal Animation

$T < 100\mathrm{nK}$

Fermi and Bose atomic gases

Fermi pressure in
quantum degenerate gases

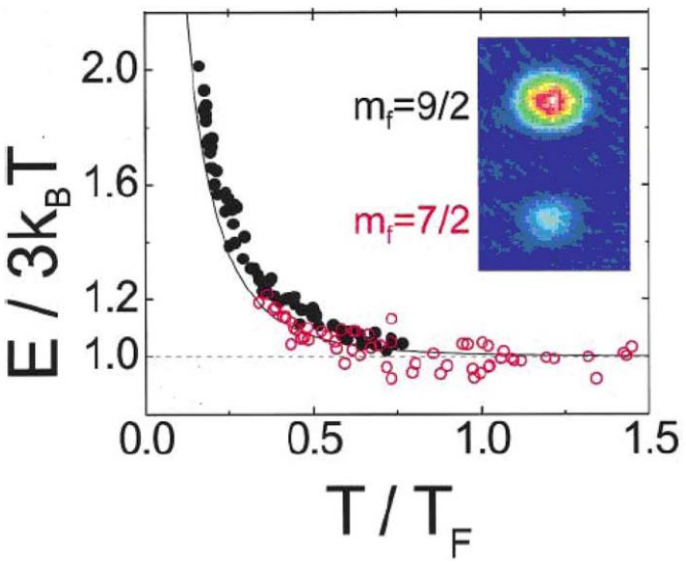

Phys. Rev. Lett. **86**, 5409 (2001).

Velocity distribution
in Bose-Einstein condensates

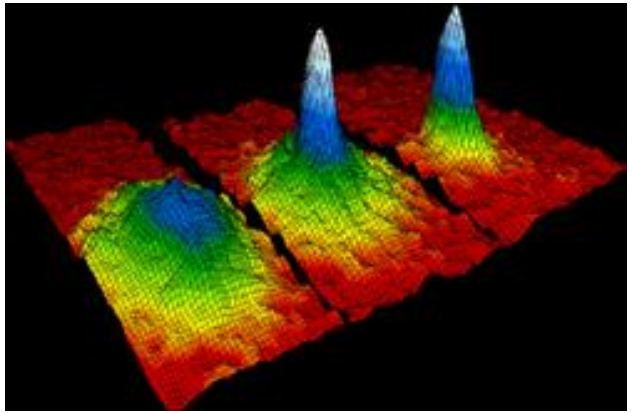

JILA

Science **269**, 198 (1995).

Fermi atoms (^{6}Li, ^{40}K, ^{173}Yb,…)

^{6}Li = 3 protons + 3 neutrons + 3 electrons
= (9 fermions)

Bose atoms (^{7}Li, ^{87}Rb, ^{174}Yb,…)

^{7}Li = 3 protons + 4 neutrons + 3 electrons
= (10 fermions)

Low dimension and lattice geometry

Optical lattice and 1D tube

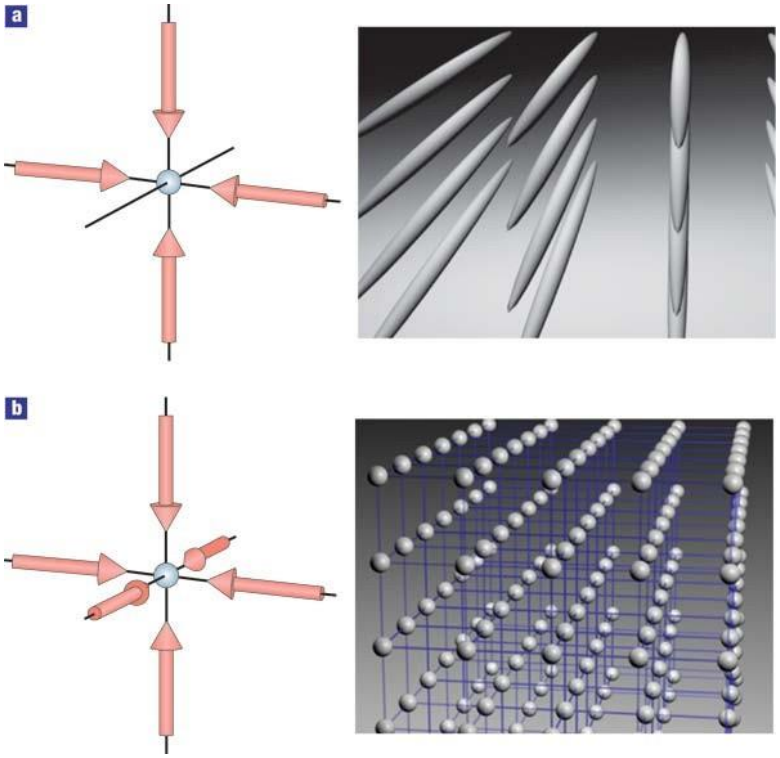

I. Bloch, Nat. Phys. **1**, 23 (2005).

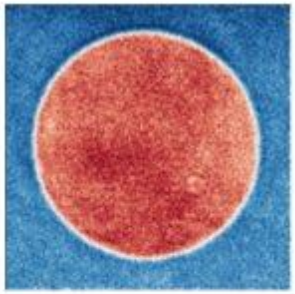

EDITORS' SUGGESTION

Two-Dimensional Homogeneous Fermi Gases

A homogeneous ultracold 2D Fermi gas is trapped in a box potential, which has advantages over harmonically trapped ones for probing strongly interacting systems.

Klaus Hueck *et al.*

Phys. Rev. Lett. **120**, 060402 (2018)

High-resolution trap potential

http://quantumgases.lens.unifi.it/exp/li

Feshbach resonance

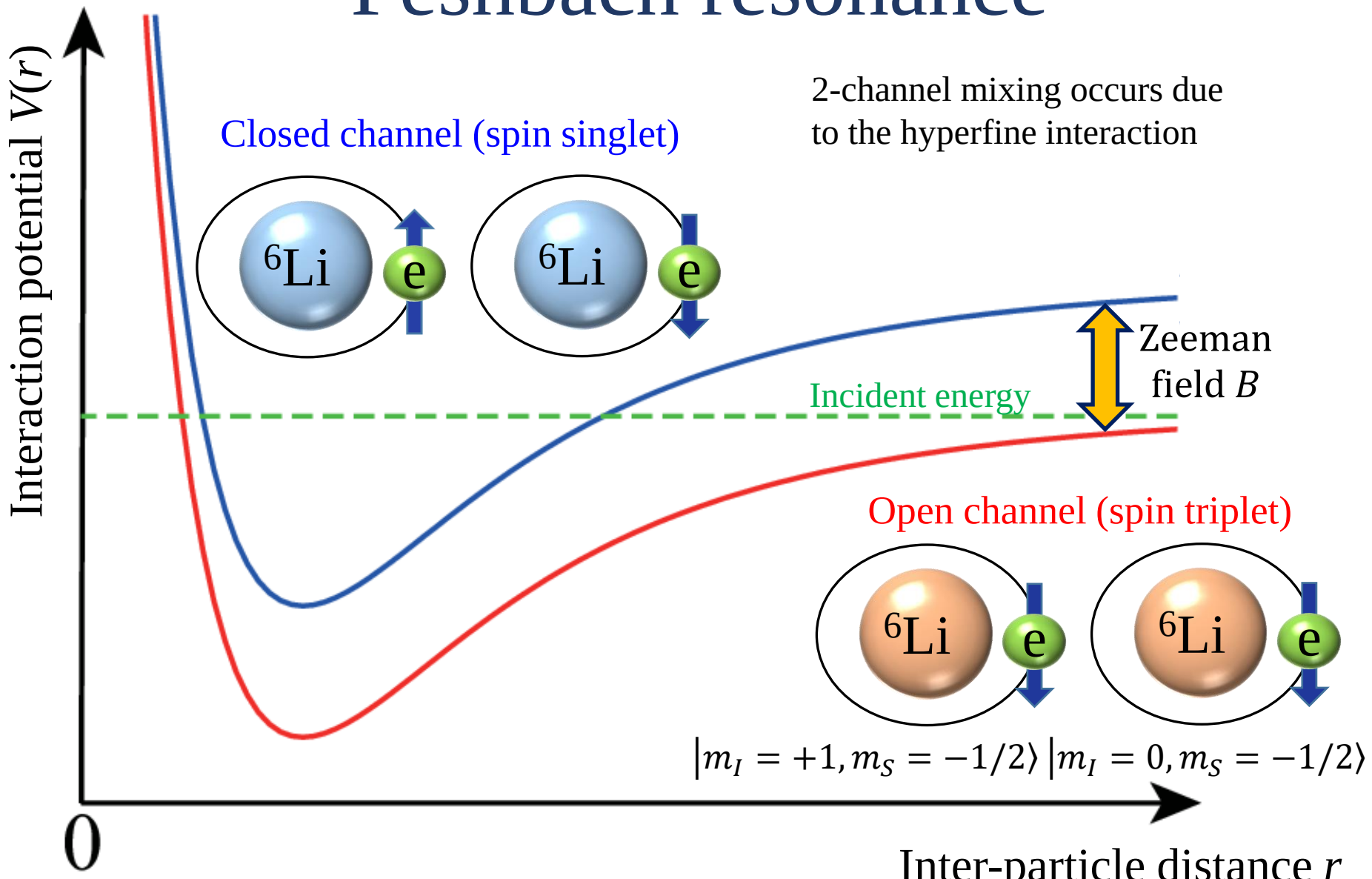

Feshbach resonance

Atoms interacts with each other via an intermediate state

⇒attraction can be tuned by an external magnetic field

Effective attraction

$$-U_{\mathrm{eff}} \simeq -\frac{g^2}{2\nu(B)}$$

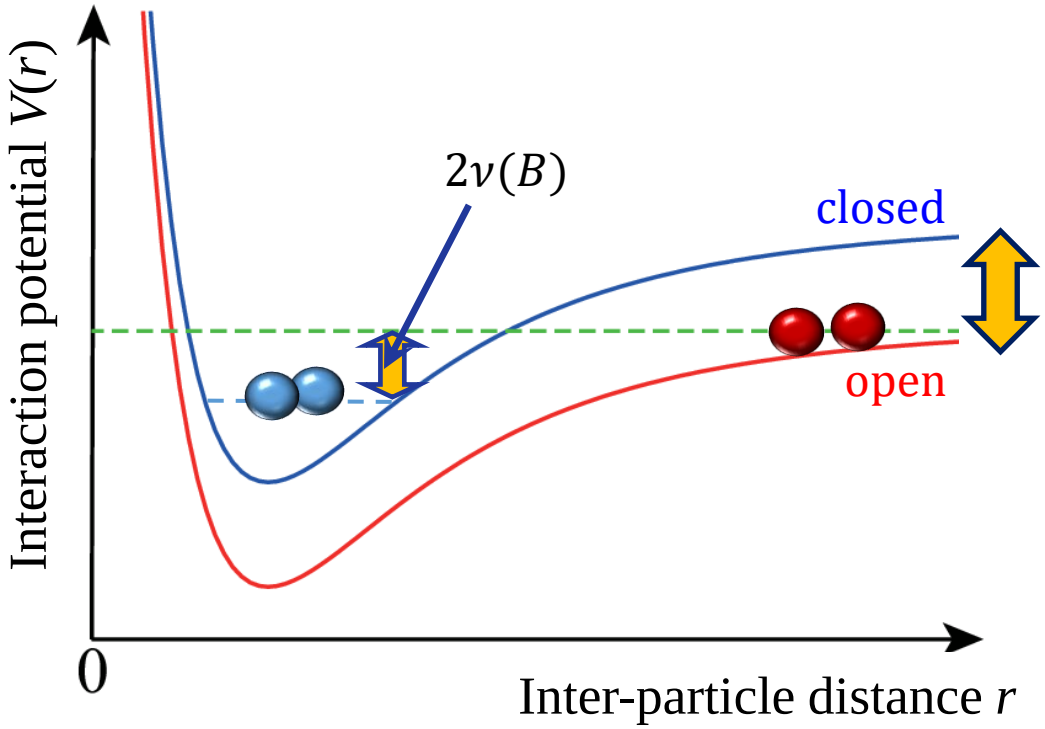

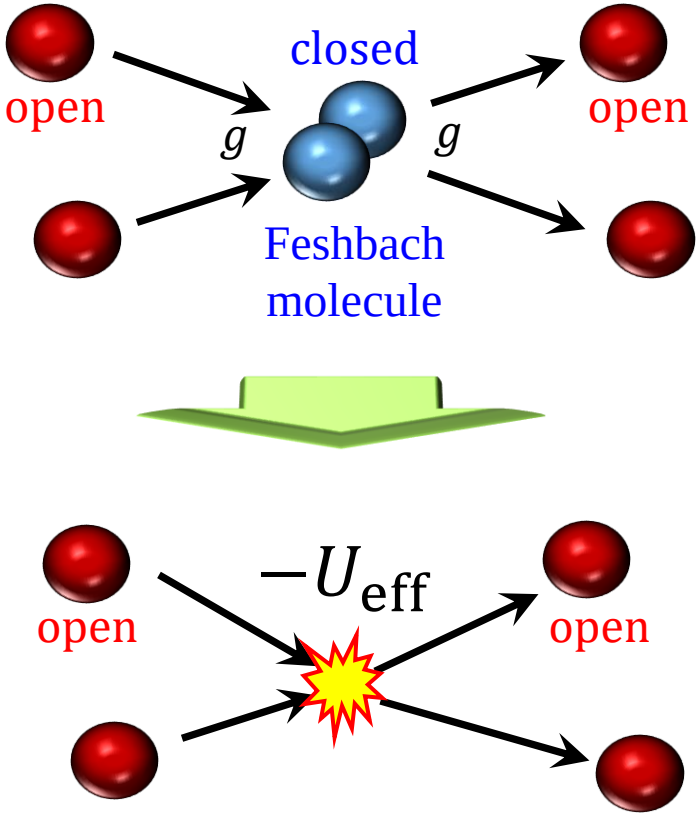

Feshbach resonance

Feshbach resonance in a ^{6}Li Fermi gas

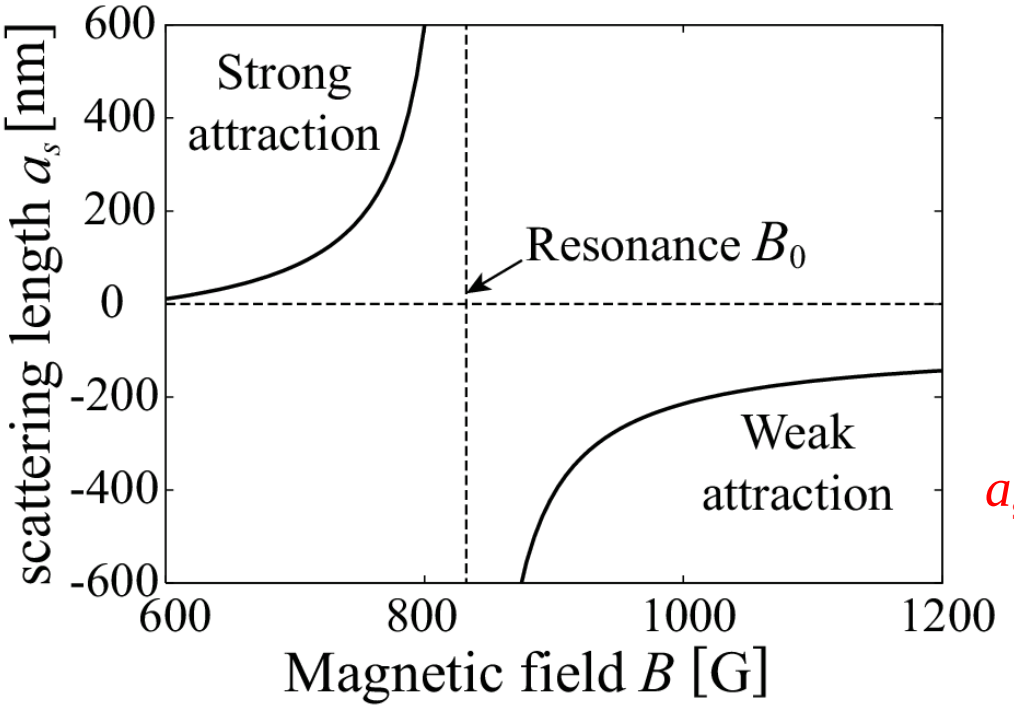

B-dependence near Feshbach resonance

$$a_s(B) = a_{\mathrm{bg}}\left(1 + \frac{W_{\mathrm{res}}}{B - B_0}\right)$$

Resonance width $W_{\mathrm{res}} = 262.3\mathrm{G}$

Background scattering length $a_{\mathrm{bg}} = -1582a_0$

a_s can be controlled precisely by tuning *B*

G. Zürn, *et al.*, PRL **110**, 135301 (2013).

Superfluidity and BCS-BEC crossover

Review: Y. Ohashi, HT, and P. van Wyk, Prog. Part. Nucl. Phys. **111**, 103739 (2020).

- Crossover from Bardeen-Cooper-Schrieffer (BCS) superfluid to Bose-Einstein condensates (BEC) of bound molecules is realized by tuning the interaction.

Phase diagram of the BCS-BEC crossover

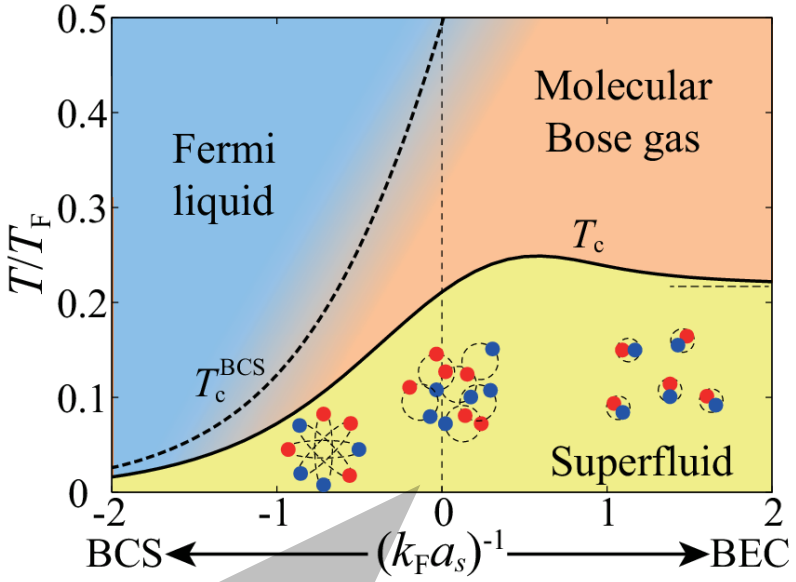

$a_s = -18.5\text{fm}$

$(k_F a_s)^{-1} \simeq 0$

http://astro.riken.jp/wordpress/?page_id=1425

Observation of BCS-BEC crossover in a ^{40}K Fermi gas

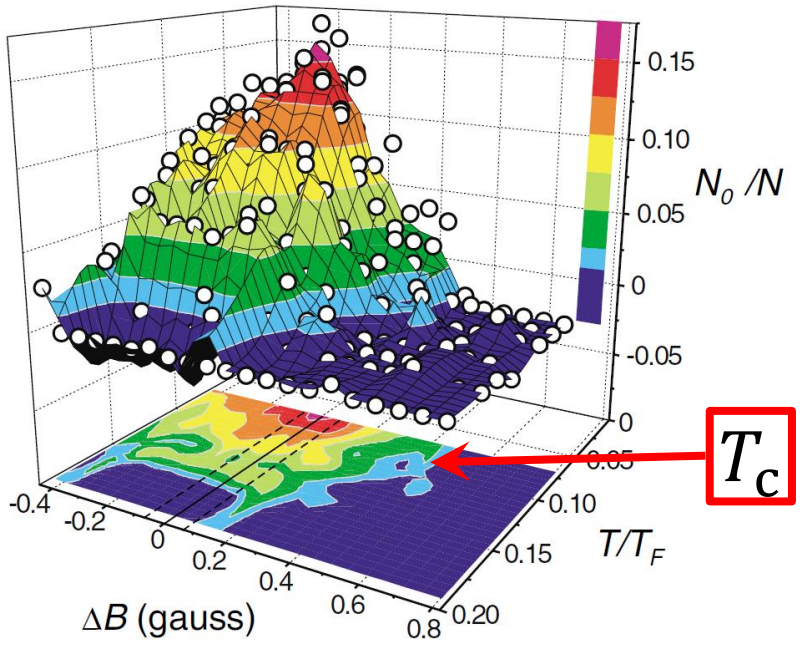

C. Regal, *et al.*, PRL **92**, 040403 (2004).

Hamiltonian

$$H = \sum_{\boldsymbol{p},\sigma} (\varepsilon_{\boldsymbol{p}} - \mu_\sigma) c^\dagger_{\boldsymbol{p}\sigma} c_{\boldsymbol{p}\sigma} + U \sum_{\boldsymbol{p},\boldsymbol{p}',\boldsymbol{q}} c^\dagger_{\boldsymbol{p}+\boldsymbol{q}/2,\uparrow} c^\dagger_{-\boldsymbol{p}+\boldsymbol{q}/2,\downarrow} c_{-\boldsymbol{p}'+\boldsymbol{q}/2,\downarrow} c_{\boldsymbol{p}'+\boldsymbol{q}/2,\uparrow}$$

$c_{\boldsymbol{p}\sigma}$: Annihilation operator

$\sigma = \uparrow, \downarrow$: pseudospin

$\varepsilon_{\boldsymbol{p}} = \dfrac{\boldsymbol{p}^2}{2m}$: Kinetic term with mass m

μ_σ :Chemical potential

Renormalization of the two-body coupling constant U

$$\frac{m}{4\pi a} = \frac{1}{U} + \frac{m\Lambda}{2\pi^2}$$

a: scattering length

Λ: Momentum cutoff

$-U$: small

$-\infty$

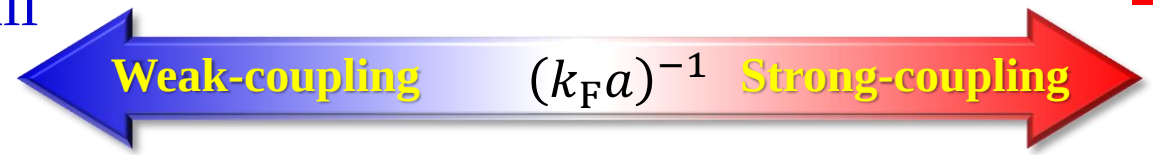

$-U$: large

$+\infty$

$a^{-1} < 0$, attractive but no 2b bound state

$a^{-1} > 0$, $E_{\text{bind}} = 1/(ma^2)$

BCS-Eagles-Leggett theory

D. M. Eagles, Phys. Rev. **186**, 456 (1969).
A. J. Leggett, *in Modern Trends in the Theory of Condensed Matter,* Springer Verlag, Berlin,1980,p.13.

Mean field Hamiltonian

$$H_{\mathrm{MF}} = \sum_{\boldsymbol{p},\sigma} \left(\varepsilon_{\boldsymbol{p}} - \mu_\sigma\right) c^\dagger_{\boldsymbol{p}\sigma} c_{\boldsymbol{p}\sigma} - \sum_{\boldsymbol{p}} \left[\Delta c^\dagger_{\boldsymbol{p},\uparrow} c^\dagger_{-\boldsymbol{p},\downarrow} + \Delta^* c_{-\boldsymbol{p},\downarrow}\, c_{\boldsymbol{p},\uparrow}\right] - \frac{|\Delta|^2}{U}$$

$$\Delta = -U \sum_{\boldsymbol{p}} \langle c_{-\boldsymbol{p},\downarrow} c_{\boldsymbol{p},\uparrow} \rangle$$:Mean field for BCS superfluid

Gap equation

$$1 = -\frac{4\pi a}{m} \sum_{\boldsymbol{p}} \left[\frac{1}{2E_{\boldsymbol{p}}} - \frac{1}{2\varepsilon_{\boldsymbol{p}}}\right]$$

Number density equation

$$\rho = \sum_{\boldsymbol{p}} \left[1 - \frac{\varepsilon_{\boldsymbol{p}} - \mu}{E_{\boldsymbol{p}}}\right]$$

$\varepsilon_{\boldsymbol{p}} = p^2/2m$:Kinetic energy

$E_{\boldsymbol{p}} = \sqrt{\left(\varepsilon_{\boldsymbol{p}} - \mu\right)^2 + |\Delta|^2}$:BCS quasiparticle dispersion

BCS-Eagles-Leggett theory

$$1 = -\frac{4\pi a}{m}\sum_{\boldsymbol{p}}\left[\frac{1}{2E_{\boldsymbol{p}}} - \frac{1}{2\varepsilon_{\boldsymbol{p}}}\right]$$

$$\rho = \sum_{\boldsymbol{p}}\left[1 - \frac{\varepsilon_{\boldsymbol{p}} - \mu}{E_{\boldsymbol{p}}}\right]$$

<u>Weak-coupling BCS</u>

$$\Delta = \frac{8}{e^2}E_{\mathrm{F}}e^{\frac{\pi}{2k_{\mathrm{F}}a}}$$

$$\mu = E_{\mathrm{F}}$$

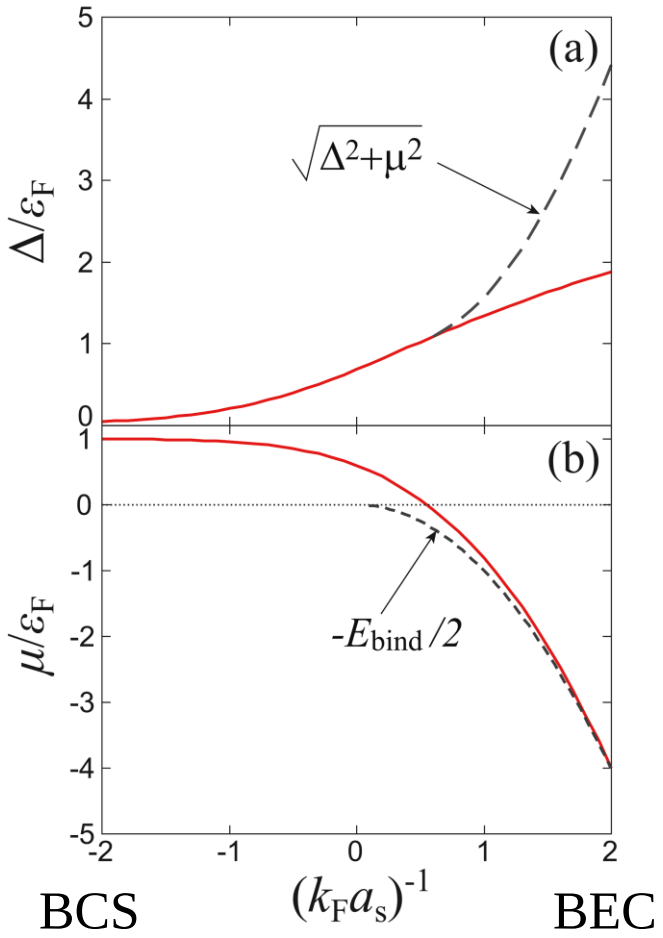

<u>Strong-coupling BEC</u>

$$\Delta = \frac{4|\mu|}{\sqrt{3\pi}(k_F a)^{-\frac{3}{2}}} \ll |\mu|$$

$$\mu = -\frac{E_{\mathrm{bind}}}{2}$$

Y. Ohashi, HT, and P. van Wyk, Prog. Part. Nucl. Phys. **111**, 103739 (2020).

BCS-Eagles-Leggett theory

- Quasiparticle dispersion $E_{\boldsymbol{p}} = \sqrt{(\varepsilon_{\boldsymbol{p}} - \mu)^2 + |\Delta|^2}$

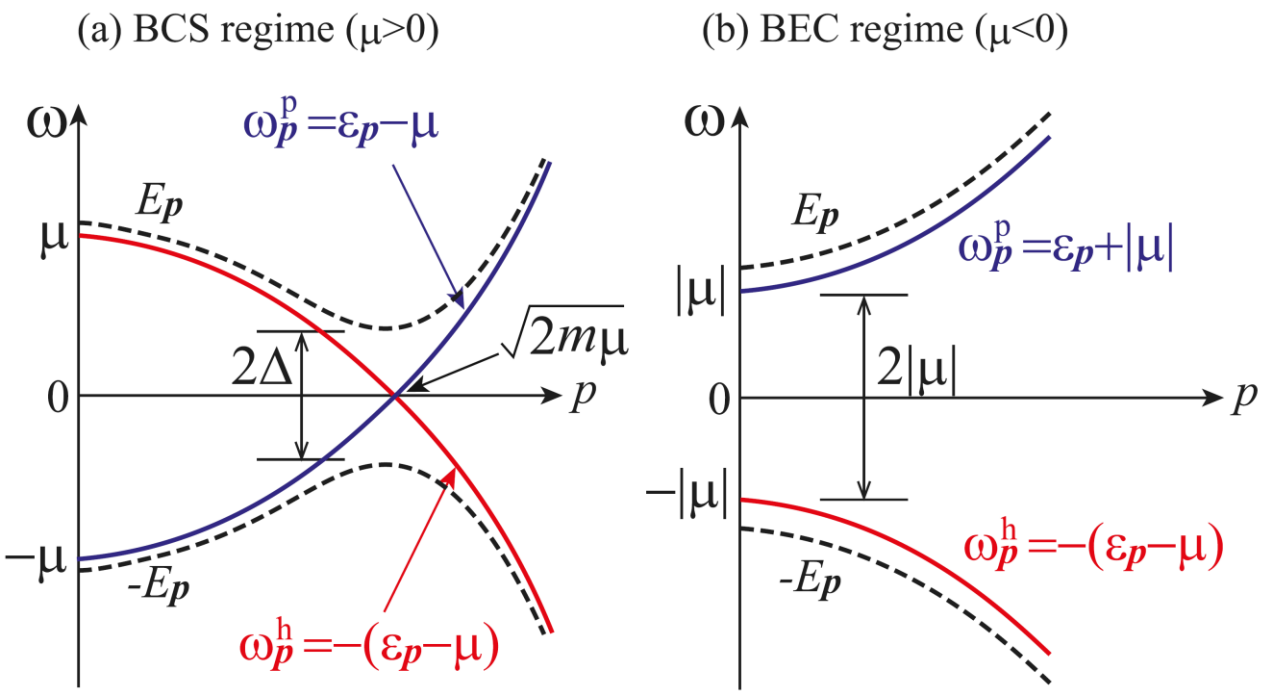

Cooper pair breaking $\sim 2\Delta$

Molecule dissociation $\sim 2\sqrt{|\Delta|^2 + \mu^2} \simeq E_{\mathrm{bind}}$

Y. Ohashi, HT, and P. van Wyk, Prog. Part. Nucl. Phys. **111**, 103739 (2020).

Outline

- Cold atoms and BCS-BEC crossover
- Strong pairing fluctuations
- Unitary Fermi gas and neutron matter
- Role of the multi-band configuration
- Beyond pairing effect
- Summary

Strong pairing fluctuations and pseudogaps

Review: Y. Ohashi, HT, and P. van Wyk, Prog. Part. Nucl. Phys. **111**, 103739 (2020).

Phase diagram of from physical quantities

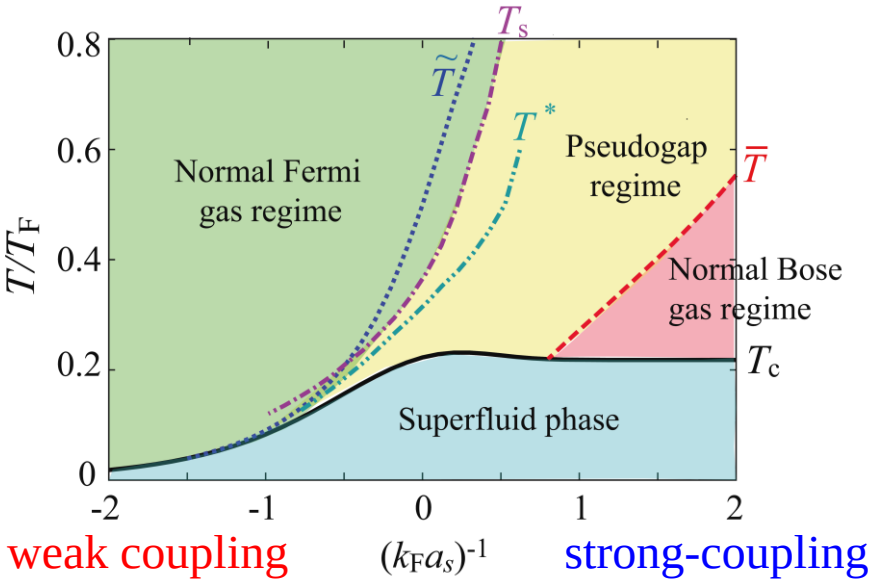

Single-particle dispersion and density of states

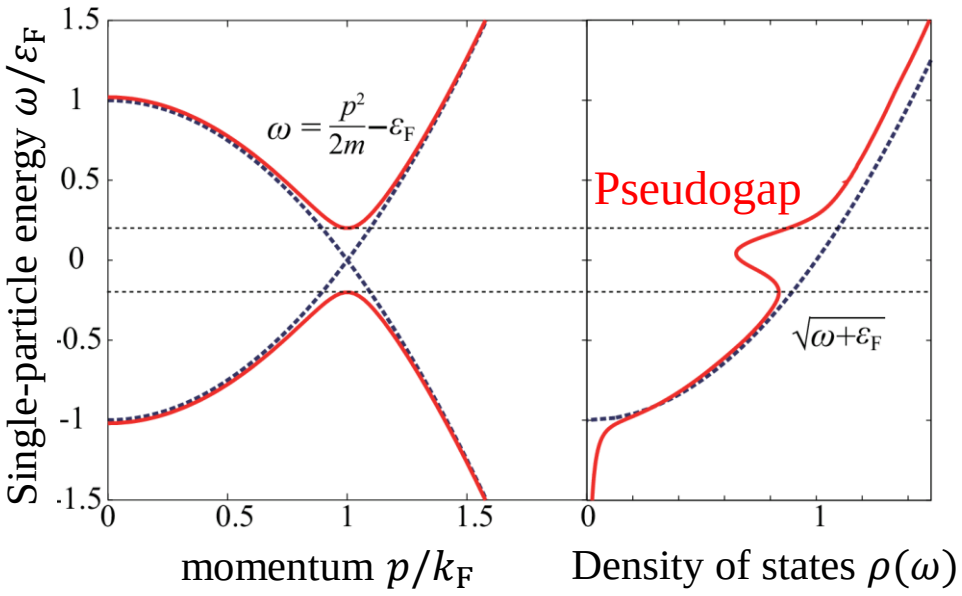

T_s: Spin susceptibility starts to drop
T^*: Density of states starts to show a dip
$\tilde{T}$: Specific heat becomes minimum

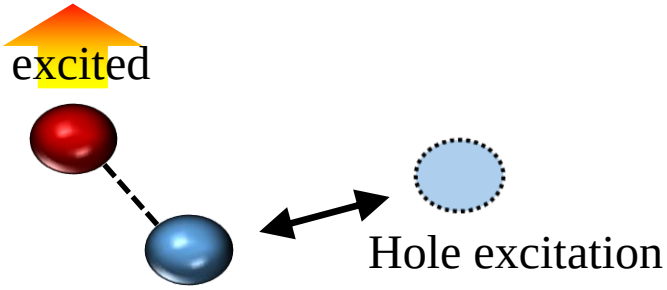

Pairing pseudogap effect across the different energy scales

Dip-like structure in density of states or level density even in the normal phase

BCS-BEC crossover in Li_xZrNCl

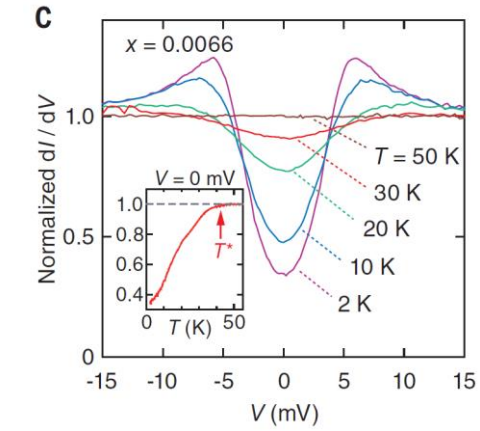

Y. Nakagawa, et al., Science **372**, 6538 (2021).

Nuclear matter

A. Schnell, et al., PRL **83**, 1926 (1999).

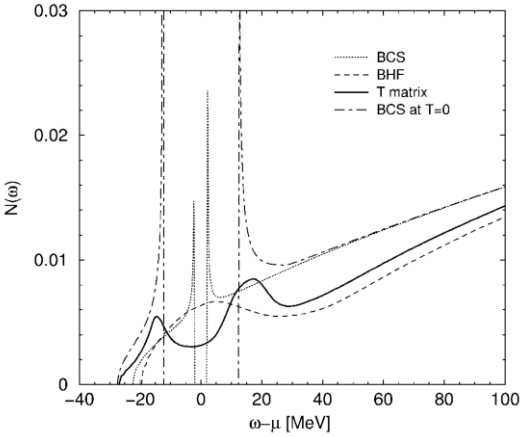

Neutron matter

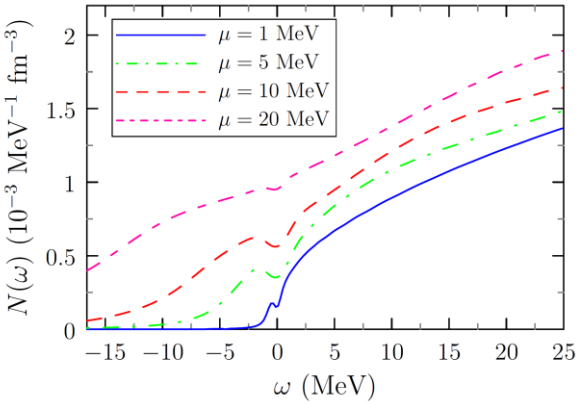

D. Durel, et al., Universe **2020**, 6(11), 208

Color superconductivity

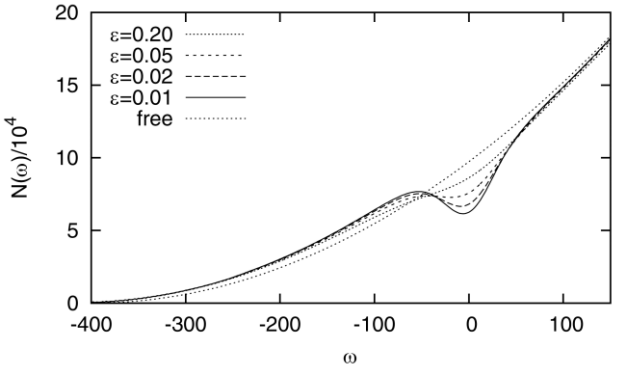

M. Kitazawa, et al., PRD **70**, 056003 (2004).

Existence of pairing pseudogaps in cold-atom experiments

Pairing pseudogap is a long standing issue in an ultracold Fermi gas

Momentum-resolved photoemission spectra

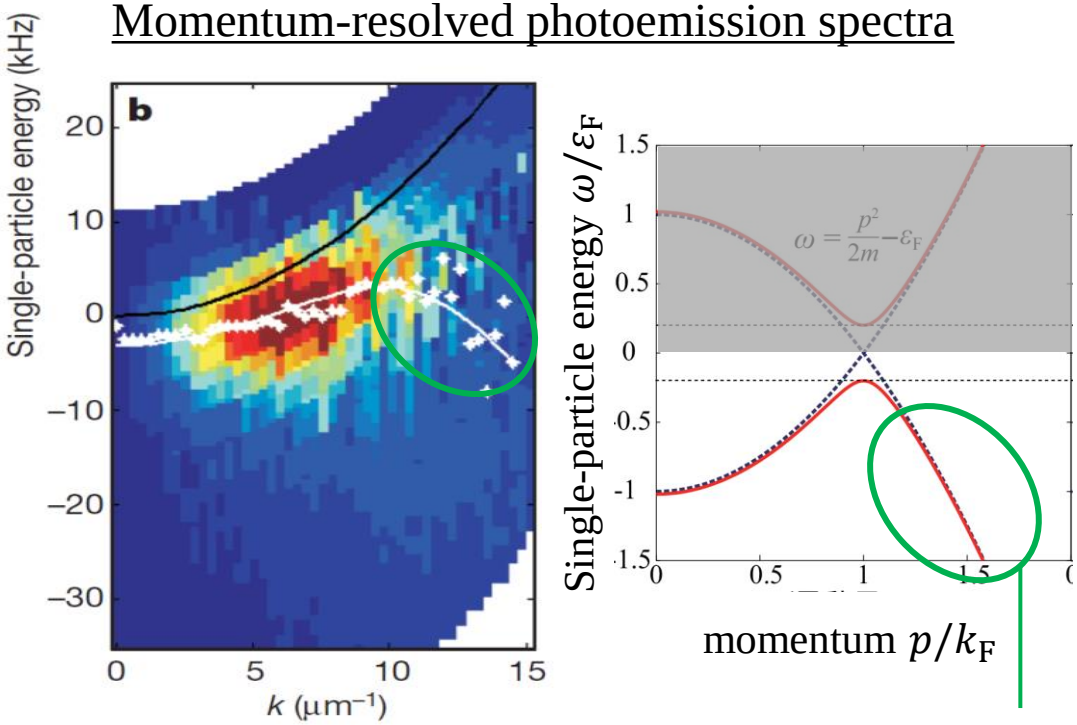

Back bending curve

J. T. Stewart, et al., Nature **454**, 744 (2008).

➡ Supporting the pseudogap

Local pressure measurement

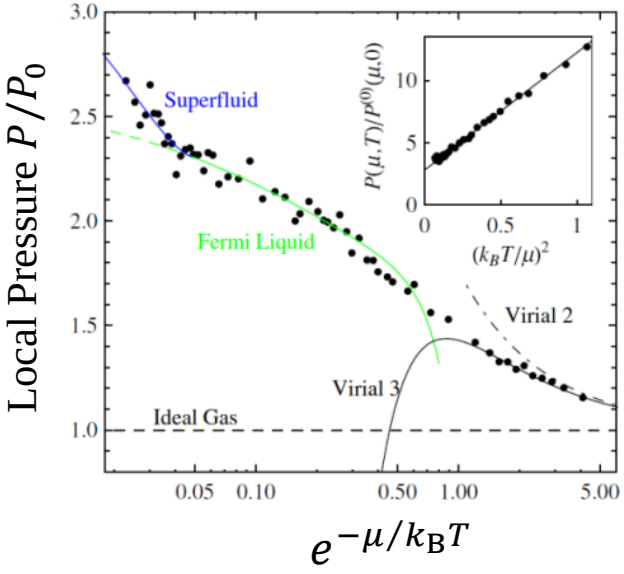

S. Nascimbène, et al., New Journal of Physics **12** (2010) 103026

➡ Supporting the Fermi liquid

Diagrammatic approaches

Review: Y. Ohashi, HT, and P. van Wyk, Prog. Part. Nucl. Phys. **111**, 103739 (2020).

Single-particle self-energy

T-matrix approx. (TMA) | Extended TMA (ETMA) | Self-consistent TMA (SCTMA, LW)

$\Sigma_\sigma =$ (a) 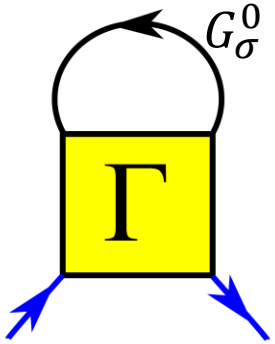 (b) 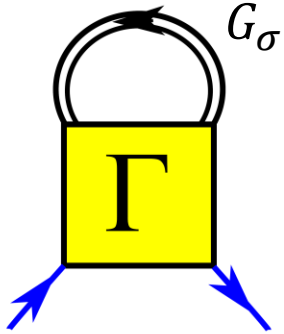 (c) 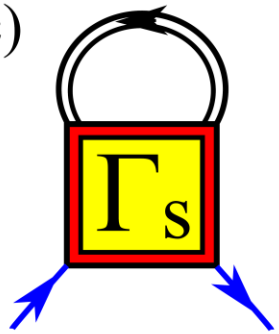

Many-body *T*-matrix

(d) 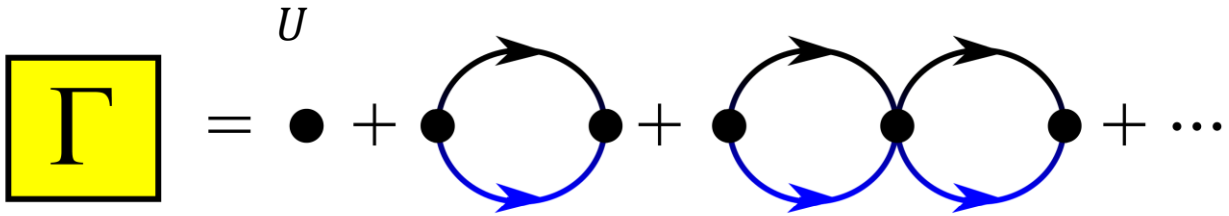

(e) 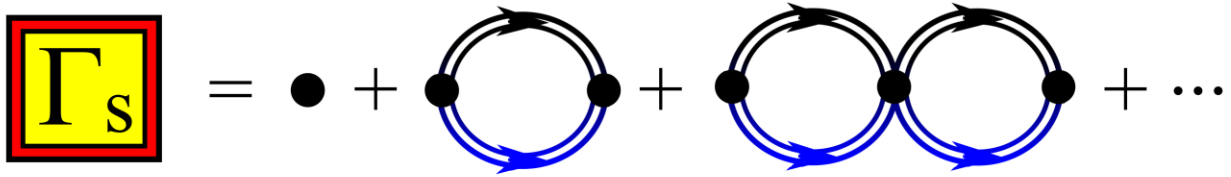

Recent studies of pseudogap effect on the spin susceptibility

Drop of the spin susceptibility above T_c: Signature of pseudogap (PRA, **89**, 033617 (2014).)

Recent measurement in a trapped Fermi gas

Y. Long, et al., PRL **126**, 153402 (2021).

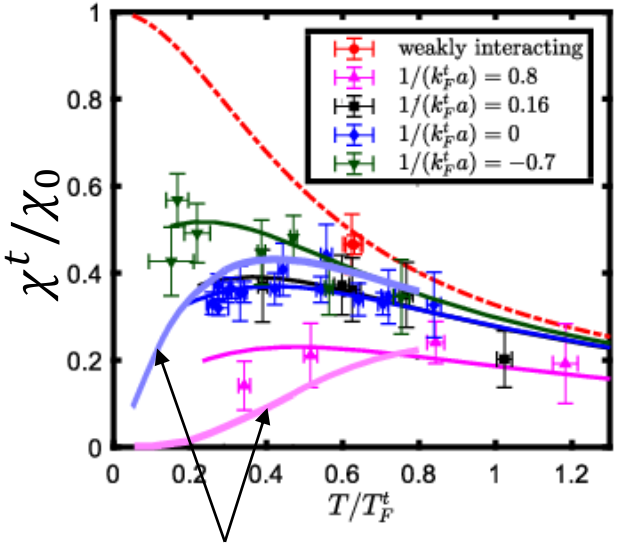

ETMA+LDA

HT, et al., PRA **96**, 033614 (2017).

Trap effects are not negligible

Quantum Monte Carlo

Common consensus has been not obtained yet.

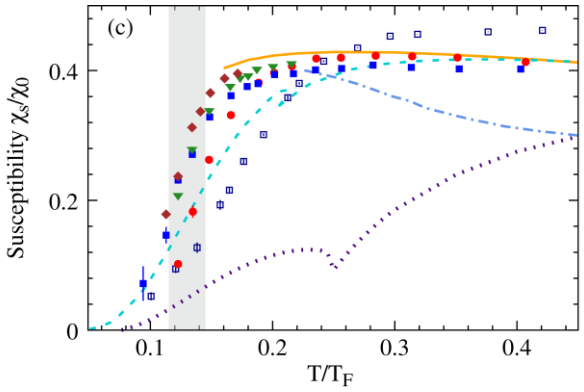

S. Jensen, *et al.*, Phys. Rev. Lett. **124**, 090604 (2020).

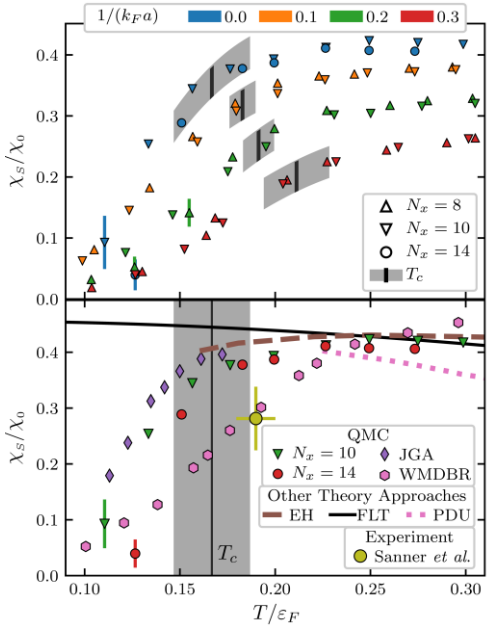

A. Richie-Halford, *et al.*, Phys. Rev. Lett. **125**, 060403 (2020).

Although not reaching the thermodynamic limit yet, the pseudogap signal is hardly seen at unitarity.

Pseudogap can be confirmed at $(k_F a)^{-1} = 0.3$. Still possibility of pseudogap at unitarity.

Tunneling transport phenomena in strongly-interacting interface

G. Del Pace, *et al.*, PRL **126**, 055301 (2021).

Spin-1/2 Fermi gas with tunable interaction

How does tunneling transport reflect effects of the strong interaction?

Barrier $V(x)$

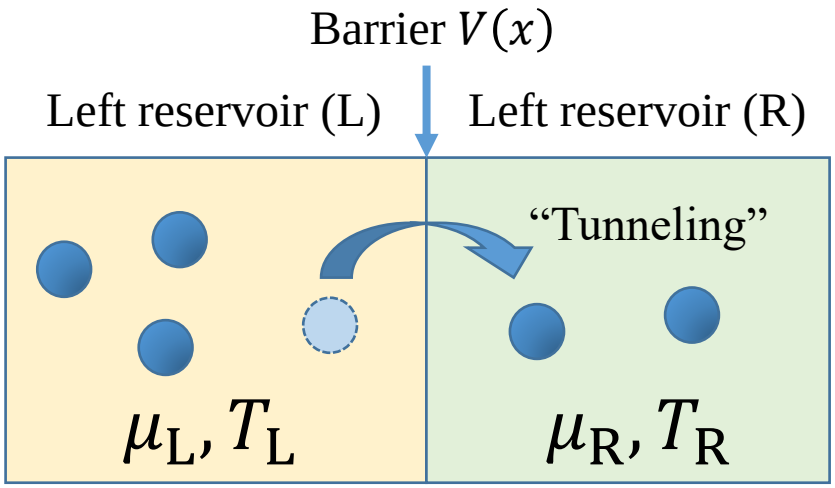

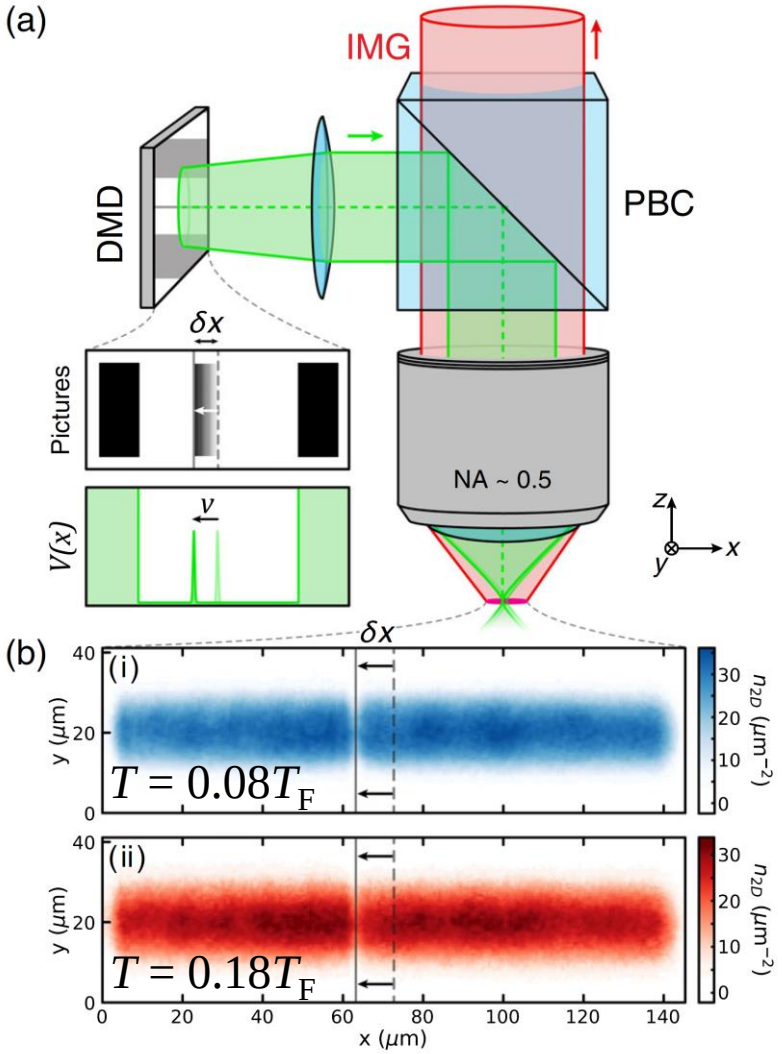

Anomalous tunneling transport

- Extremely large mass conductance G in the crossover

From PRL **126**, 055301 (2021).

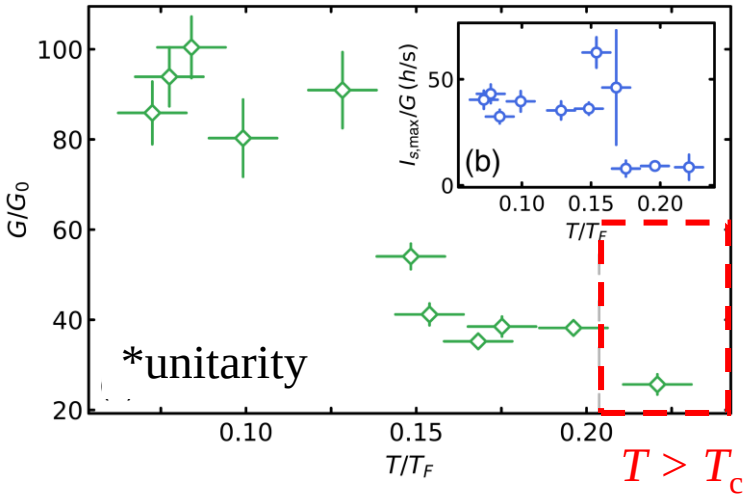

G_0: non-interacting case

Larger than $10 \times G_0$ even above T_c

1. Quasiparticle transport with pseudogap effect?

➡No! The pseudogap suppresses the density of state (DOS) around the Fermi level

Pseudogapped DOS

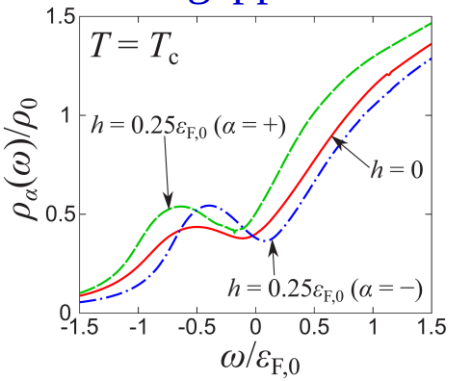

Y. Sekino, HT, and S. Uchino, Phys. Rev. Research **2**, 023152 (2020).

2. Preformed-pair tunneling transport?

➡Probably yes. However, how do they occur? Are there any clear evidences ?

HT, D. Oue, and M. Matsuo, PRA **106**, 033310 (2022).
HT, D. Oue, M. Matsuo, and K. Kato, arXiv:2202.03873

Interaction-induced multi-particle transport

HT, D. Oue, and M. Matsuo, PRA **106**, 033310 (2022).

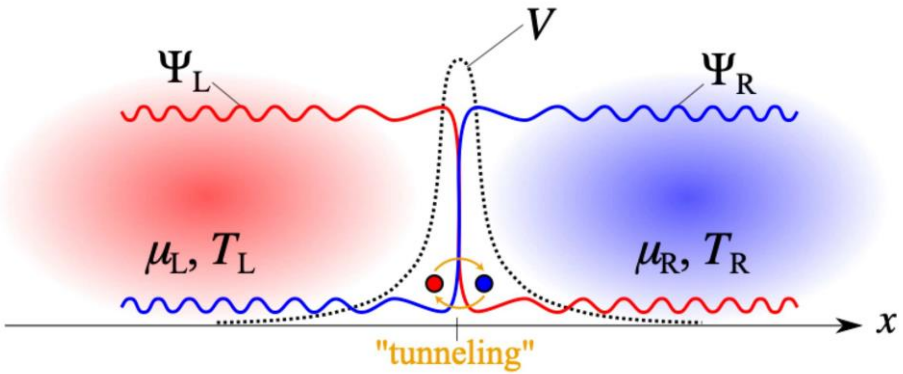

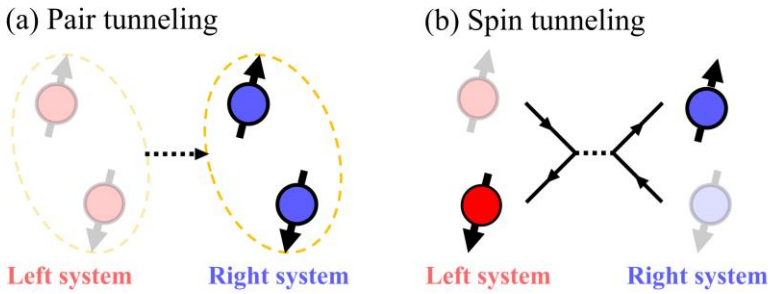

- Pair- and spin-tunneling processes naturally occur in strongly interacting systems via interaction Hamiltonians.

$$\hat{H} = \int d^3\boldsymbol{r} \sum_\sigma \hat{\psi}^\dagger_\sigma(\boldsymbol{r}) \hat{h}_\sigma(\boldsymbol{r}) \hat{\psi}_\sigma(\boldsymbol{r}) + g \int d^3\boldsymbol{r} \hat{\psi}^\dagger_\uparrow(\boldsymbol{r}) \hat{\psi}^\dagger_\downarrow(\boldsymbol{r}) \hat{\psi}_\downarrow(\boldsymbol{r}) \hat{\psi}_\uparrow(\boldsymbol{r})$$

$$\hat{\psi}_\sigma(\boldsymbol{r}) = \hat{\psi}_{\sigma,\mathrm{L}}(\boldsymbol{r}) + \hat{\psi}_{\sigma,\mathrm{R}}(\boldsymbol{r})$$

$$H_{1\mathrm{t}} = \sum_{\boldsymbol{p},\boldsymbol{k},\sigma} \mathcal{T}_{\boldsymbol{k},\boldsymbol{p},\sigma} \left[c^\dagger_{\boldsymbol{k},\sigma,\mathrm{L}} c_{\boldsymbol{p},\sigma,\mathrm{R}} + c^\dagger_{\boldsymbol{k},\sigma,\mathrm{R}} c_{\boldsymbol{p},\sigma,\mathrm{L}} \right]$$

$$H_{\mathrm{pair}} = \sum_{\boldsymbol{q}} \tilde{g} \left[P^\dagger_{\boldsymbol{q},\mathrm{L}} P_{-\boldsymbol{q},\mathrm{R}} + \mathrm{h.c.} \right],$$

$$H_{\mathrm{spin}} = \sum_{\boldsymbol{q}} \tilde{g} \left[S^+_{\boldsymbol{q},\mathrm{L}} S^-_{-\boldsymbol{q},\mathrm{R}} + S^+_{-\boldsymbol{q},\mathrm{R}} S^-_{\boldsymbol{q},\mathrm{L}} \right],$$

Detecting preformed-pair current through nonequilibrium noise

HT, D. Oue, M. Matsuo, and T. Kato, arXiv:2202.03873

Quasiparticle tunneling

$$H_{1\mathrm{T}} = \sum_{\boldsymbol{p},\boldsymbol{k},\sigma} \left[t_{\boldsymbol{p},\boldsymbol{k}} c^{\dagger}_{\boldsymbol{p},\sigma,\mathrm{L}} c_{\boldsymbol{k},\sigma,\mathrm{R}} + \mathrm{h.c.} \right]$$

Pair tunneling

$$H_{2\mathrm{T}} = \sum_{\boldsymbol{q},\boldsymbol{q}'} \left[w_{\boldsymbol{q},\boldsymbol{q}'} P^{\dagger}_{\boldsymbol{q},\mathrm{L}} P_{\boldsymbol{q}',\mathrm{R}} + \mathrm{h.c.} \right]$$

Fermion annihilation operator

$$c_{\boldsymbol{p},\sigma,\mathrm{j}}$$

(momentum $\boldsymbol{p}$, spin $\sigma = \uparrow,\downarrow$, reservoir j=L,R)

Pair annihilation operator

$$P_{\boldsymbol{q},\mathrm{j}} = \sum_{\boldsymbol{p}} c_{-\boldsymbol{p}+\boldsymbol{q}/2,\downarrow,\mathrm{j}} c_{\boldsymbol{p}+\boldsymbol{q}/2,\uparrow,\mathrm{j}}$$

Current operator

$$\hat{I} = i[\hat{N}_{\mathrm{L}}, H] \qquad \hat{N}_{\mathrm{j}} = \sum_{\boldsymbol{p},\sigma} c^{\dagger}_{\boldsymbol{p},\sigma,\mathrm{j}} c_{\boldsymbol{p},\sigma,\mathrm{j}}$$

Non-equilibrium noise

$$\mathcal{S} = \frac{1}{2} \int_{-\infty}^{\infty} dt \left(\langle \hat{I}(t)\hat{I}(0) \rangle + \langle \hat{I}(0)\hat{I}(t) \rangle \right)$$

Fano factor

$$F = \frac{\mathcal{S}}{I}$$

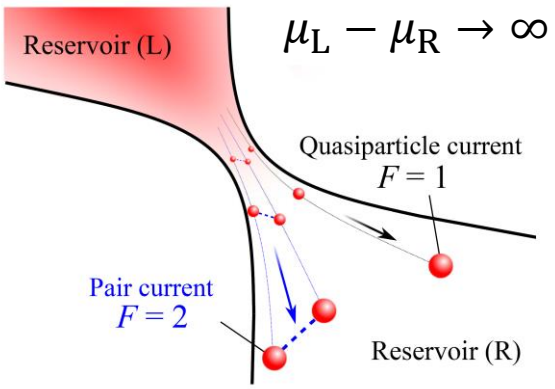

Detecting preformed-pair current through nonequilibrium noise

HT, D. Oue, M. Matsuo, and T. Kato, arXiv:2202.03873

Schwinger-Keldysh + Many-body T-matrix approaches

Fano factor above T_c

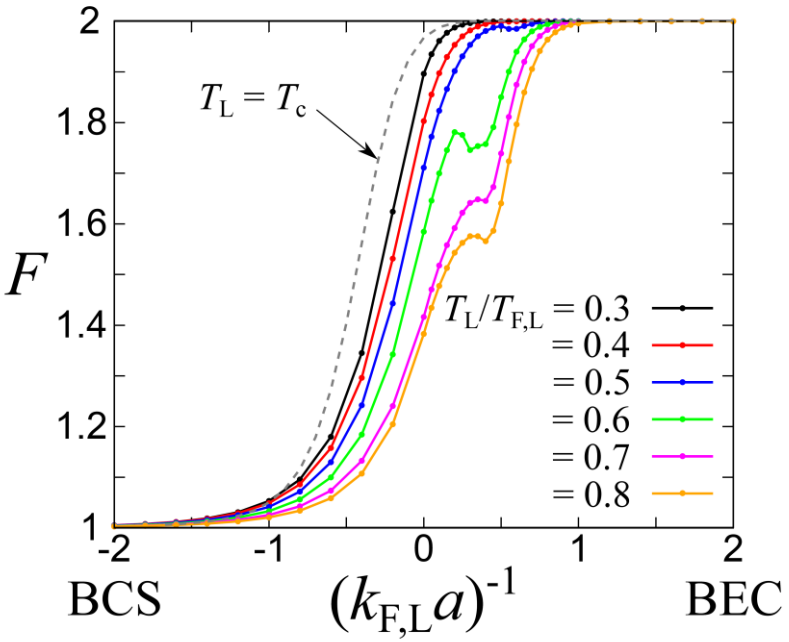

Preformed pair current

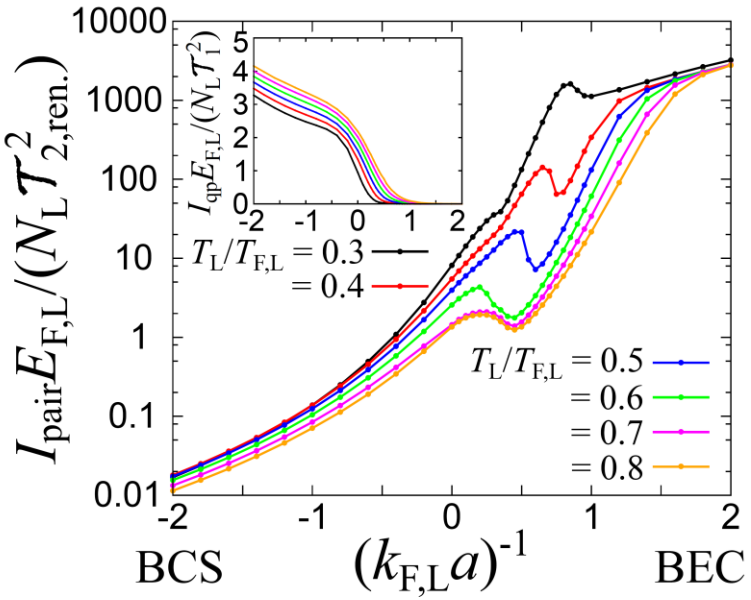

$$F = \frac{\mathcal{S}}{I} = \frac{\mathcal{S}_{qp} + \mathcal{S}_{pair}}{I_{qp} + I_{pair}}$$

The change of F reflects the dominant current carrier

Toward spintronics application

Spin tunneling process is crucial for application to spintronics simulation

Spin tunneling Hamiltonian

$$H_{\mathrm{ex}} = \sum_{k,q} [\mathcal{T}_{k,q} S_k^+ s_q^- + \mathrm{H.c.}]$$

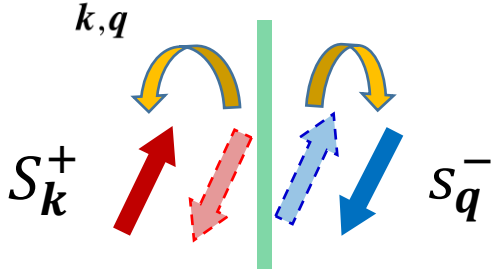

T. Kato, *et al*., PRB **99**, 144411 (2019).

?

Atomtronics

Ferromagnetism in repulsive Fermi gases

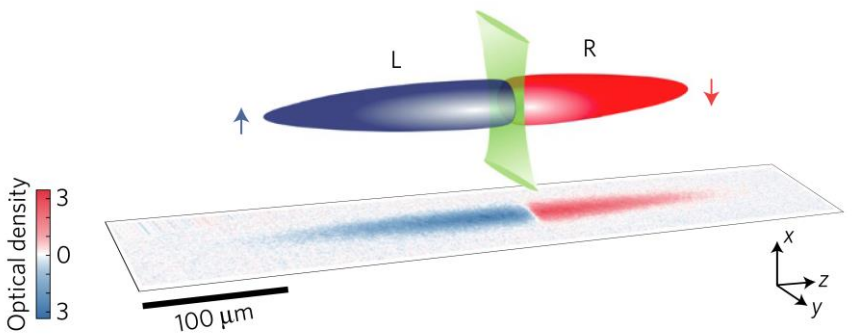

G. Valtolina, *et al*., Nat. Phys. **13**, 704 (2017).

Spintronics

Spin Seebeck/pumping effect

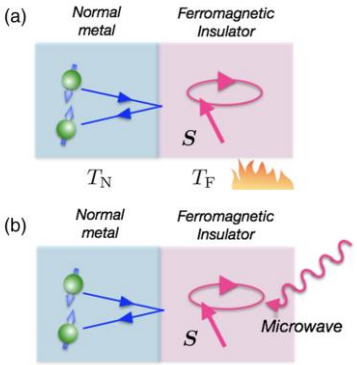

M. Matsuo et al., PRL **120**, 037201 (2018).

Spin Peltier effect

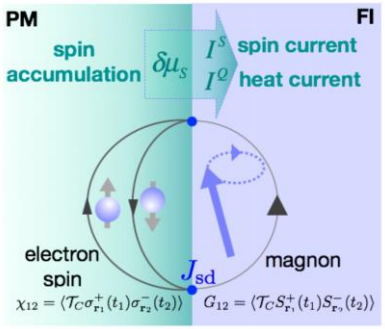

Y. Ohnuma, et al., PRB **96**, 134412 (2017).

Magnon tunneling transport

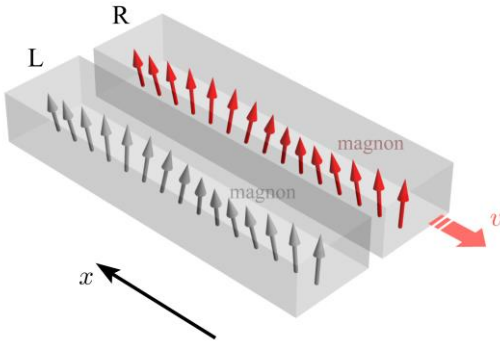

D. Oue and M. Matsuo, PRB **105**, L020302 (2022).

Outline

- Cold atoms and BCS-BEC crossover
- Strong pairing fluctuations
- Unitary Fermi gas and neutron matter
- Role of the multi-band configuration
- Beyond pairing effect
- Summary

Unitary Fermi gas and universality

Scale invariance because of no length scales associated with interaction ($a \to \infty$)

Universal thermodynamics

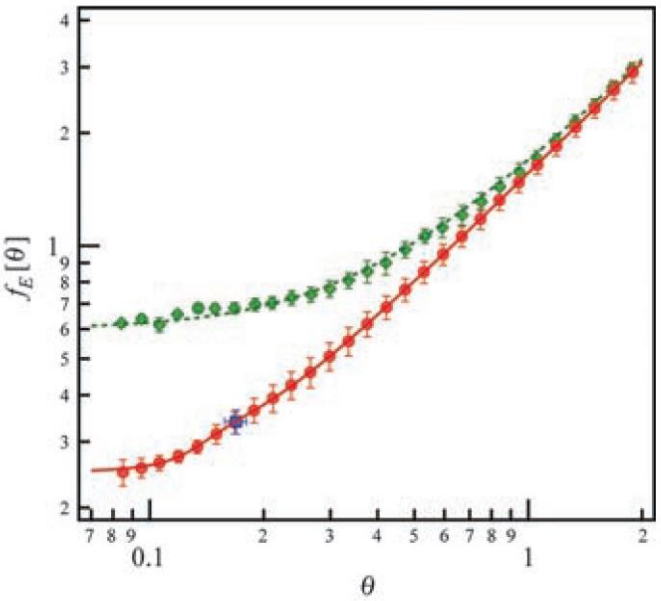

M. Horikoshi, et al., Science **327**, 442 (2010).

Ideal Fermi gas: $E_{\text{ideal}} = f_0(n, T)$

Interacting Fermi gas: $E = g(n, a, T)$

Unitary Fermi gas: $E_{\text{UFG}} = f(n, T)$

At $T = 0$, only one parameter is relevant

Compressibility $\kappa = \frac{1}{\xi}\kappa_0$

Sound velocity $v_s = \sqrt{\frac{\xi}{3}}v_F$

Internal energy $E = \frac{3}{5}\xi n\varepsilon_F$

Pressure $P = \xi^{-\frac{3}{2}}P_0$

Bertsch parameter

$\xi \simeq 0.37$

G. F. Bertsch, Challenge problem in many-body physics (1999)

Unitary Fermi gas and astrophysics

Universal thermodynamics

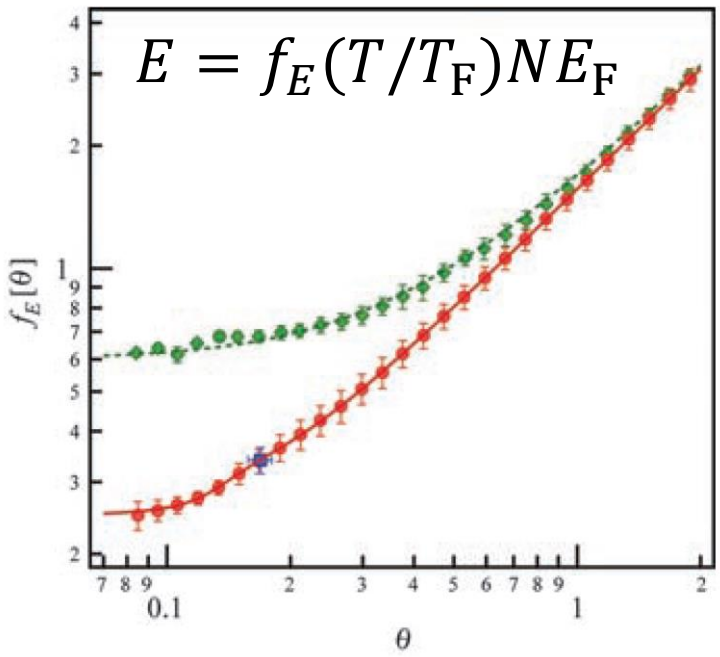

M. Horikoshi, *et al.*, Science, **327**, 442 (2010).

- neutron-matter equation of state (T = 0)

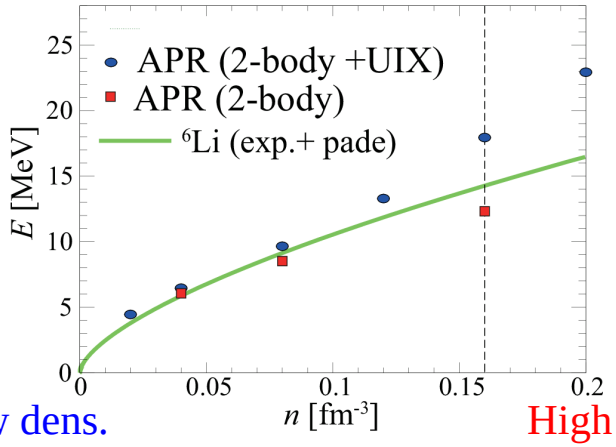

Low dens. High dens.

M. Horikoshi, *et al.*, PRX, **7**, 041004 (2017).

- High-temperature supernova matter

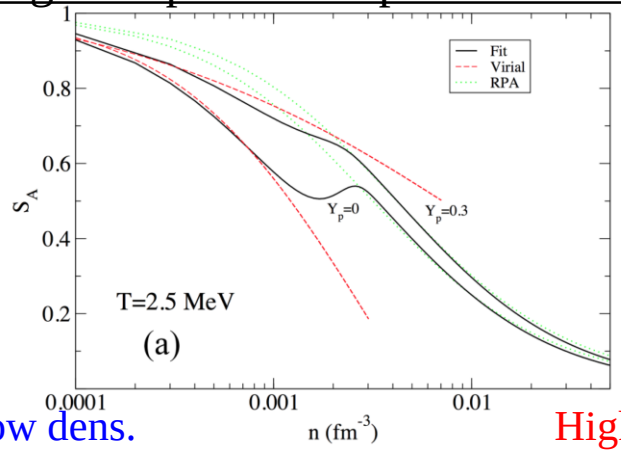

Low dens. High dens.

C. J. Horowitz, *et al.*, PRC, **95**, 025801 (2017).

Another unitary Fermi gas

➡ 1D Fermi gas with *p*-wave interaction

HT, et al. PRA **104**, 023319 (2021).

Unitary Fermi gas and neutron matter

- The low-density neutron matter is also dominated by the s-wave scattering like an ultracold Fermi gas

Phase shift (effective range expansion)

$$k\cot\delta_k = -\frac{1}{a_s} + \frac{1}{2}k^2 r_e$$

a_s: s-wave scattering length

r_e: effective range

	Cold atom	Neutrons
a_s	$-\infty\sim\infty$	-18.5 fm
r_{eff}	~ 0	2.8 fm
density	$\sim 10^{15}$ cm^{-3}	~ 0.17 fm^{-3}
$(k_F a_s)^{-1}$	$-\infty\sim\infty$	$-\infty\sim 0$

Phase shift of NN scattering

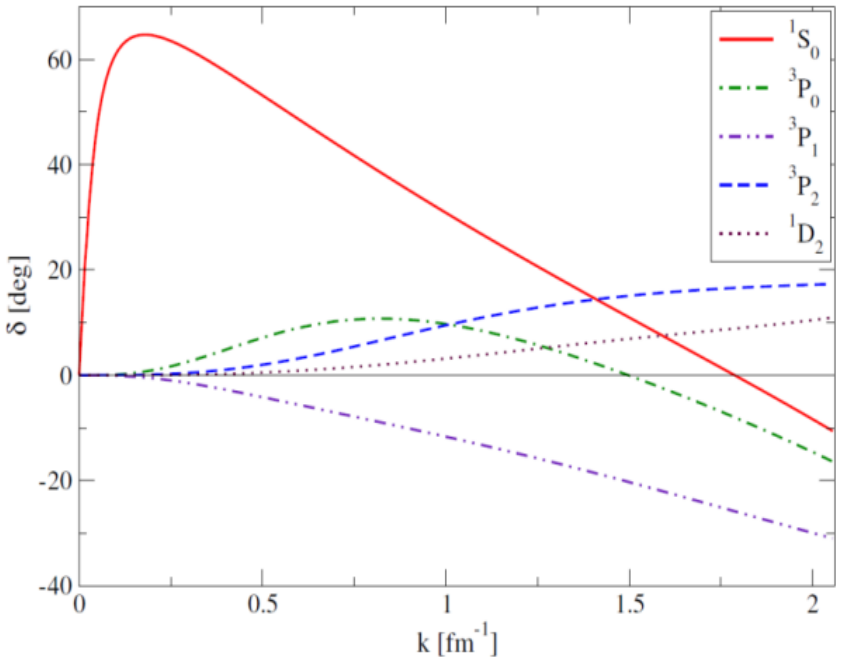

A. Gezerlis, *et al*, arXiv : 1406.6109v2

$*$ k_F: Fermi momentum

Experiment and theory

Exp. 1 : M. Horikoshi, M. Koashi, HT, Y. Ohashi, and M. Kuwata-Gonokami, PRX **7**, 041004 (2017).
Exp. 2 : S. Hoinka, P. Dyke, M. Lingham, J. Kinnunen, G. Bruun, and C. J. Vale, Nat. Phys. **13**, 943 (2017).

Internal energy

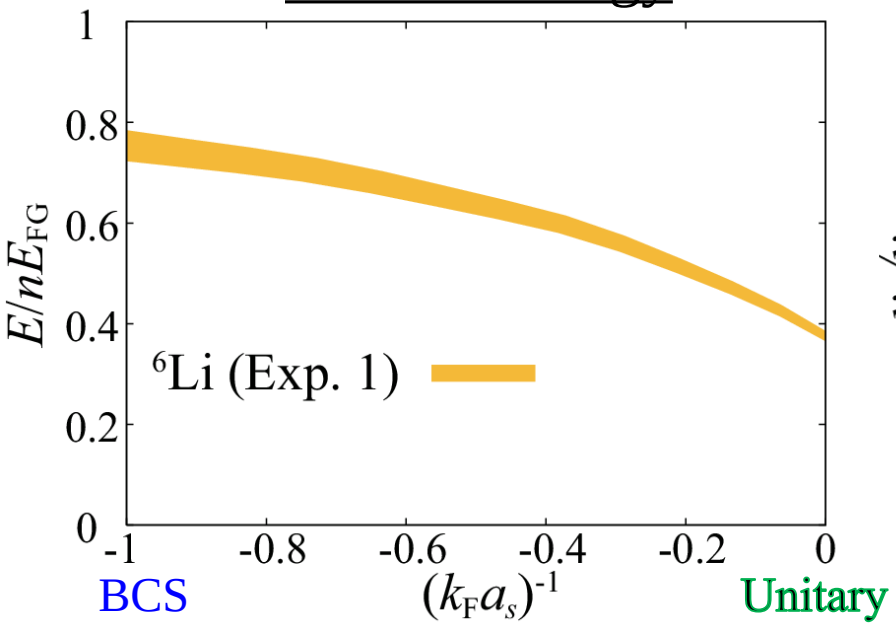

Speed of sound

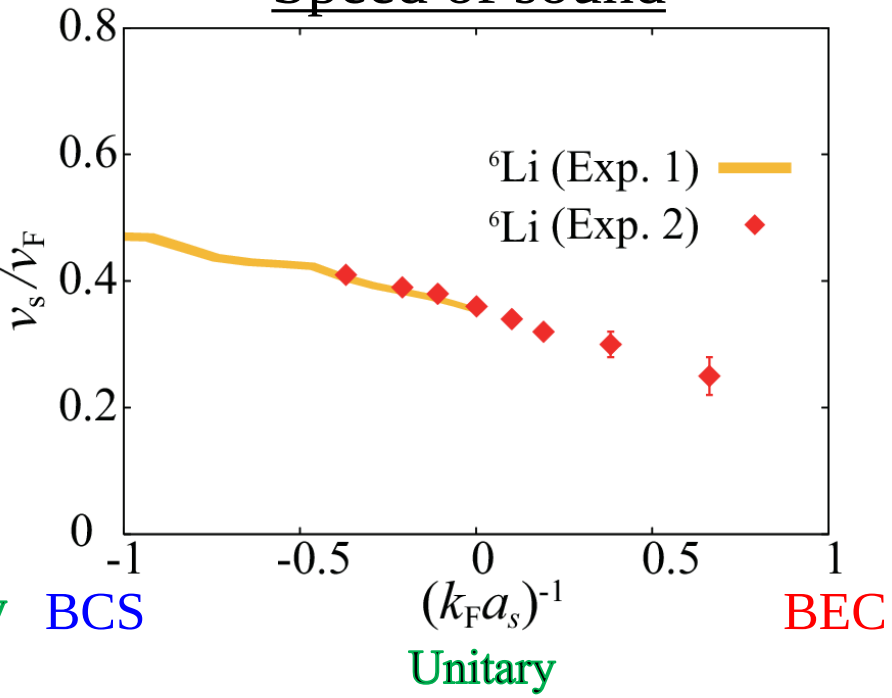

The relative error is within only 4%

Experiment and theory

Exp. 1 : M. Horikoshi, M. Koashi, HT, Y. Ohashi, and M. Kuwata-Gonokami, PRX **7**, 041004 (2017).
Exp. 2 : S. Hoinka, P. Dyke, M. Lingham, J. Kinnunen, G. Bruun, and C. J. Vale, Nat. Phys. **13**, 943 (2017).
ETMA: HT P. van Wyk, R. Hanai, D. Kagamihara, D. Inotani, M. Horikoshi, and Y. Ohashi, PRA **95**, 043625 (2017).

Internal energy

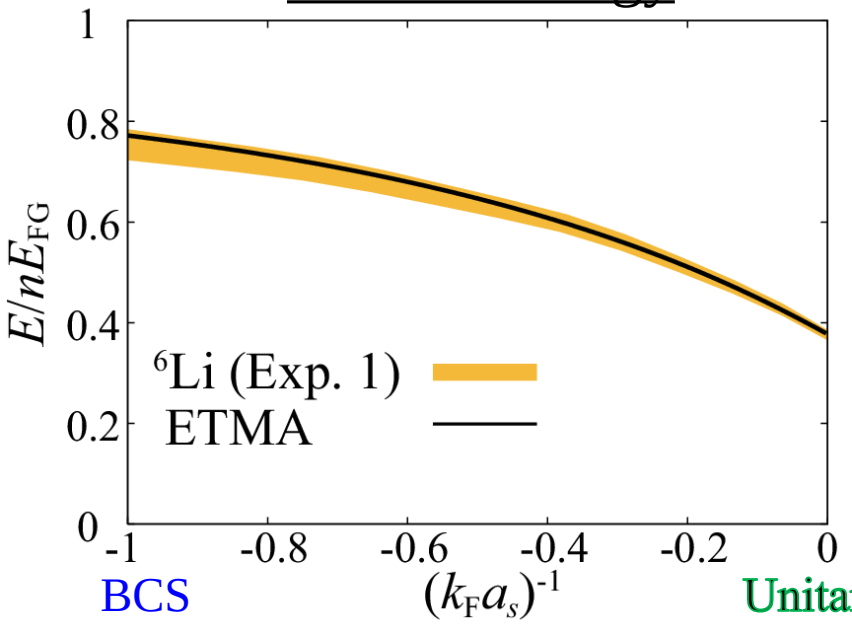

Speed of sound

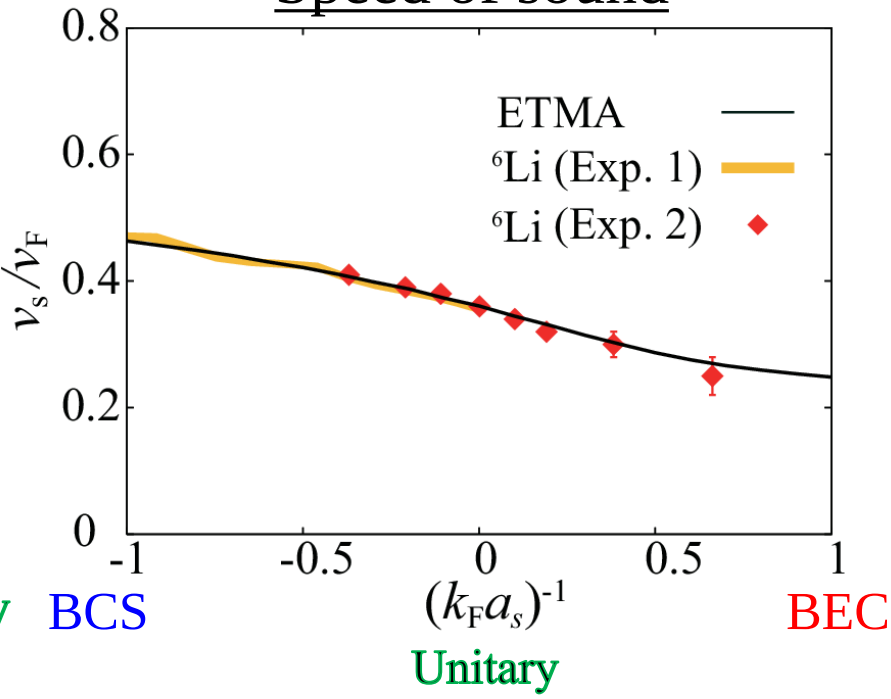

The relative error is within only 4%

Unitary Fermi gas and neutron matter

- The low-density neutron matter is also dominated by the s-wave scattering like an ultracold Fermi gas

M. Horikoshi, M. Koashi, HT, Y. Ohashi, and M. Kuwata-Gonokami, PRX, **7**, 041004 (2017).

▸ Precise measurement of cold atom EOS

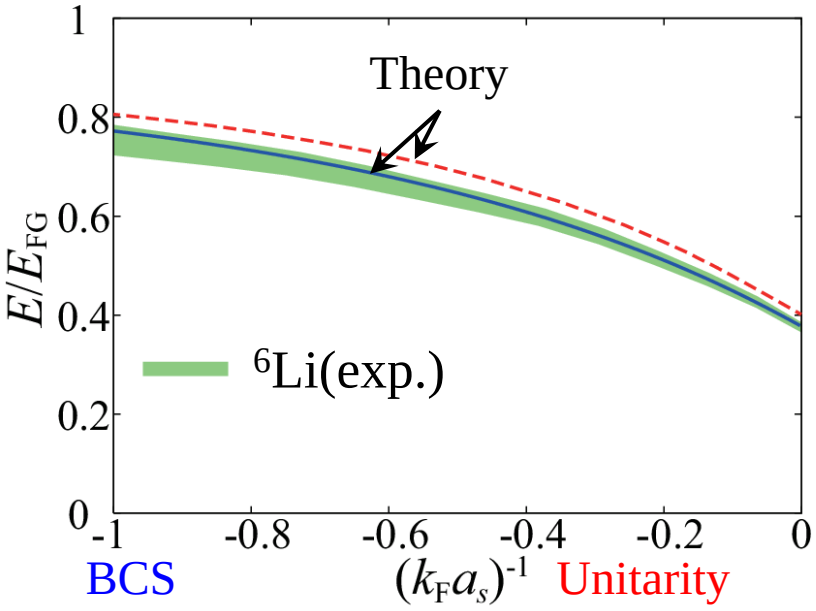

Scale trans.

▸ EOS of neutron matter and cold atom

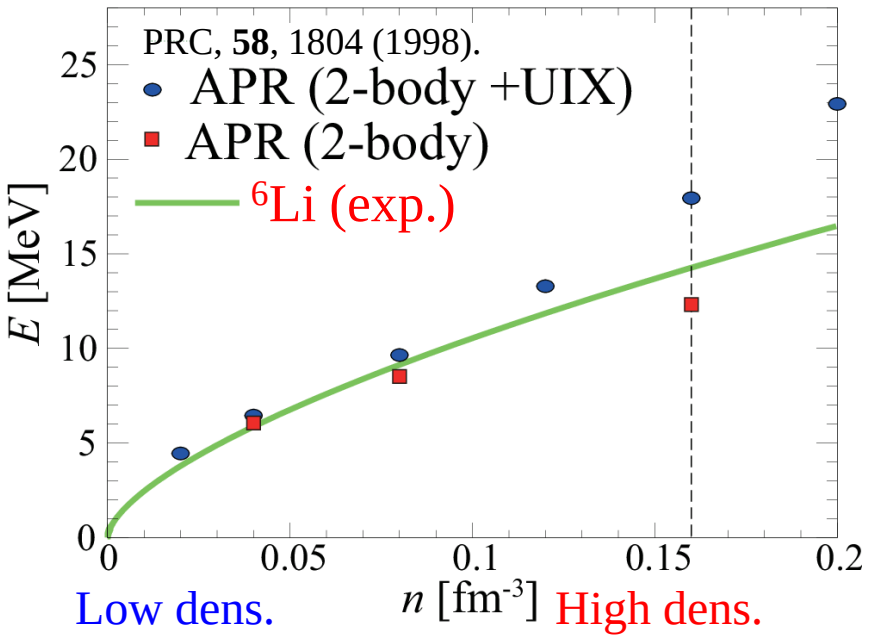

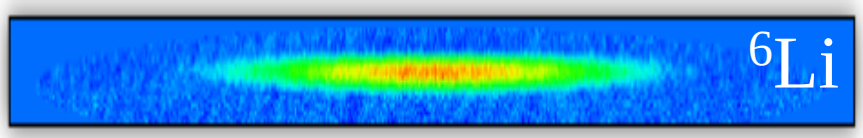

Agreement in the low density region

Unitary Fermi gas and neutron matter

Comparison of pairing gaps

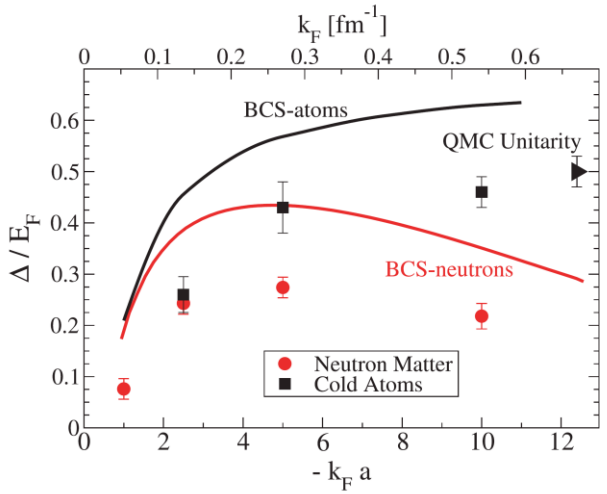

PRC **77**, 032801(R) (2008).

Spin susceptibility in neutron matter

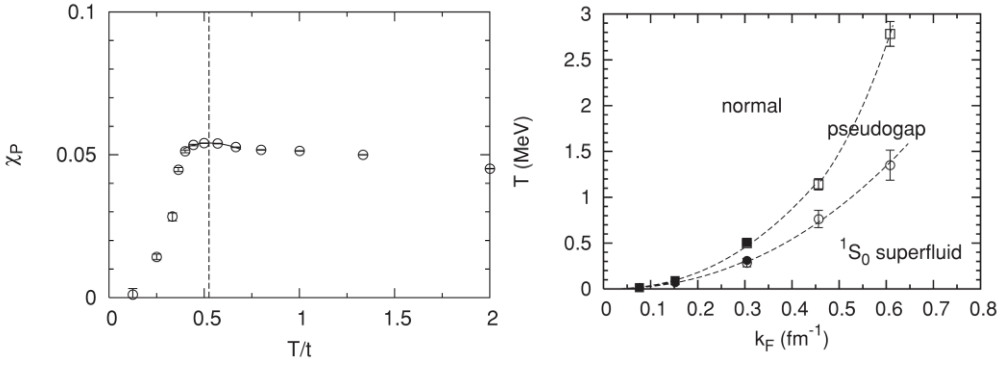

T. Abe and R. Seki, PRC **79**, 054002 (2009).

Latest results of pairing gaps

Neutron matter (AFDMC)

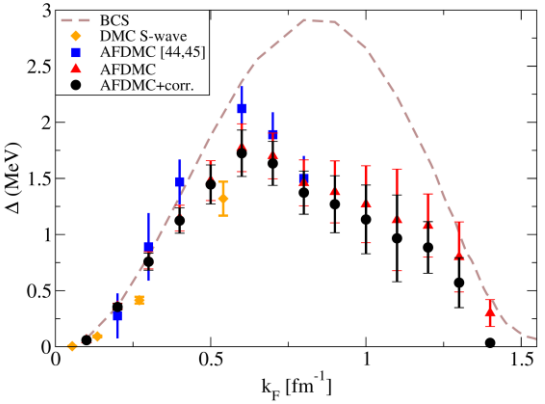

S. Gandolfi, et al., Condens. Matter **2022**, *7*(1), 19

Ultracold Fermi gas (expt.)

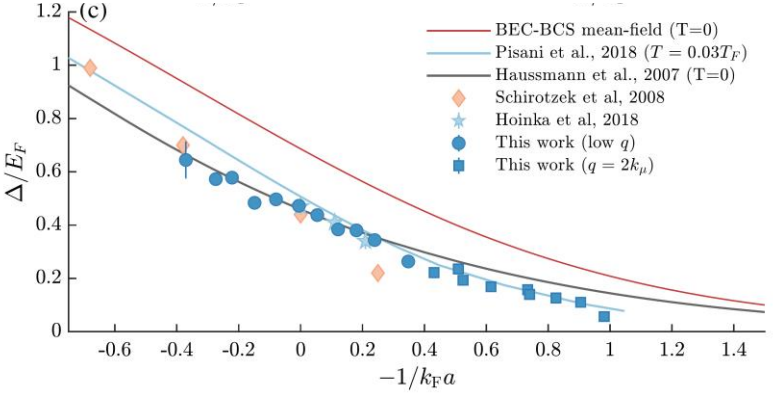

H. Biss, et al., PRL **128**, 100401 (2022).

“BCS-BCS” crossover in dilute neutron matter

P. Van Wyk, HT, D. Inotani, A. Ohnishi, and Y. Ohashi, PRA, **97**, 013601 (2018).
HT, T. Hatsuda, P. van Wyk, and Y. Ohashi, Sci. Rep. **9**, 18477 (2019).

Neutron-star equation of state

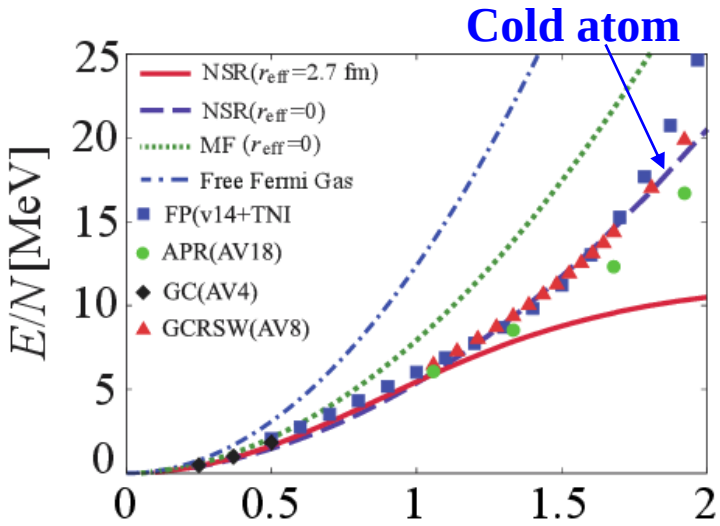

small $|k_{\rm F}a|$

$(k_{\rm F}a)^{-1} = -\infty$

$k_{\rm F}r = 0$

large $|k_{\rm F}a|$

$(k_{\rm F}a)^{-1} = -0.02$

$k_{\rm F}r = 5.6$

Neutron-neutron scattering

$a = -18.5$ fm $\quad r = 2.8$ fm

$T_{\rm c}$-dome of neutron superfluid

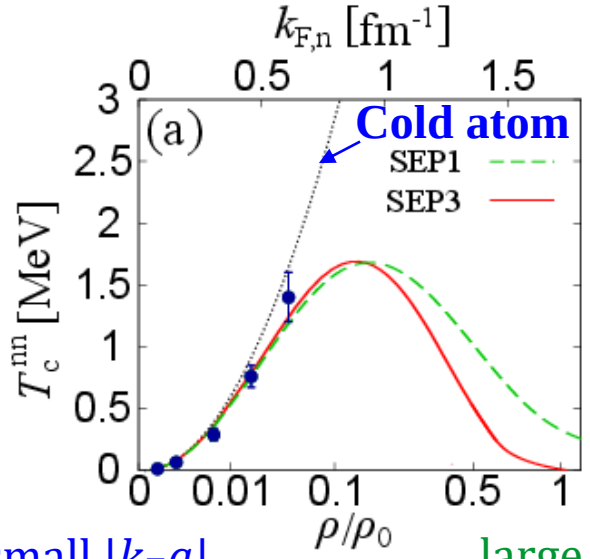

small $|k_{\rm F}a|$

large $|k_{\rm F}a|$

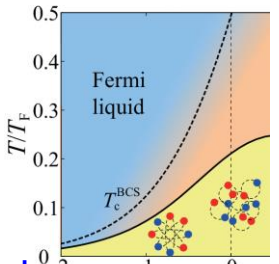

small $|k_{\rm F}a|$ large $|k_{\rm F}a|$

“BCS-BCS” crossover in dilute neutron matter

P. Van Wyk, HT, D. Inotani, A. Ohnishi, and Y. Ohashi, PRA, **97**, 013601 (2018).
HT, T. Hatsuda, P. van Wyk, and Y. Ohashi, Sci. Rep. **9**, 18477 (2019).

Neutron-star equation of state

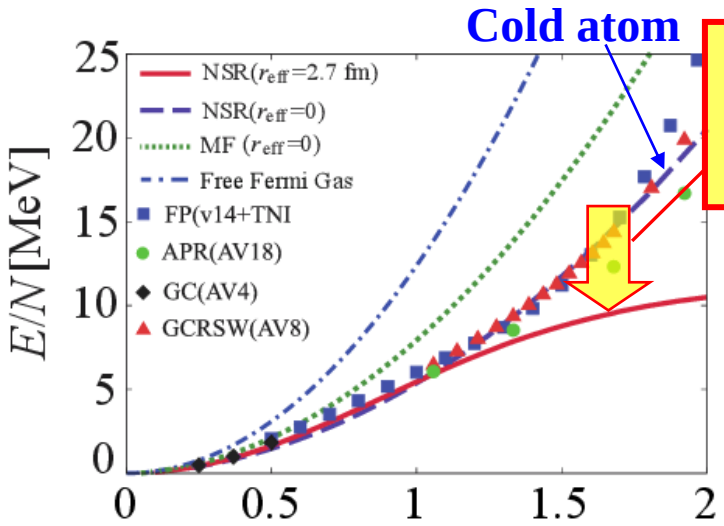

Effective range correction
$k_{\rm F}r \gtrsim 1$

$T_{\rm c}$-dome of neutron superfluid

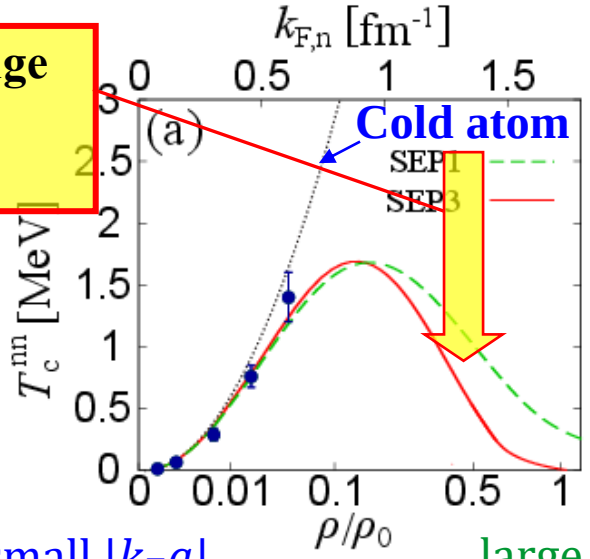

small $|k_{\rm F}a|$ large $|k_{\rm F}a|$

small $|k_{\rm F}a|$ large $|k_{\rm F}a|$

$(k_{\rm F}a)^{-1} = -\infty$

$k_{\rm F}r = 0$

$(k_{\rm F}a)^{-1} = -0.02$

$k_{\rm F}r = 5.6$

Neutron-neutron scattering
$a = -18.5$ fm $\quad r = 2.8$ fm

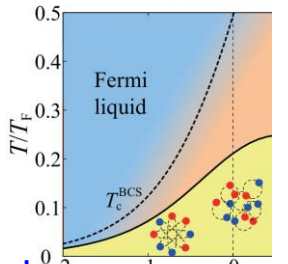

small $|k_{\rm F}a|$ large $|k_{\rm F}a|$

Density-induced BEC-BCS crossover

HT and H. Liang, PRA 106, 043308 (2022).

*Change of the carrier density ≃ Change of interactions?

The one parameter (i.e., a) is not enough to characterize the density-induced crossover

Phase shift

$$k\cot\delta_k = -\frac{1}{a} + \frac{1}{2}k^2 r$$

a: s-wave scattering length

r: effective range

Cold atoms (zero-range interaction, $r/a = 0$)

No bound state (e.g., neutron matter) ($r/a < 0$)

Bound state exists (e.g., nuclear matter) ($r/a > 0$)

➡ layer SC, exciton, etc,…would also be on the red line

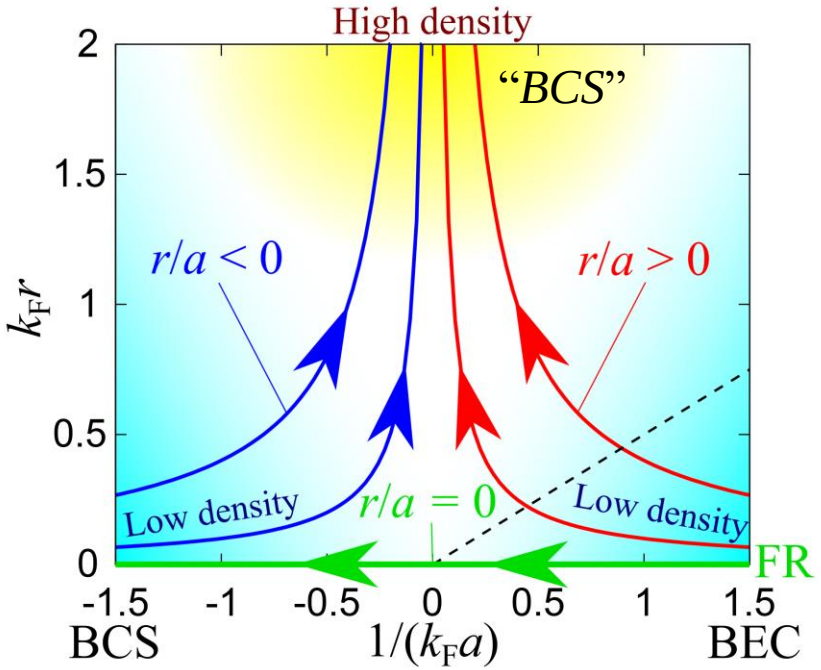

Dashed line: $\cot\delta_s(k = k_F) = 0$

HT, JPSJ **88**, 093001 (2019).

“BEC-BCS” crossover in nuclear systems

If a two-body bound state (e.g., deuteron, hadron in QC_2D, 2D SC) is present in vacuum, BEC(dilute)-BCS(dense) crossover can be achieved.

Density-induced BEC-BCS crossover in symmetric nuclear matter (neutron-proton)

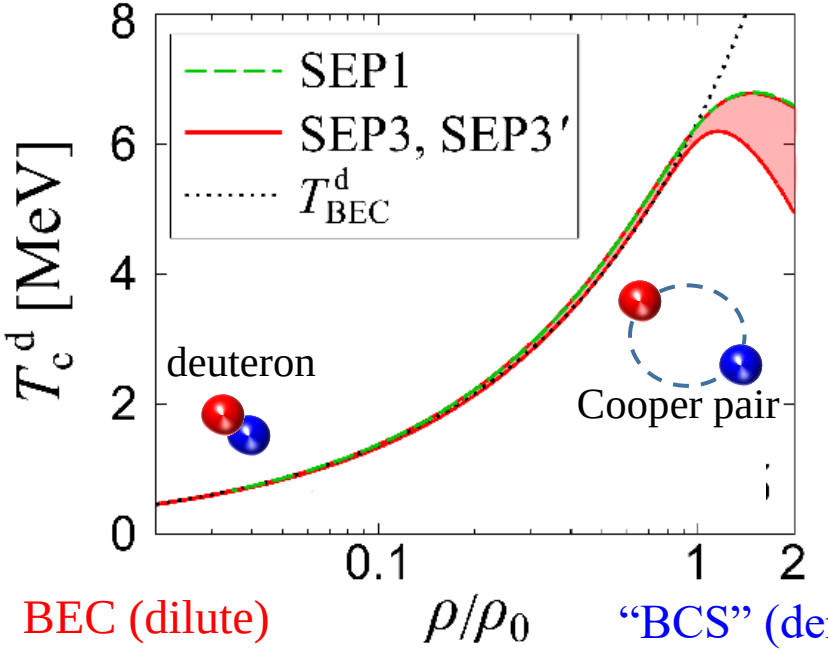

HT, T. Hatsuda, P. van Wyk, and Y. Ohashi, Sci. Rep. **9**, 18477 (2019).

Density-induced BEC-BCS crossover in QC_2D

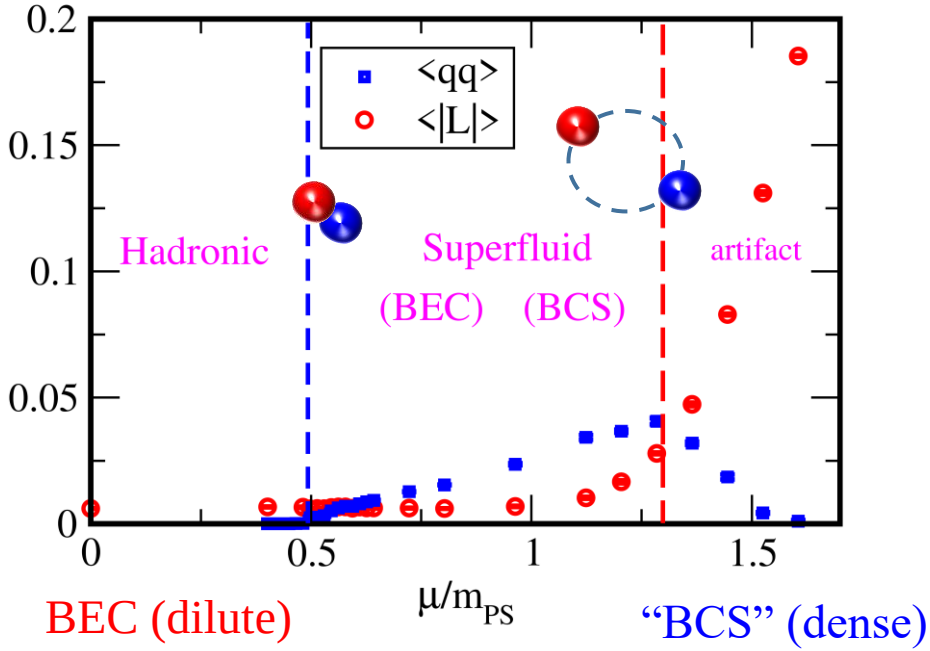

K. Iida, E. Itou, and T.-G. Lee, JHEP 01(2020)181

*np scattering length $a_{\rm np} = 5.42$ fm, effective range $r_{\rm np} = 1.76$ fm

“BEC-BCS” crossover in condensed-matter systems

Scattering length (interaction) CANNOT be tuned ➡ Density can be tuned

BEC-BCS crossover in Li_xZrNCl (lithium-intercalated layered nitride)

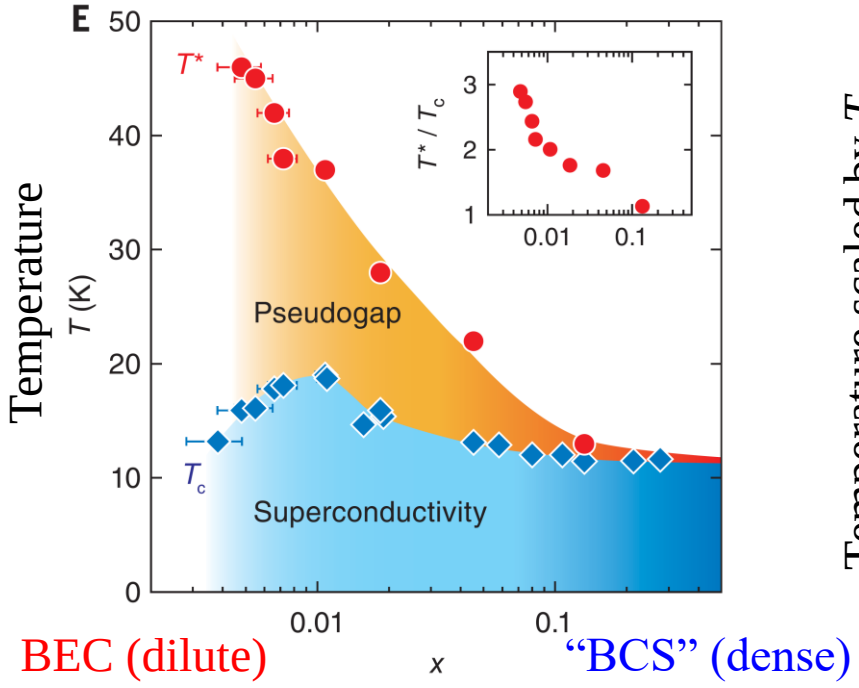

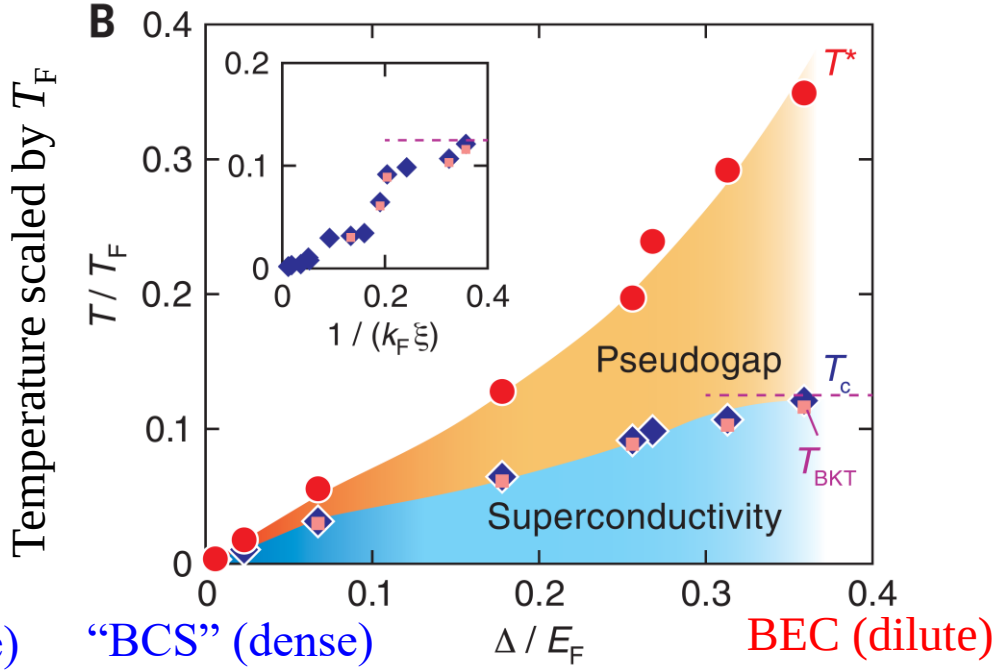

Y. Nakagawa, *et al.*, Science **372**, 6538 (2021).

Others: FeSe [PNAS **111**, 16309 (2014).], Organic SC [PRX **12**, 011016 (2022).], Excitons in bilayer graphene [Science **375**, 6577 (2022).], etc…

Trans-scale low-dimensionality

Pair sizes in 2D and 3D Fermi gases

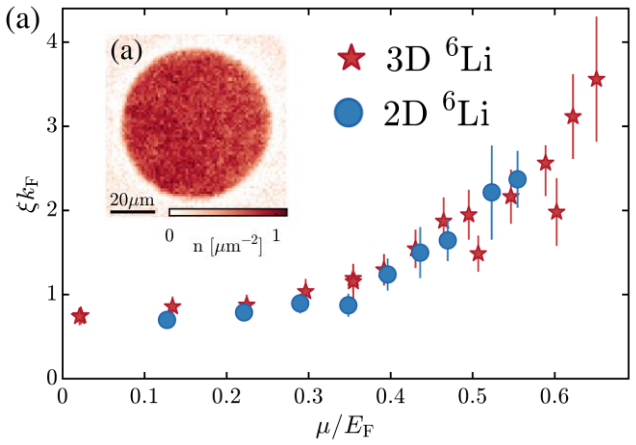

L. Sobirey, et al., PRL **129**, 083601 (2022)

Gate-controlled superconductor

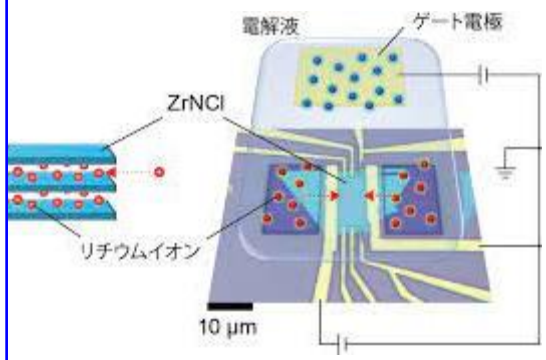

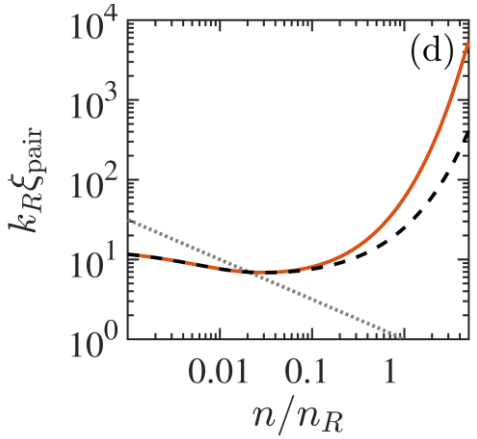

Y. Nakagawa, et al., Science **372**, 6538 (2021).

Shi, *et al*., EPL **139**, 36004 (2022).

Nuclear pasta in neutron star

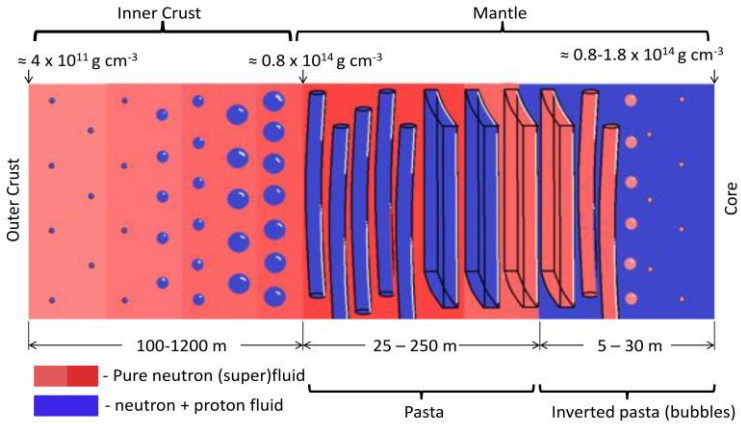

arXiv:1112.2018

Dineutron pair size in the slab phase

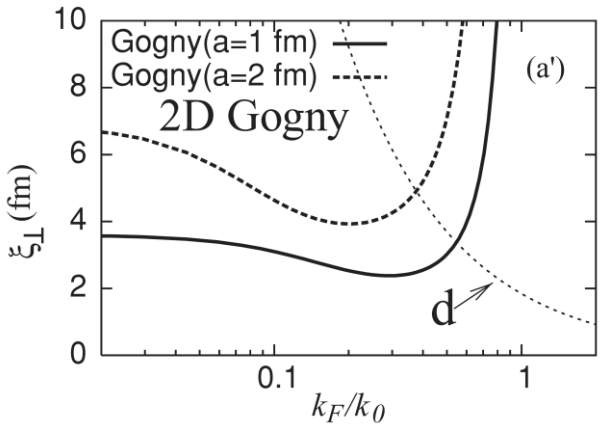

Y. Kanada-En'yo, et al., PRC **79**, 054305 (2009).

Outline

- Cold atoms and BCS-BEC crossover
- Strong pairing fluctuations
- Unitary Fermi gas and neutron matter
- Role of the multi-band configuration
- Beyond pairing effect
- Summary

BCS-BEC crossover in two-band superconductors/superfluids

Yb Fermi gas near orbital Feshbach resonance

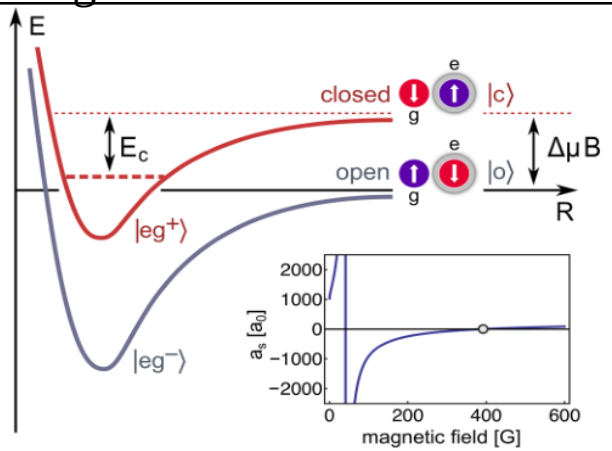

G. Pagano, et al., Phys. Rev. Lett. **115**,265301 (2015).

Missing pseudogap in two-band BCS-BEC crossover

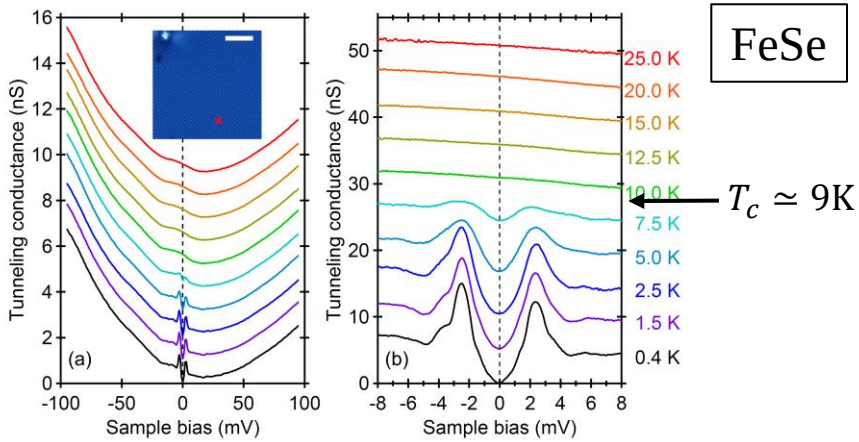

T. Hanaguri, *et al*., Phys. Rev. Lett. **122**, 077001 (2019).

Multiband effects?

- Coupled shallow and deep bands

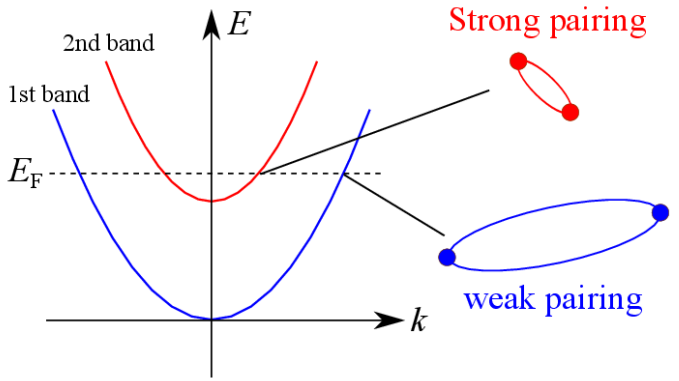

- Interband pair-exchange coupling

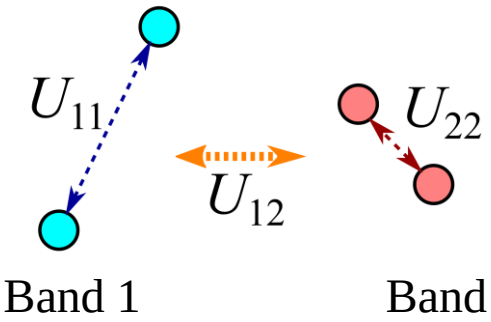

H. Suhl, et al., PRL **3**, 552 (1959).
J. Kondo, Prog. Theor. Phys. **29**, 1 (1963).

Two-band Hamiltonian

$$H = \sum_{\boldsymbol{k},\sigma,i} \xi_{\boldsymbol{k}\sigma i}\, c^{\dagger}_{\boldsymbol{k}\sigma i} c_{\boldsymbol{k}\sigma i} + \sum_{i,j} U_{ij} \sum_{\boldsymbol{k},\boldsymbol{k}',\boldsymbol{q}} c^{\dagger}_{\boldsymbol{k}+\boldsymbol{q}/2\uparrow i} c^{\dagger}_{-\boldsymbol{k}+\boldsymbol{q}/2\downarrow i} c_{-\boldsymbol{k}+\boldsymbol{q}/2\downarrow j} c_{\boldsymbol{k}+\boldsymbol{q}/2\uparrow j}$$

$c_{\boldsymbol{k}\sigma i}$: annihilation operator of a fermion

k: momentum

$\sigma = \uparrow, \downarrow$: spin

$i = 1,2$: band index

$$\xi_{\boldsymbol{k}\sigma i} = \frac{k^2}{2m_i} - \mu_i$$

μ_i: chemical potential m_i: mass $(m_1 = m_2)$

$\mu_2 = \mu_1 - E_{\mathrm{g}}$

E_{g}: Energy difference between two bands

U_{11}, U_{22}: intraband couplings

U_{12}, U_{21}: interband couplings

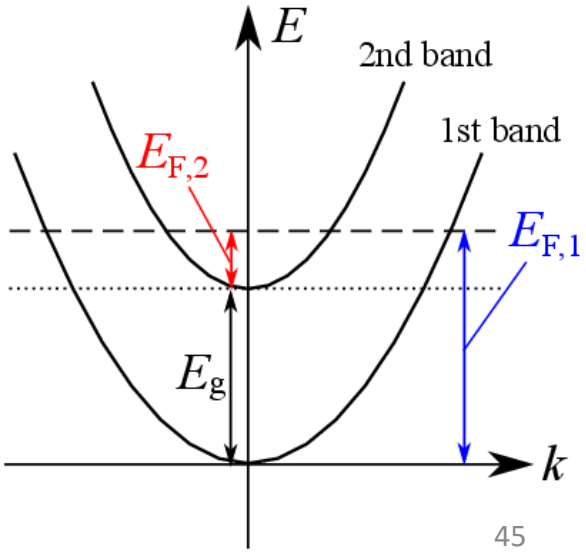

Enhanced critical temperature

HT, Y. Yerin, A. Perali, and P. Pieri, Phys. Rev. B **99**, 180503(R) (2019).

Interband pair-transfer mechanism leads to various nontrivial properties (e.g., enhancement of T_c, screened pair fluctuations, hidden pseudogap)

Many-body two-band T-matrix approximation

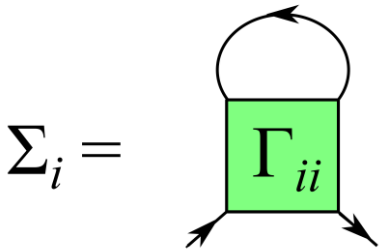

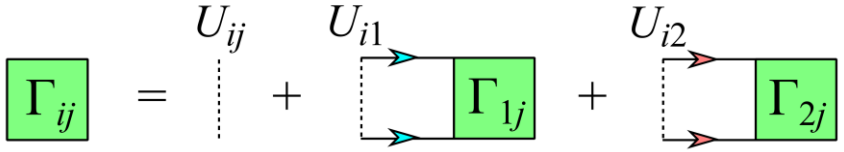

i, j: band index

U_{12}: interband pair scattering

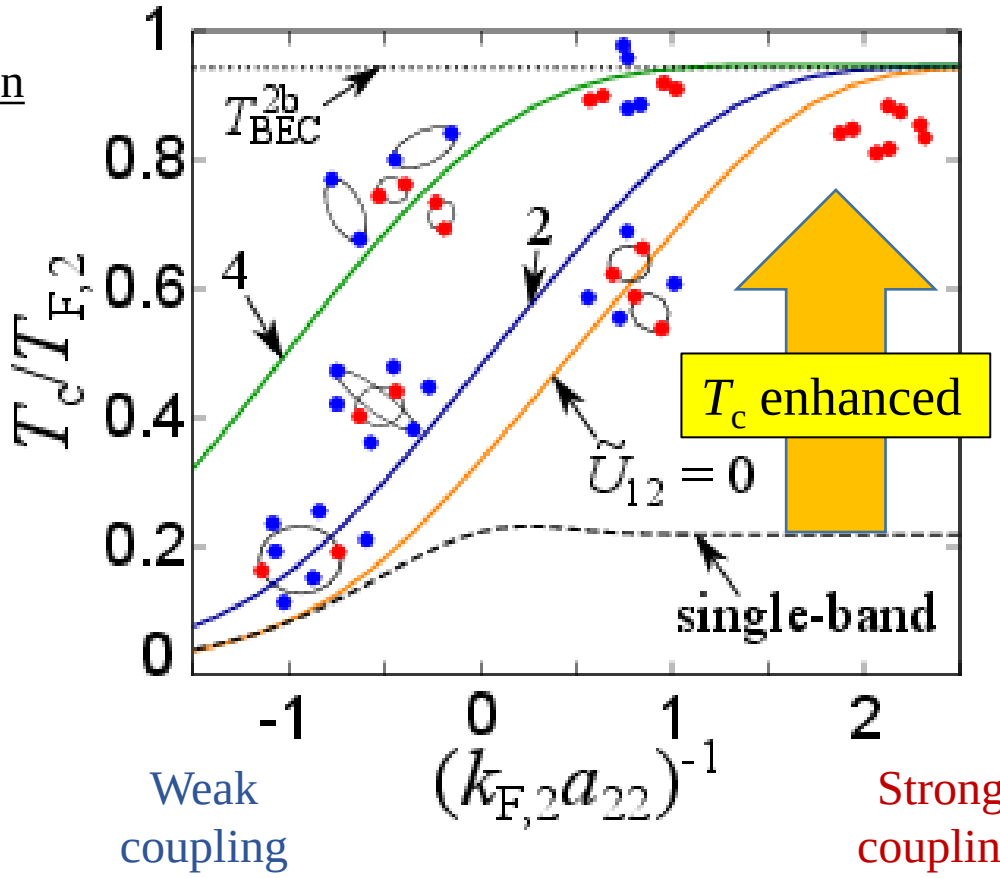

Interaction in the shallow band

Enhanced critical temperature

HT, Y. Yerin, A. Perali, and P. Pieri, Phys. Rev. B **99**, 180503(R) (2019).

Interband pair-transfer mechanism leads to various nontrivial properties (e.g., enhancement of T_c, screened pair fluctuations, hidden pseudogap)

Non-interacting case

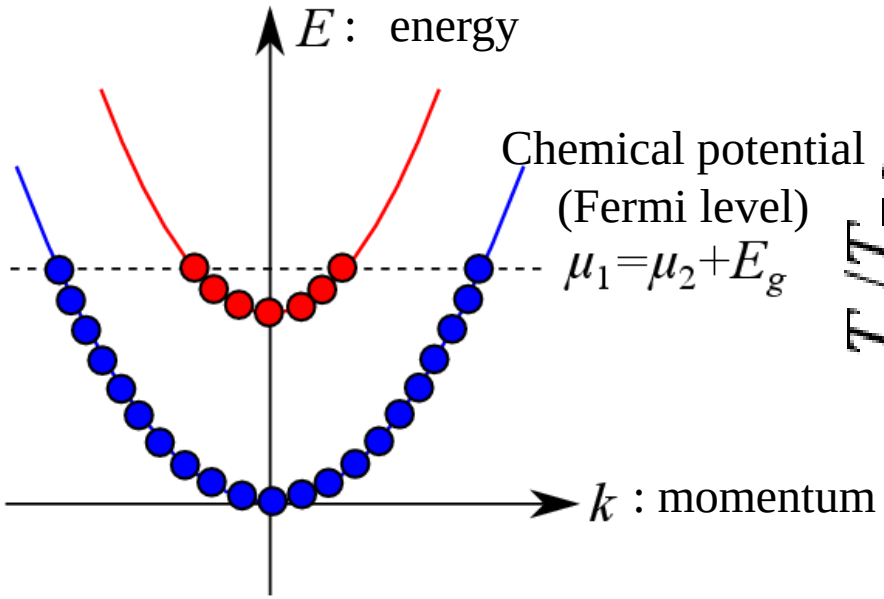

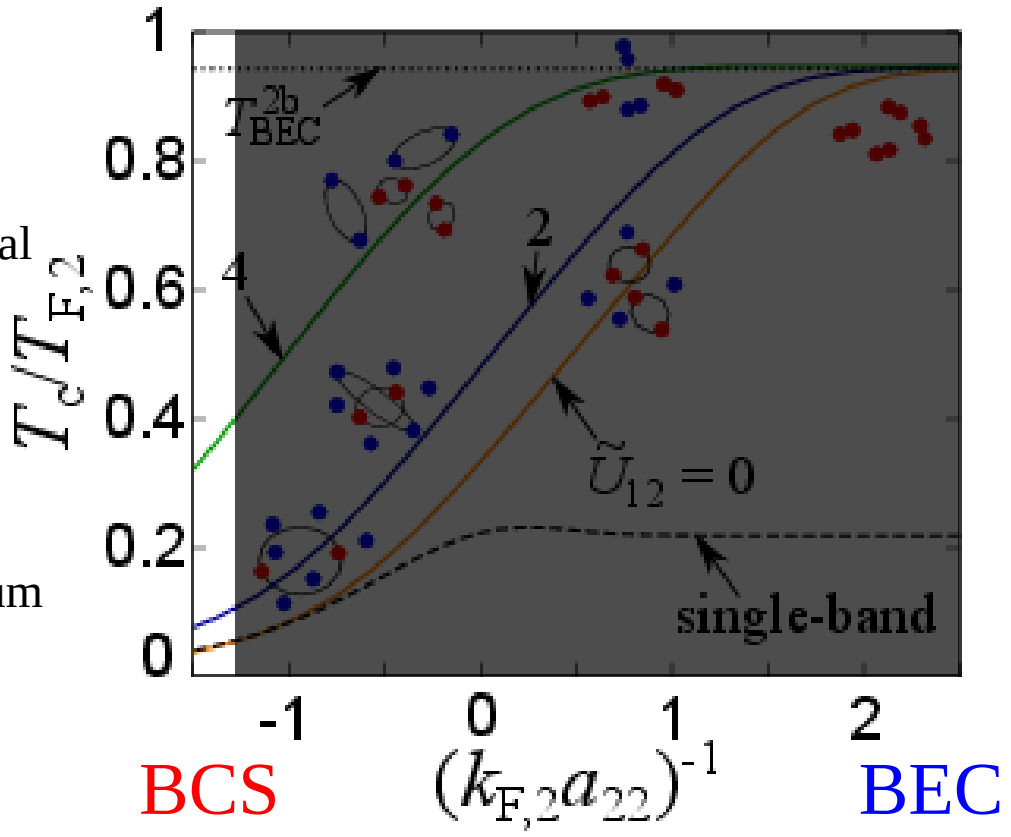

U_{12}: interband pair scattering

Interaction in the shallow band

Enhanced critical temperature

HT, Y. Yerin, A. Perali, and P. Pieri, Phys. Rev. B **99**, 180503(R) (2019).

Interband pair-transfer mechanism leads to various nontrivial properties (e.g., enhancement of T_c, screened pair fluctuations, hidden pseudogap)

Weakly-interacting shallow band

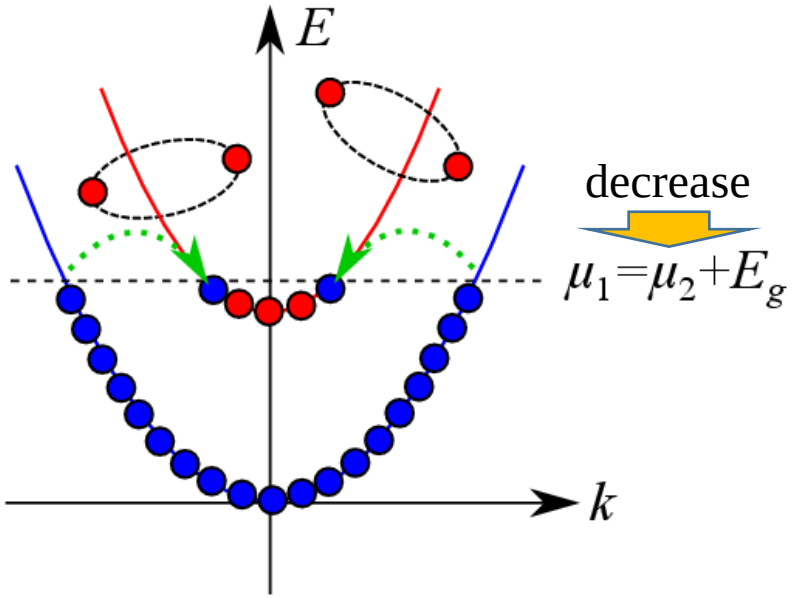

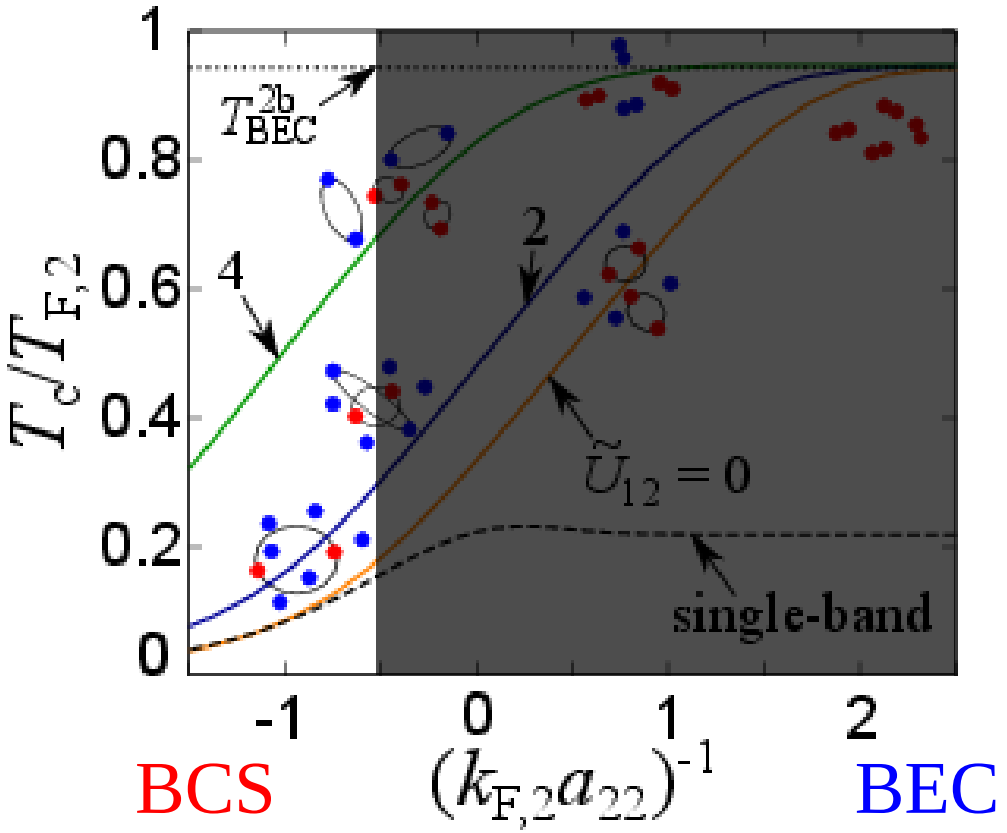

U_{12}: interband pair scattering

Interaction in the shallow band

Enhanced critical temperature

HT, Y. Yerin, A. Perali, and P. Pieri, Phys. Rev. B **99**, 180503(R) (2019).

Interband pair-transfer mechanism leads to various nontrivial properties (e.g., enhancement of T_c, screened pair fluctuations, hidden pseudogap)

Weakly-interacting shallow band

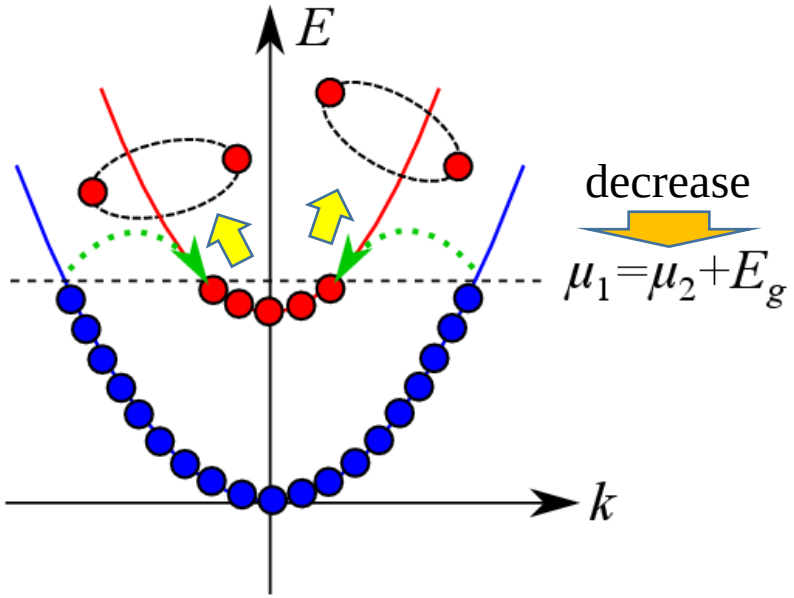

T_c enhanced!

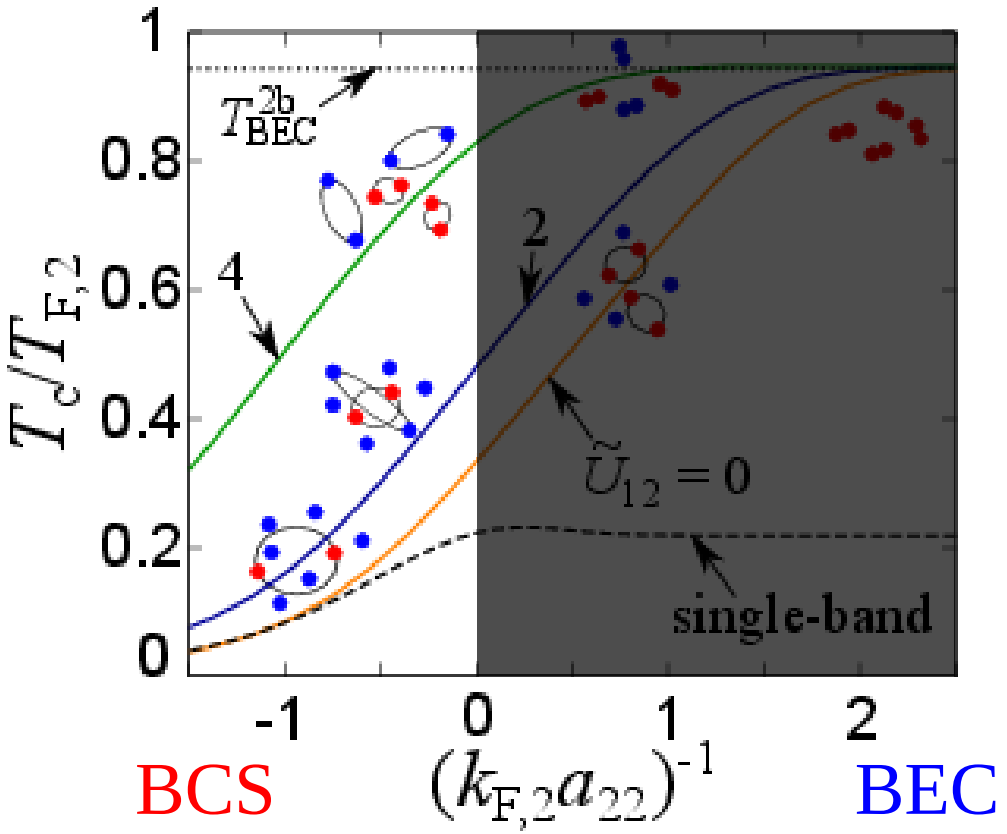

U_{12}: interband pair scattering

Interaction in the shallow band

Enhanced critical temperature

HT, Y. Yerin, A. Perali, and P. Pieri, Phys. Rev. B **99**, 180503(R) (2019).

Interband pair-transfer mechanism leads to various nontrivial properties (e.g., enhancement of T_c, screened pair fluctuations, hidden pseudogap)

Strongly-interacting shallow band

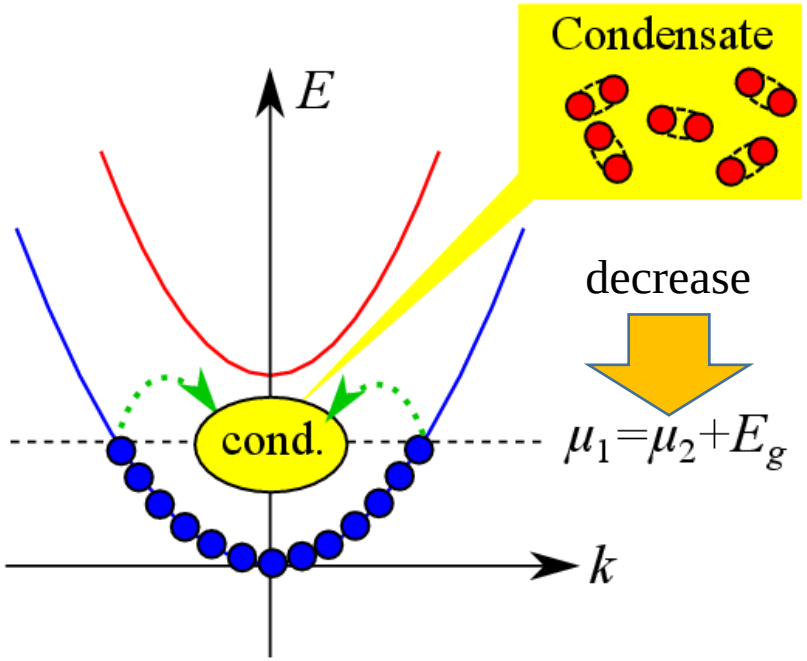

"Resonance"

PRR **4**, 013032 (2022).

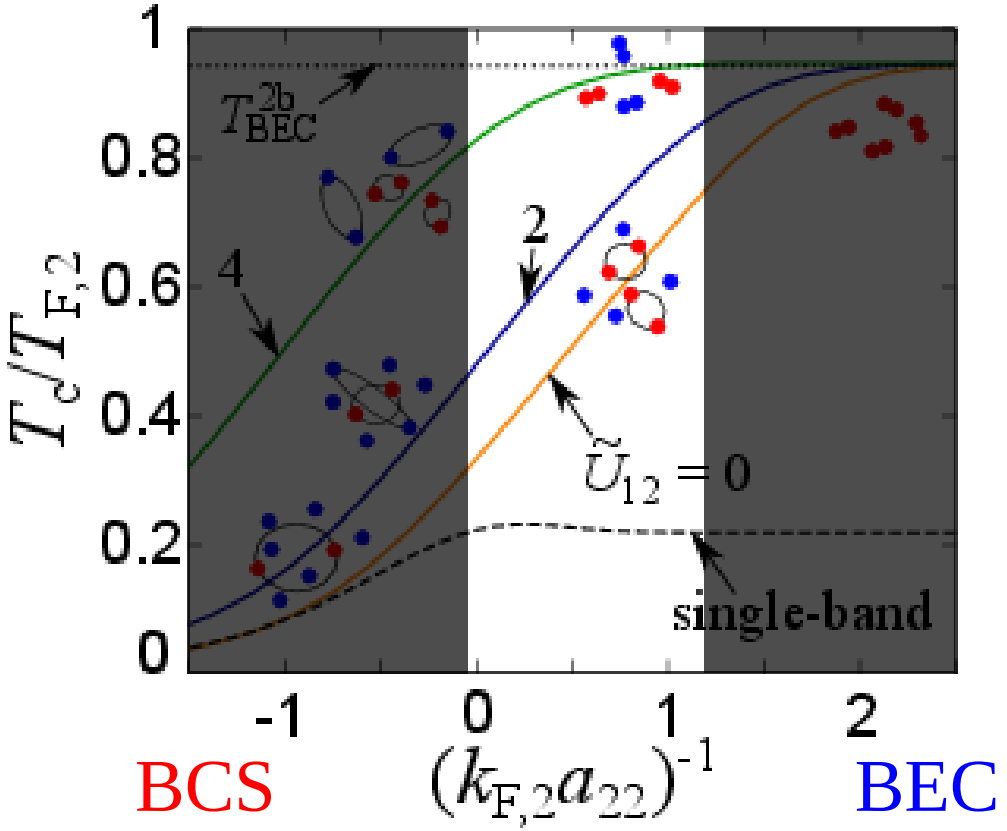

U_{12}: interband pair scattering

Interaction in the shallow band

Enhanced critical temperature

HT, Y. Yerin, A. Perali, and P. Pieri, Phys. Rev. B **99**, 180503(R) (2019).

Interband pair-transfer mechanism leads to various nontrivial properties (e.g., enhancement of T_c, screened pair fluctuations, hidden pseudogap)

Strongly-interacting shallow band

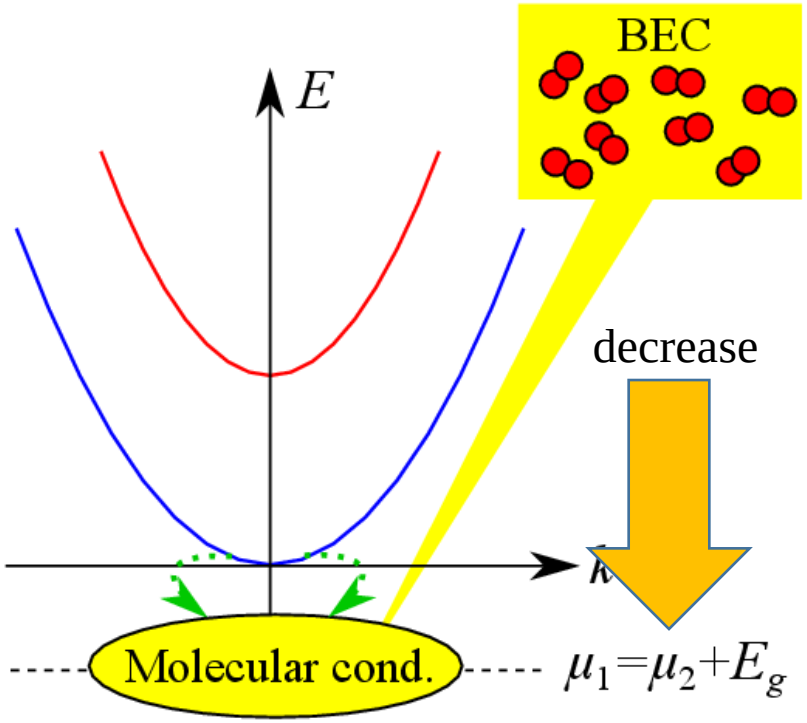

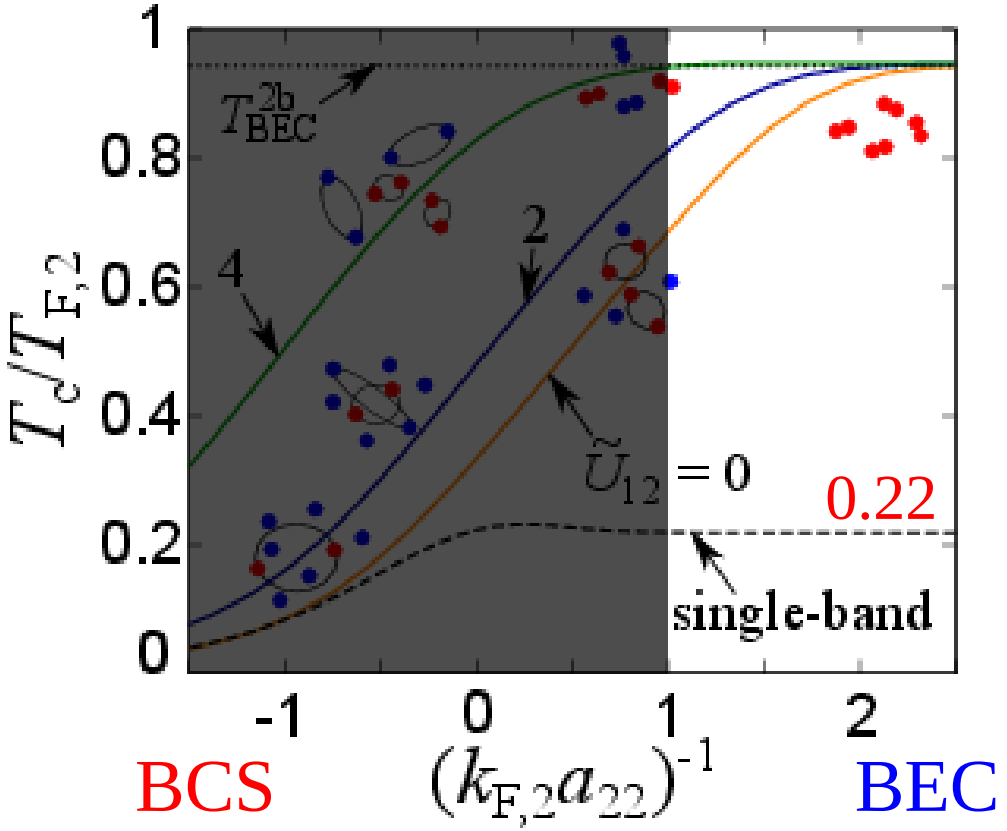

All particles (not only shallow but also deep bands) contribute to condensation in the BEC limit

Shrinking of the pseudogap regime

HT, Y. Yerin, P. Pieri, and A. Perali, Phys. Rev. B **102**, 220504(R) (2020).

Shrinking of the pseudogap regime can be understood as screened pairing fluctuations originating from interband particle transfer

Shrinking of the pseudogap regime

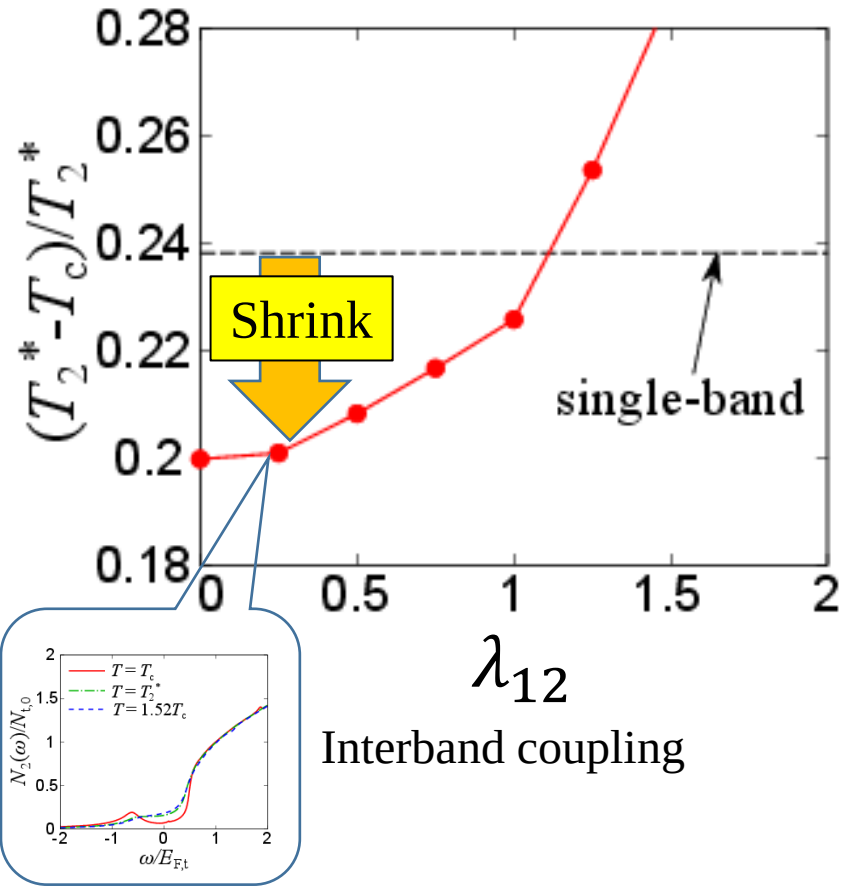

Interband coupling

Viewpoint of "particle transfer"

$$\frac{\delta N_{\mathrm{fluc}}}{N} > \frac{\delta N_{\mathrm{fluc},2}}{N_2}$$

"Single-band" "Two-band"

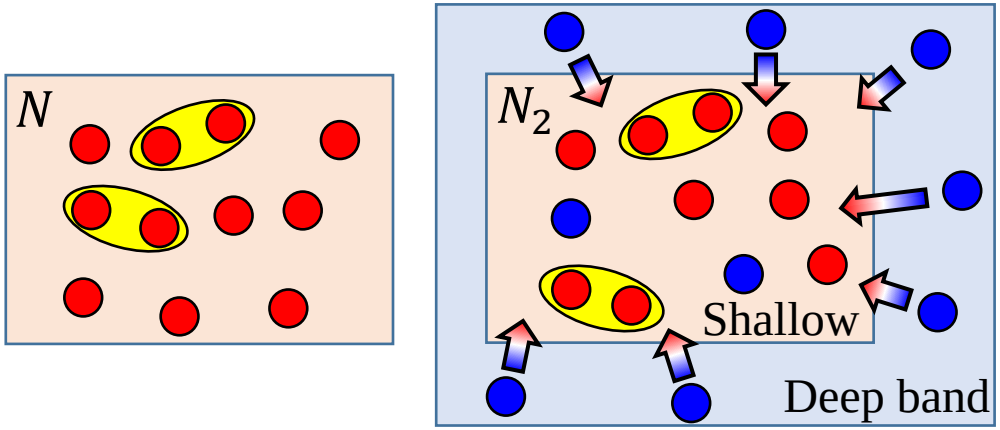

fluctuation contribution: $\delta N_{\mathrm{fluc},(2)}$

System with particle number $N_{(2)}$

Enhanced pairing near the incipient band

K. Ochi, HT, K. Iida, and H. Aoki, Phys. Rev. Research **4**, 013032 (2022).

Two-band SC with incipient heavy band

Band 1 (dispersive)
Band 2 (incipient heavy)

Two-channel (Feshbach resonance)

Open channel
Closed channel

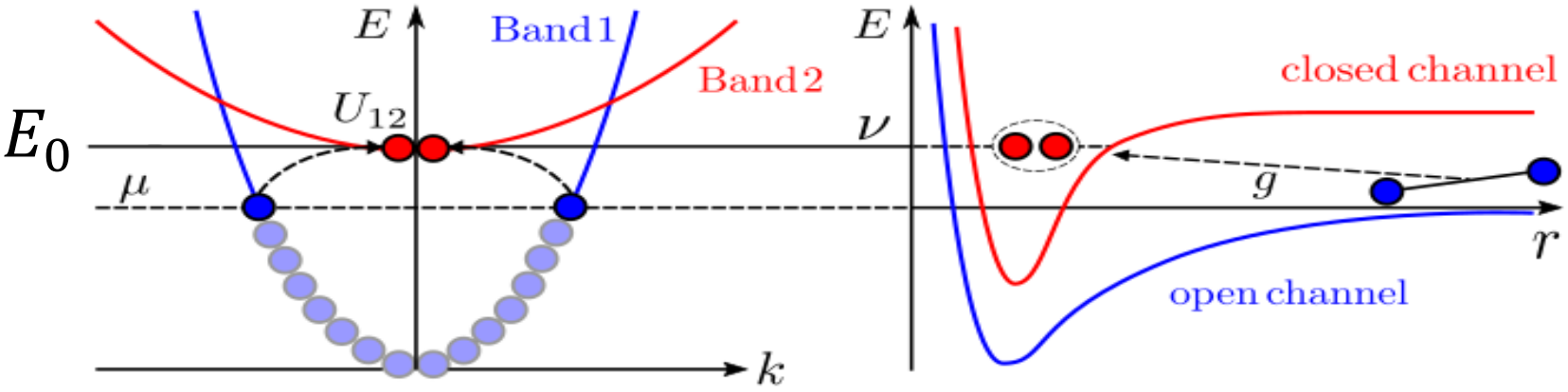

Effective interaction

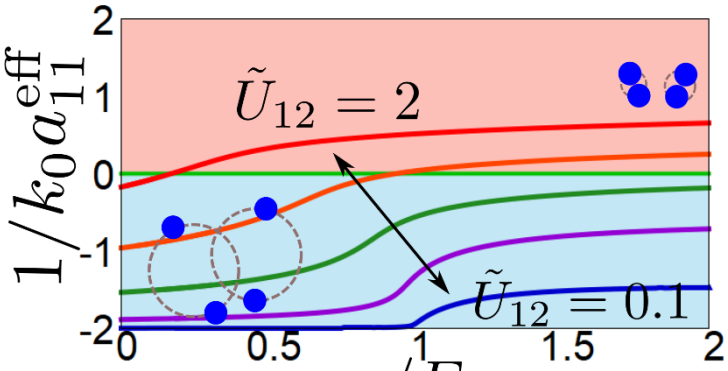

Strong coupling (BEC)

Unitarity limit

Weak coupling (BCS)

Hidden pseudogap

STM Differential conductance is associated with two DOSs

$$\frac{dI}{dV} = t_1^2 N_r N_1(\omega) + t_2^2 N_r N_2(\omega)$$

N_r: DOS in ref. sys.

t_i: Tunneling amplitude

Total density of states ($t_1 = t_2$, at $T = T_c$)

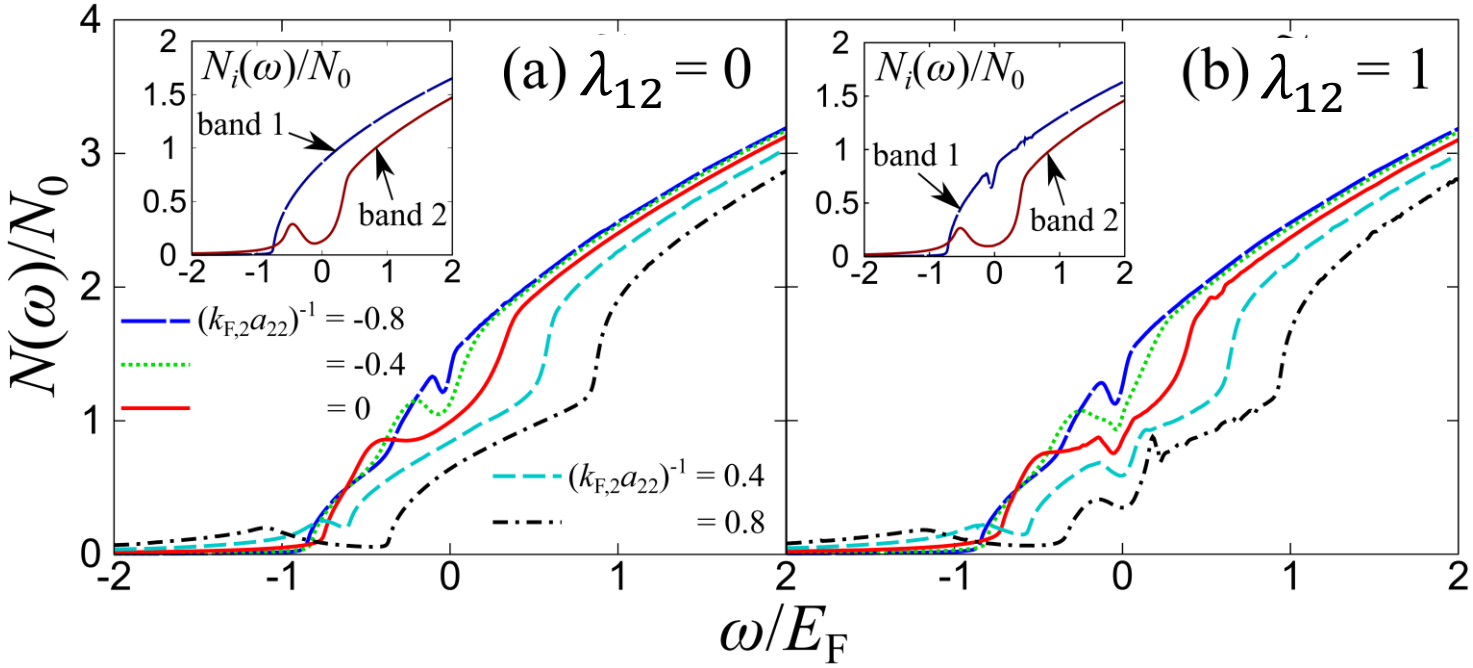

Masking of the pseudogap in the hot band becomes significant in the crossover regime

HT, P. Pieri, and A. Perali, Condensed Matter **6**, 8 (2021).

Outline

- Cold atoms and BCS-BEC crossover
- Strong pairing fluctuations
- Unitary Fermi gas and neutron matter
- Role of the multi-band configuration
- Beyond pairing effect
- Summary

Why pairs or dimers?

- The quantum cluster formation is related to the internal degrees of freedom and Pauli's exclusion principle

e.g. Spin-1/2 fermions with s-wave interaction

"attraction"

➡Cooper pair or dimer

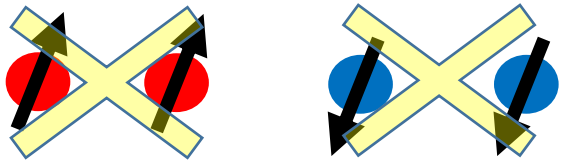

"Pauli's exclusion principle"

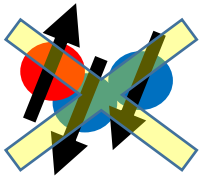

"Trimer"

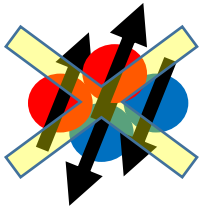

"Tetramer"

Why pairs or dimers?

- The quantum cluster formation is related to the internal degrees of freedom and Pauli's exclusion principle

e.g. Spin-1/2 fermions with s-wave interaction

"attraction"

➡Cooper pair or dimer

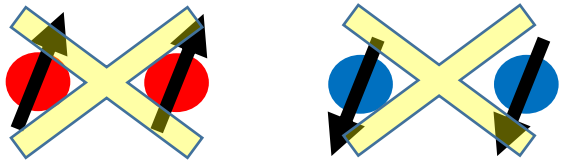

"Pauli's exclusion principle"

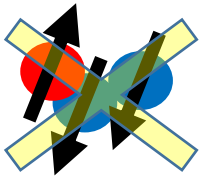

"Trimer"

Three-color fermions (e.g. quarks)

"Baryon"

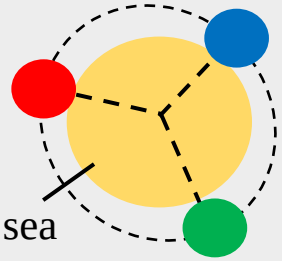

Fermi sea

"Cooper triple"

Three-body crossover?

- BCS-BEC crossover (from Cooper pairs to dimers)

Two-component Fermi gas

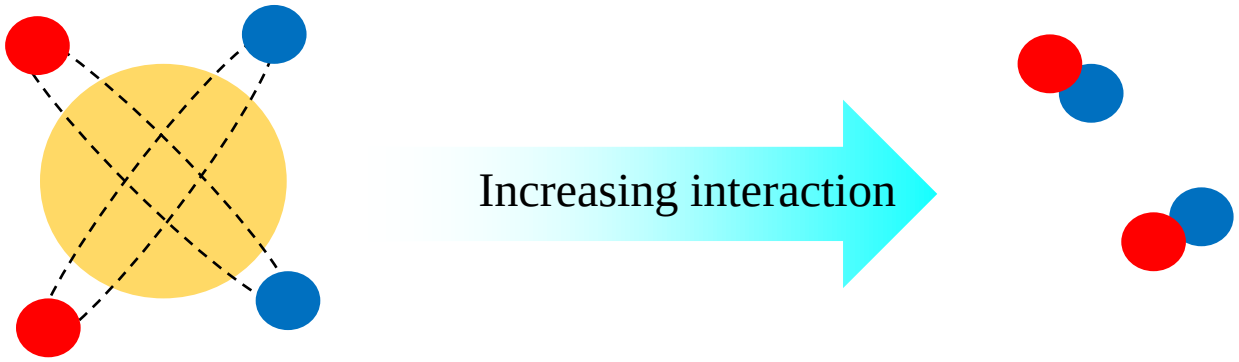

- Novel Crossover from Cooper triples to trimers

Three-component Fermi gas

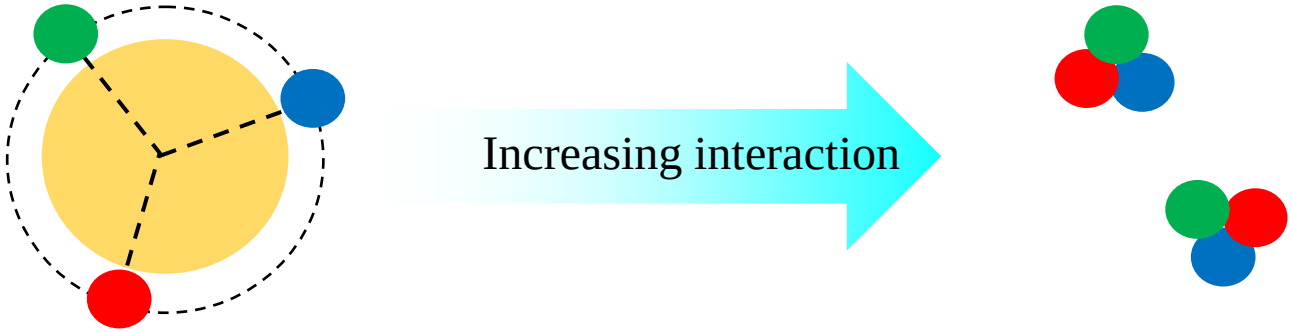

Density-induced multibody crossover

BEC-BCS crossover

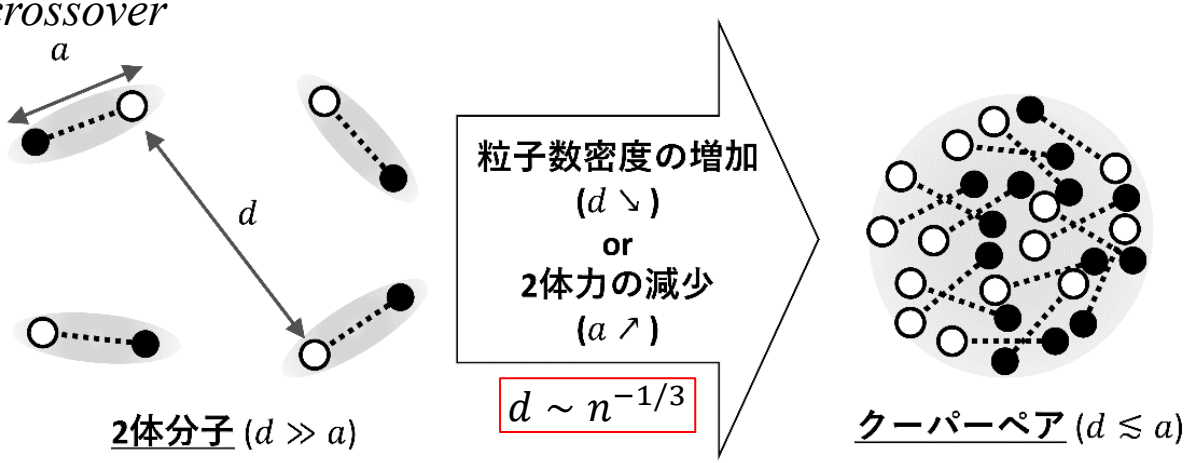

BT-CT crossover

d: 平均粒子間距離　a: 分子の大きさ

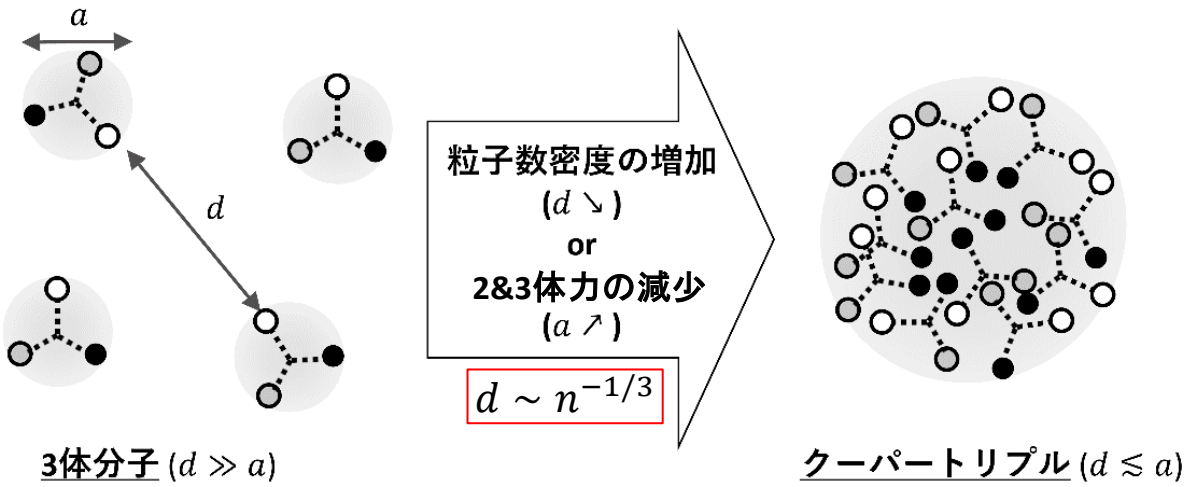

d: 平均粒子間距離　a: 分子の大きさ

飯田圭, 鷹野正利, 田島裕之, 岩波書店『科学』10月号 (2022).

Many-body physics in three-component fermions

Finte-density QCD phase diagram

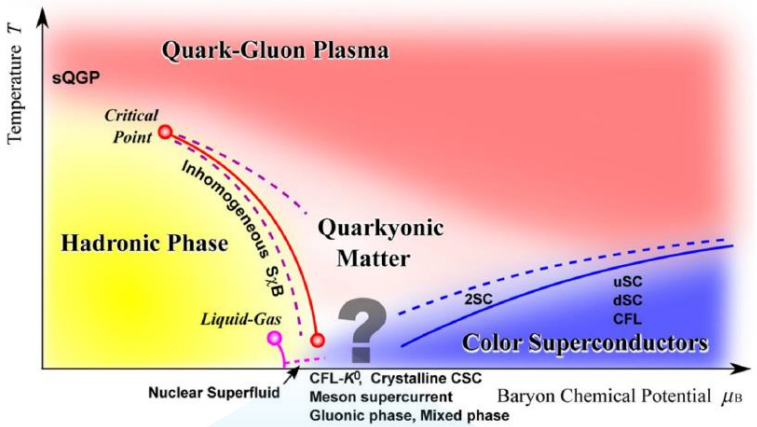

K. Fukushima and T. Hatsuda, Rept. Prog. Phys. **74**, 014001 (2011).

Quark-hadron continuity

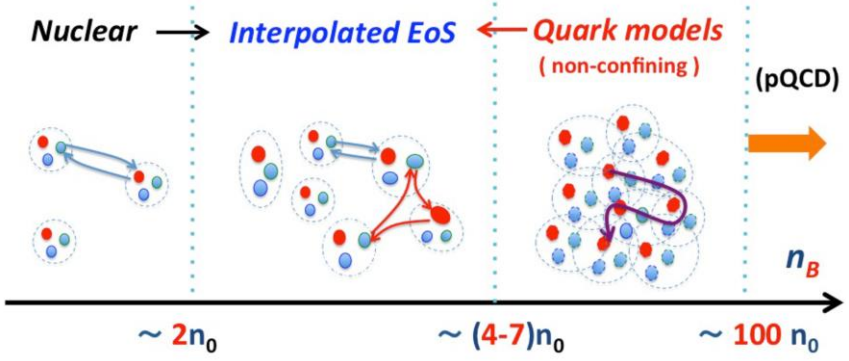

G. Baym, *et al.*, Rep. Prog. Phys. **81**, 056902 (2018).

Phase diagram in SU(3) Fermi gases

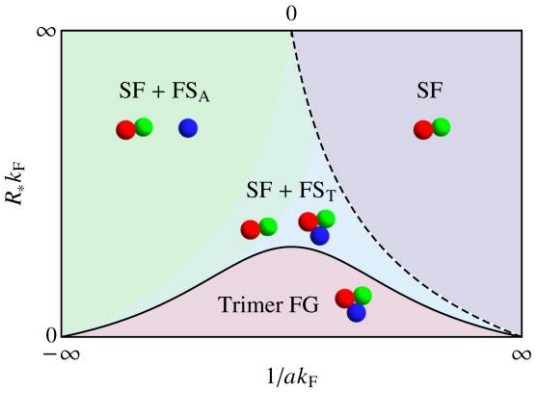

Y. Nishida, Phys. Rev. Lett. **109**, 240401 (2012).

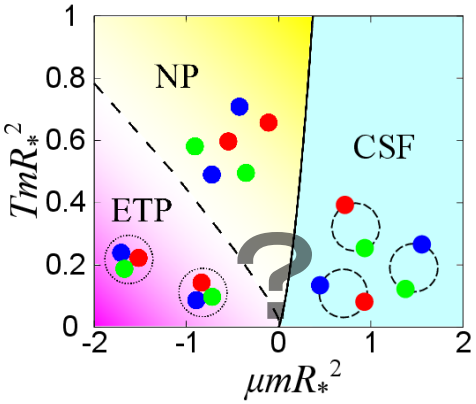

HT and P. Naidon, New J. Phys. **21**, 073051 (2019).

Trimer resonance (exp.)

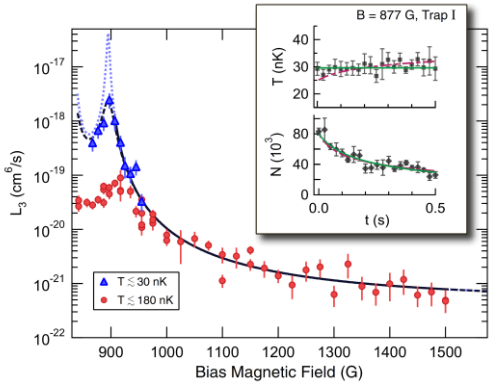

J. R. Williams, *et al.*, Phys. Rev. Lett. **103**, 130404 (2009).

EOS (1D worldline QMC)

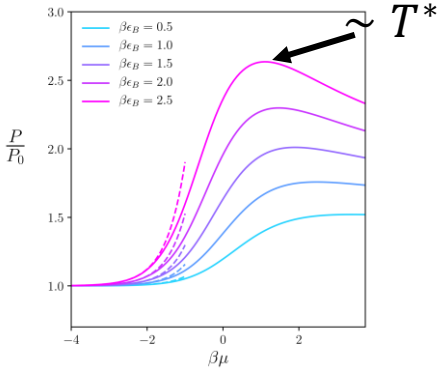

J. McKenny, *et al.*, Phys. Rev. A **102**, 023313 (2020).

Three-component Fermi gas

- Hamiltonian: $H = H_0 + V_2 + V_3$

One-body term

$$H_0 = \sum_{\boldsymbol{k},i} \xi_{\boldsymbol{k},i} c^\dagger_{\boldsymbol{k},i}\, c_{\boldsymbol{k},i}$$

$\xi_{\boldsymbol{k},i} = \frac{k^2}{2m_i} - \mu_i$: non-rela. kinetic energy

$i = \mathrm{r, g, b}$: pseudo-color (hyperfine states)

$c_{\boldsymbol{k},i}$, $c^\dagger_{\boldsymbol{k},i}$: fermionic annihilation/creation operator

Two-body interaction

$$V_2 = \sum_{i\neq j} \sum_{\boldsymbol{k},\boldsymbol{q},\boldsymbol{P}} g_{ij} c^\dagger_{\boldsymbol{k}+\frac{\boldsymbol{P}}{2},i} c^\dagger_{-\boldsymbol{k}+\frac{\boldsymbol{P}}{2},j} c_{-\boldsymbol{q}+\frac{\boldsymbol{P}}{2},j} c_{\boldsymbol{q}+\frac{\boldsymbol{P}}{2},i}$$

Three-body interaction

$$V_3 = U_{123} \sum_{\boldsymbol{k},\boldsymbol{q},\boldsymbol{k}',\boldsymbol{q}',\boldsymbol{P}} c^\dagger_{\frac{\boldsymbol{P}}{3}+\boldsymbol{k}-\frac{\boldsymbol{q}}{2},\mathrm{r}} c^\dagger_{\frac{\boldsymbol{P}}{\boldsymbol{3}}+\boldsymbol{q},\mathrm{g}} c^\dagger_{\frac{\boldsymbol{P}}{3}-\boldsymbol{k}-\frac{\boldsymbol{q}}{2},\mathrm{b}} c_{\frac{\boldsymbol{P}}{3}-\boldsymbol{k}'-\frac{\boldsymbol{q}'}{2},\mathrm{b}} c_{\frac{\boldsymbol{P}}{\boldsymbol{3}}+\boldsymbol{q}',\mathrm{g}} c_{\frac{\boldsymbol{P}}{3}+\boldsymbol{k}'-\frac{\boldsymbol{q}'}{2},\mathrm{r}}$$

Variational ansatz for Cooper pairs and triples

Variational equation: $\delta\langle\psi|E-H|\psi\rangle=0$

Cooper pair on the top of Fermi sea

$$|\Psi_{\mathrm{CP}}\rangle=\sum_{|\boldsymbol{p}|\geqslant k_{\mathrm{F}}}\Phi_{\boldsymbol{p}}\hat{B}^{\dagger}_{\boldsymbol{p}\gamma,-\boldsymbol{p}\gamma'}|\mathrm{FS}\rangle$$

$$\hat{B}^{\dagger}_{\boldsymbol{k}_1\gamma,\boldsymbol{k}_2\gamma'}=\hat{c}^{\dagger}_{\boldsymbol{k}_1,\gamma}\hat{c}^{\dagger}_{\boldsymbol{k}_2,\gamma'}$$

Cooper pair energy per atom measure from E_{F}

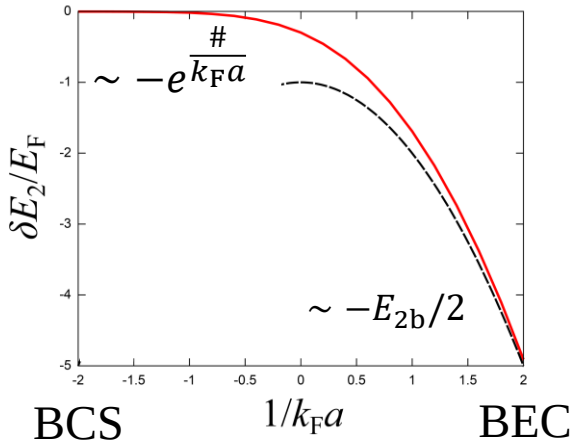

Cooper triple on the top of Fermi sea

$$|\Psi_{\mathrm{CT}}\rangle=\sum_{|\boldsymbol{k}_1|\geqslant k_{\mathrm{F}}}\sum_{|\boldsymbol{k}_2|\geqslant k_{\mathrm{F}}}\sum_{|\boldsymbol{k}_3|\geqslant k_{\mathrm{F}}}\mathcal{O}_{\boldsymbol{k}_1,\boldsymbol{k}_2,\boldsymbol{k}_3}\hat{C}^{\dagger}_{\boldsymbol{k}_1,\boldsymbol{k}_2,\boldsymbol{k}_3}\delta_{\boldsymbol{k}_1+\boldsymbol{k}_2+\boldsymbol{k}_3,\boldsymbol{0}}|\mathrm{FS}\rangle$$

$$\hat{C}^{\dagger}_{\boldsymbol{k}_1,\boldsymbol{k}_2,\boldsymbol{k}_3}=\frac{1}{6}\sum_{\gamma_1,\gamma_2,\gamma_3}\varepsilon_{\gamma_1\gamma_2\gamma_3}\hat{c}^{\dagger}_{\boldsymbol{k}_1,\gamma_1}\hat{c}^{\dagger}_{\boldsymbol{k}_2,\gamma_2}\hat{c}^{\dagger}_{\boldsymbol{k}_3,\gamma_3}$$

Reproducing usual three-body equation if we replace $|\mathrm{FS}\rangle$ with $|0\rangle$, or in the strong-coupling case where E_{F} is negligible.

Cooper pair and triple binding energies

Competition between pair (dashed line) and triple (solid line) formations

Large binding

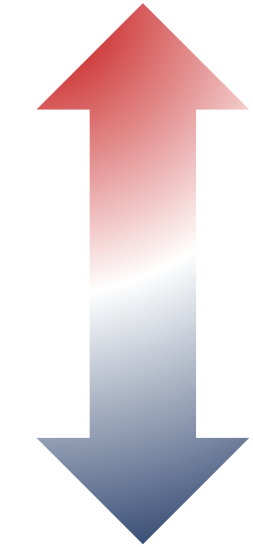

Small binding

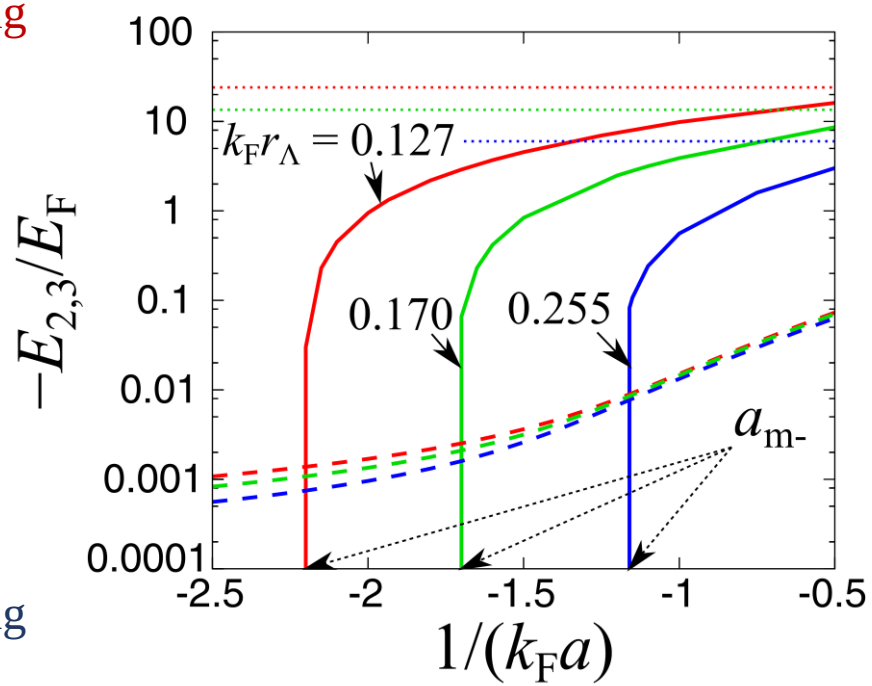

Weak-coupling ⟵ ⟶ Strong-coupling

$* \; g_{12} = g_{23} = g_{31}, U_{123} = 0$ $\quad r_\Lambda = \frac{4}{\pi\Lambda}$: range parameter $\quad \Lambda$: momentum cutoff

Cooper pair and triple binding energies

Competition between pair (dashed line) and triple (solid line) formations

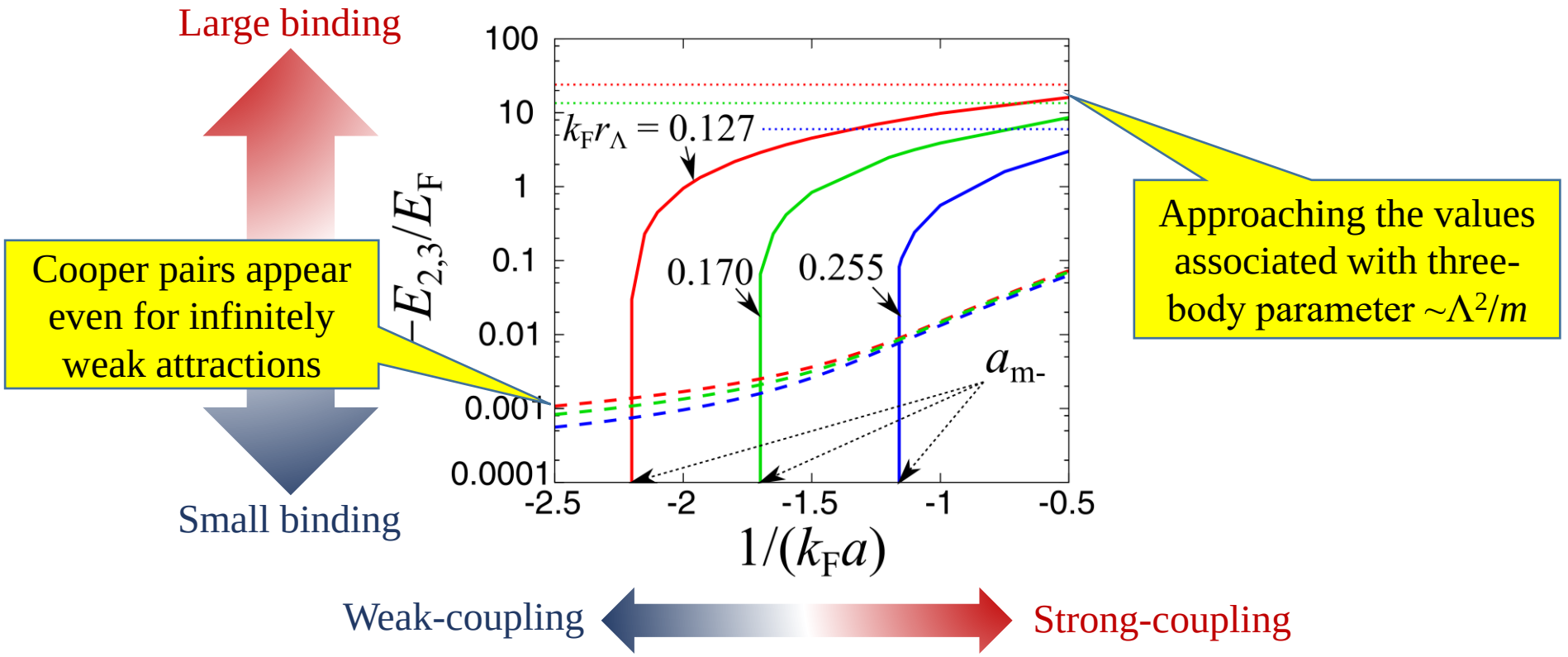

$* \; g_{12} = g_{23} = g_{31}, U_{123} = 0$ $\quad r_\Lambda = \frac{4}{\pi\Lambda}$: range parameter $\quad \Lambda$: momentum cutoff

Crossover from Cooper triples to bound trimer near a triatomic resonance

HT, S. Tsutsui, T. M. Doi, and K. Iida, Phys. Rev. A **104**, 053328 (2021).

- The CT-BT crossover occurs with increasing the pairing interaction near the triatomic resonance ($a = a_-$) where bound trimers start to appear in vacuum.
- Cooper triples can be detected by the medium shift of triatomic resonance ($a_- \to a_{\mathrm{m}-}$).

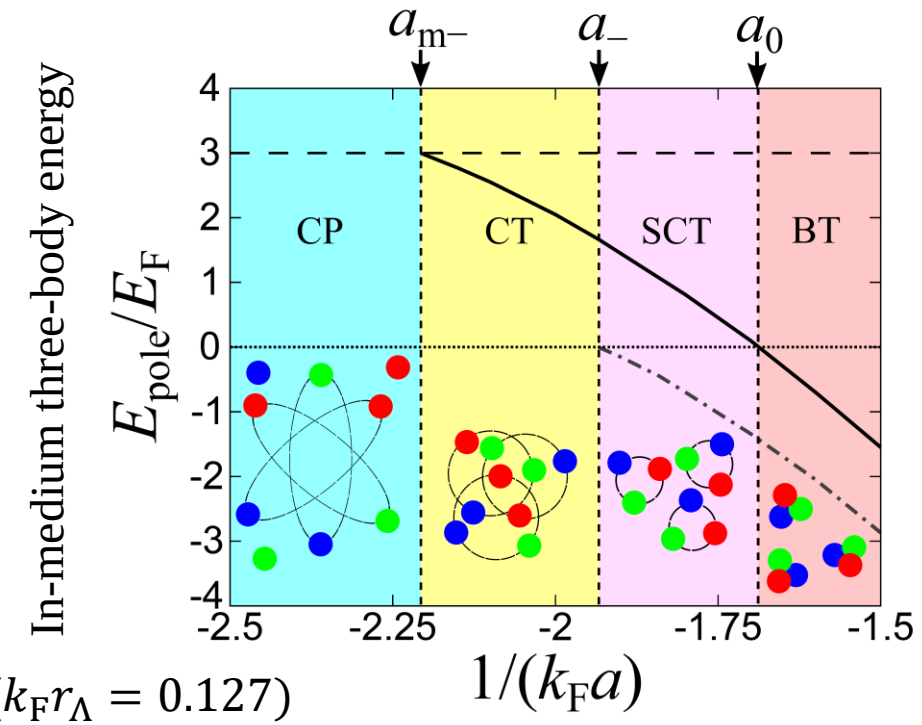

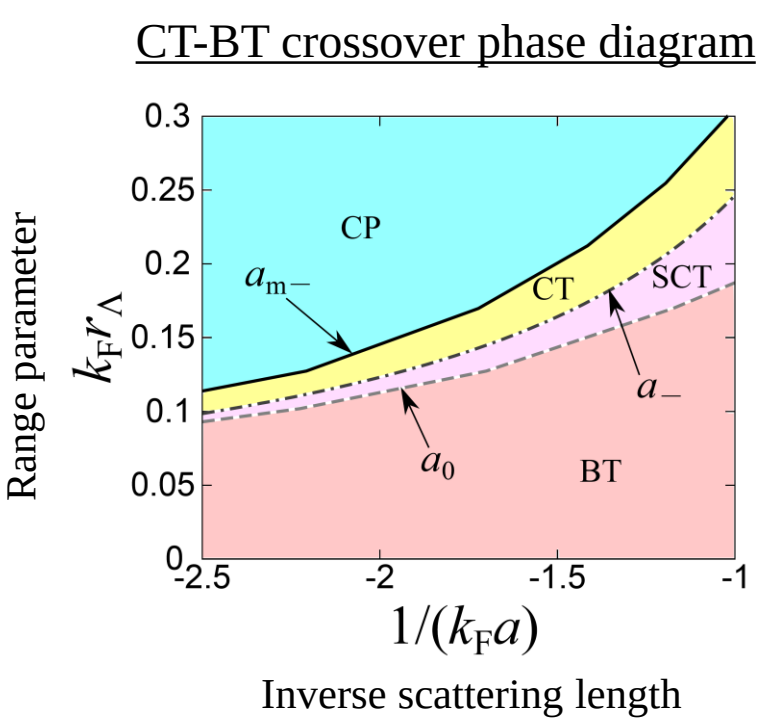

CP: Cooper pair, CT: Cooper triple, SCT: Squeezed Cooper triple, BT: Bound trimer

Three-body decay rate

HT, S. Tsutsui, T. M. Doi, and K. Iida, Phys. Rev. A **104**, 053328 (2021).

Imaginary three-body term for three-body loss

$$W = -i\gamma \sum_{k,k',p,p',q} c^{\dagger}_{k,1} c^{\dagger}_{p,2} c^{\dagger}_{q-k-p,3} c_{q-k'-p',3} c_{p',2} c_{k',1}$$

T. Kirk and M. Parish, Phys. Rev. A **96**, 053614 (2017).

Three-body decay rate

$$\Gamma = 2i\langle \Psi_{\mathrm{CT}} | W | \Psi_{\mathrm{CT}} \rangle$$

$$\rightarrow \langle \Psi(t) | \Psi(t) \rangle \propto e^{-\Gamma t}$$

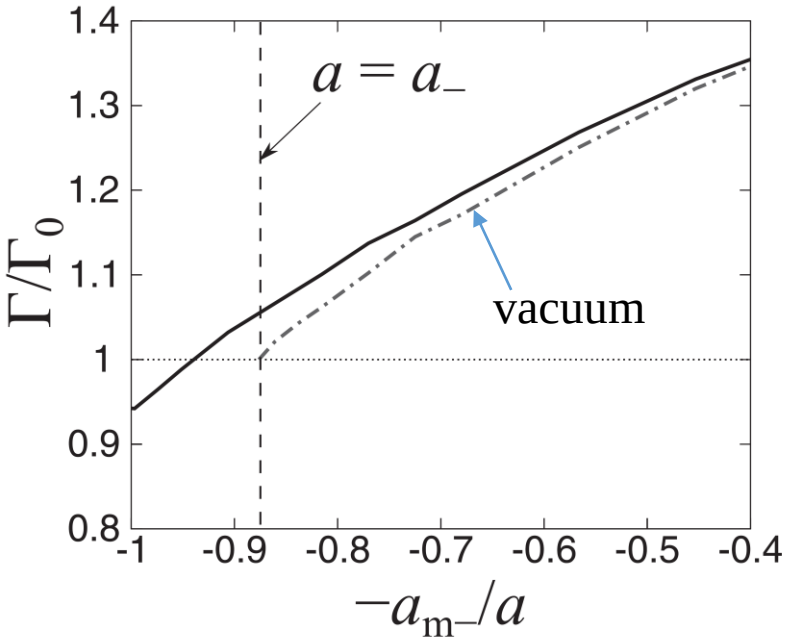

Trimer resonance in ^{6}Li 3-com. Fermi gas (exp.)

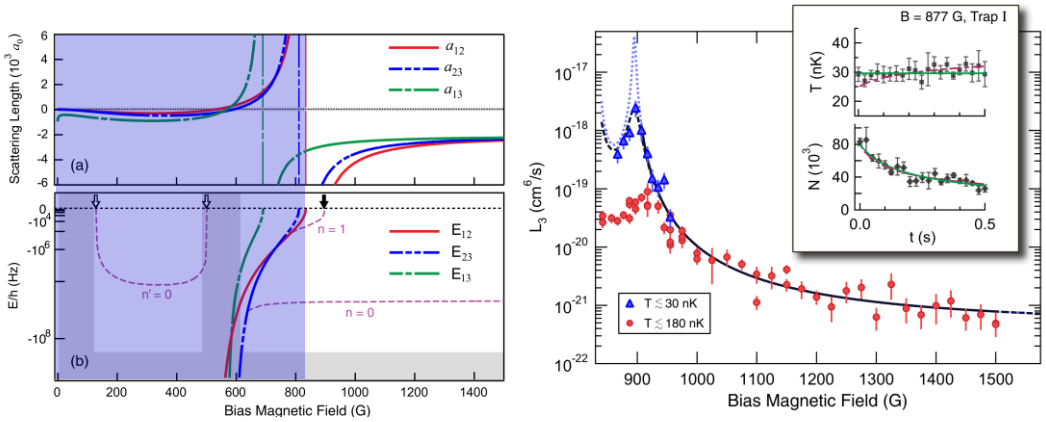

J. R. Williams, *et al*., Phys. Rev. Lett. **103**, 130404 (2009).

Three-body decay rate

HT, S. Tsutsui, T. M. Doi, and K. Iida, Phys. Rev. A **104**, 053328 (2021).

Imaginary three-body term for three-body loss

$$W = -i\gamma \sum_{k,k',p,p',q} c^{\dagger}_{k,1} c^{\dagger}_{p,2} c^{\dagger}_{q-k-p,3} c_{q-k'-p',3} c_{p',2} c_{k',1}$$

T. Kirk and M. Parish, Phys. Rev. A **96**, 053614 (2017).

Three-body decay rate

$$\Gamma = 2i\langle \Psi_{\mathrm{CT}} | W | \Psi_{\mathrm{CT}} \rangle$$

$$\rightarrow \langle \Psi(t) | \Psi(t) \rangle \propto e^{-\Gamma t}$$

Trimer resonance in ^{6}Li 3-com. Fermi gas (exp.)

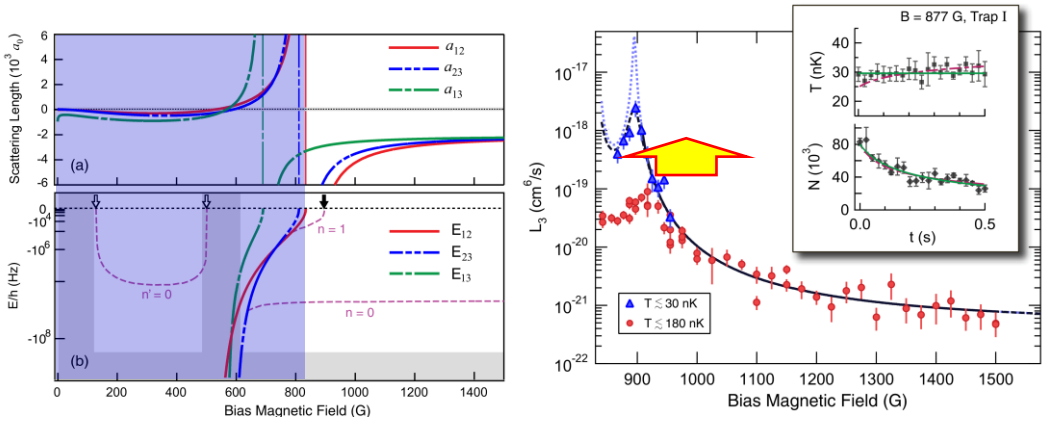

J. R. Williams, *et al*., Phys. Rev. Lett. **103**, 130404 (2009).

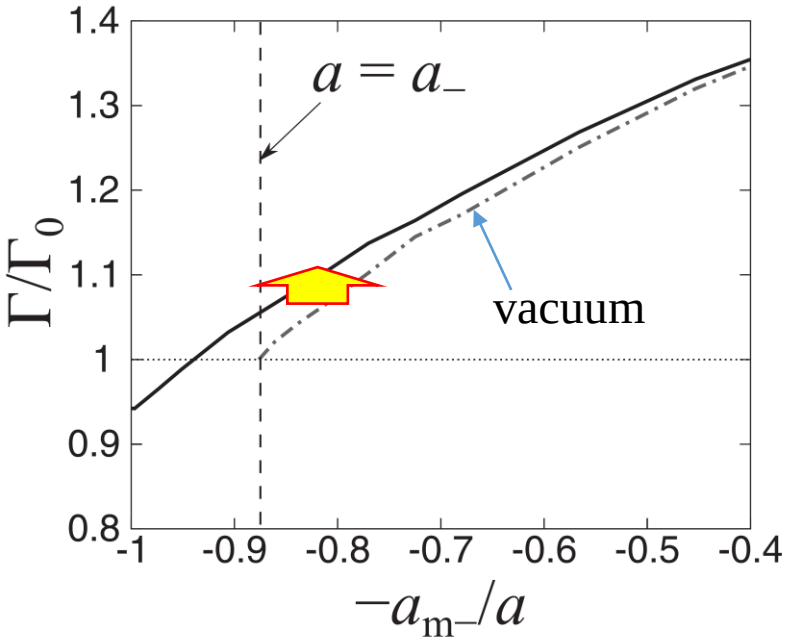

Implication for finite-density QCD

We consider a one-dimensional three-component Fermi gas where the three-body interaction is geometrically enhanced.

Similarities with dense QCD: Three colors, asymptotic freedom, sound-velocity peak

QCD matter

Three-quark interaction (flux dist.)

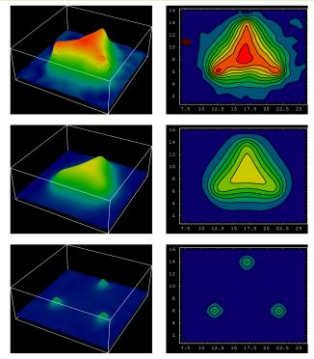

Nucl. Phys. B **119**, 751 (2003).

Sound velocity in quarkyonic matter

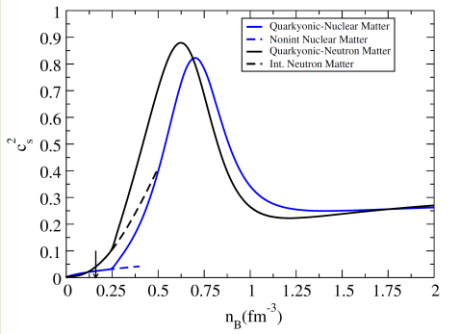

Phys. Rev. Lett. **122**, 122701 (2019).

Atomic system in this study

Scaling anomaly and asymptotic freedom

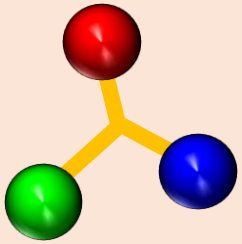

$$\frac{\partial U_{123}}{\partial \ln \Lambda} = \frac{m}{\sqrt{3\pi}} U_{123}^2$$

"Running 3body coupling"

Phys. Rev. Lett. **120**, 243002 (2018).

Compressibility (Quantum Monte Carlo)

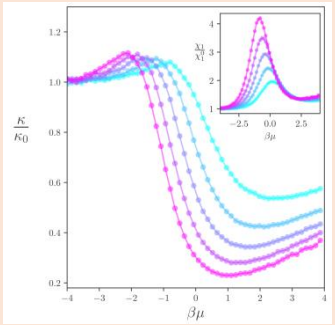

$$mc_s^2 = \frac{1}{\rho\kappa}$$

Phys. Rev. A **102**, 023313 (2020).

Three-body T-matrix in 1D

T_3 = 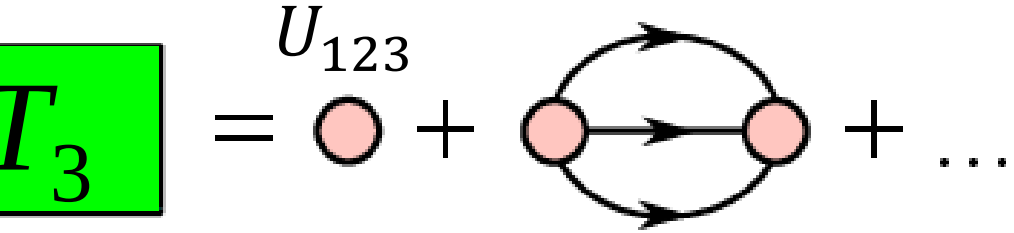

+ …

$$T_3(P,\Omega_+) = \left[\frac{1}{U_{123}} - \Xi_0(P,\Omega_+)\right]^{-1}$$

Ξ_0: Three-body propagator in vacuum

$$\Xi_0(P,\Omega_+) = \sum_{k,q} \frac{1}{\Omega_+ - \varepsilon_{\frac{P}{3}+k-\frac{q}{2}} - \varepsilon_{\frac{P}{3}+q} - \varepsilon_{\frac{P}{3}-k-\frac{q}{2}}} = -\frac{m}{2\sqrt{3}\pi}\ln\left(\frac{\Lambda^2 + P^2/6 - m\Omega_+}{P^2/6 - m\Omega_+}\right)$$

Λ: cutoff

Three-body binding energy (Scale anomaly)

$$\frac{1}{U_{123}} - \Xi_0(0,\Omega = -E_{\mathrm{B}}) = 0 \quad \Rightarrow \quad E_{\mathrm{B}} = \frac{\Lambda^2}{m}\exp\left(\frac{2\sqrt{3}\pi}{mU_{123}}\right)$$

In-medium three-body T-matrix

HT, S. Tsutsui, T. M. Doi, and K. Iida, Phys. Rev. Research **4**, L012021 (2022).

$T_3^{\mathrm{MB}} =$ 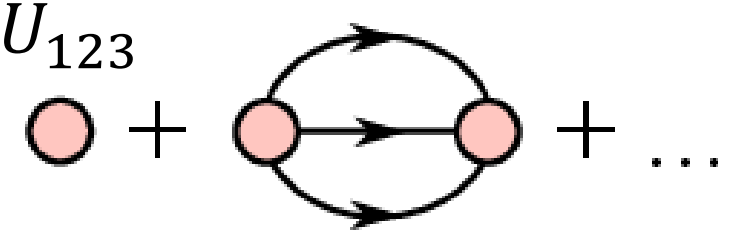 $+ \cdots$

$$T_3^{\mathrm{MB}}(P,\Omega_+) = \left[\frac{1}{U_{123}} - \Xi_{\mathrm{MB}}(P,\Omega_+)\right]^{-1}$$

Ξ_{MB}: In-medium three-particle (three-hole) propagator

$$\Xi_0(P,\Omega_+) = \sum_{k,q} \frac{F(k,q,P)}{\Omega_+ - \xi_{\frac{P}{3}+k-\frac{q}{2}} - \xi_{\frac{P}{3}+q} - \xi_{\frac{P}{3}-k-\frac{q}{2}}}$$

$F(k,q,P)$: Pauli-block operator

In-medium three-body equation

$$\frac{1}{U_{123}} - \Xi_{\mathrm{MB}}\left(P=0,\Omega_+ = -3\mu - E_{\mathrm{B}}^{\mathrm{M}}\right) = 0$$

Three-body spectral function

HT, S. Tsutsui, T. M. Doi, and K. Iida, Phys. Rev. Research **4**, L012021 (2022).

- Three-body binding is suppressed by medium corrections regardless of the scale anomaly.
- The three-body pole survives even at high density, indicating the presence of Cooper triples.

In-medium three-body spectral function

$$A_3(P,\Omega) = -\mathrm{Im}T_3^{\mathrm{MB}}(P,\Omega_+)$$

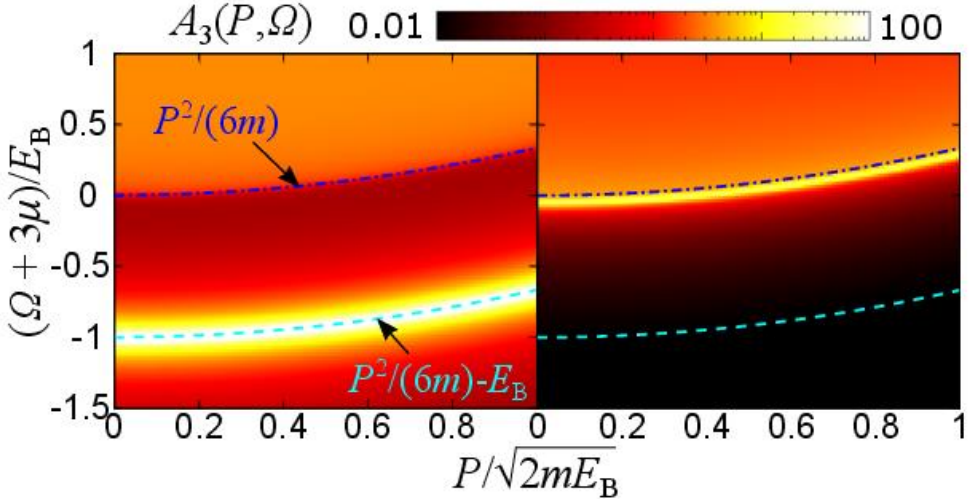

Low density
$(\mu/E_B = -1)$

High density
$(\mu/E_B = 2)$

In-medium three-body binding energy

Three-body problem

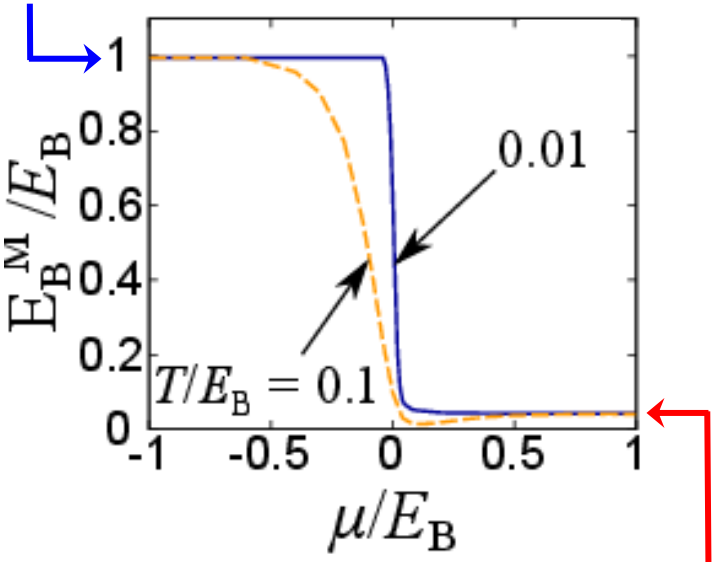

$E_B^M/E_B \simeq 0.04$

Grand-canonical phase diagram and implication for hadron-quark crossover

HT, S. Tsutsui, T. M. Doi, and K. Iida, Phys. Rev. Research **4**, L012021 (2022).

We found that the sound-velocity peak can be obtained near the region where Cooper triples start to appear from the comparison with QMC results.

Grand-canonical phase diagram

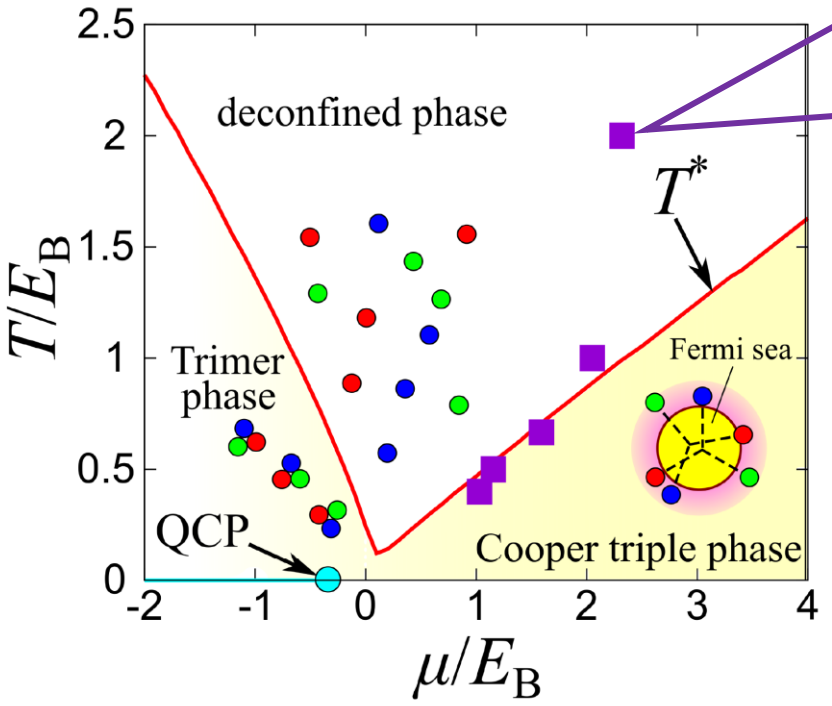

Method: diagrammatic approach

Compressibility minimum in QMC

$$mc_s^2 = \frac{1}{\rho\kappa}$$

c_s: sound velocity
κ: compressiblity

J. McKenny, *et al.*, Phys. Rev. A **102**, 023313 (2020).

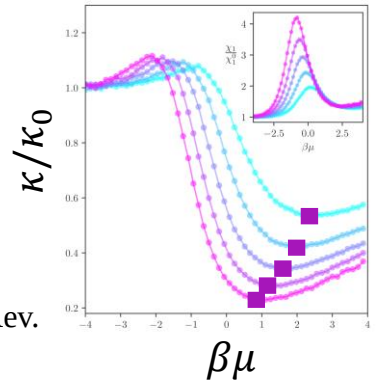

Cooper triple and quarkyonic matter*

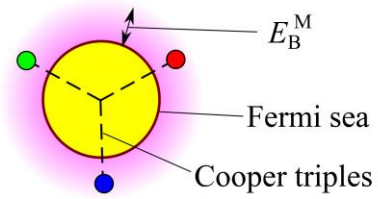

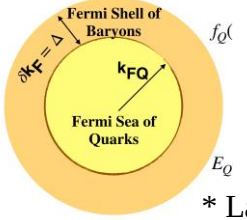

$\mu \gg E_B \gg E_B^M$

* Large N_c-limit

Phys. Rev. Lett. **122**, 122701 (2019).

Compressibility minimum across Cooper triple formation

HT, S. Tsutsui, T. M. Doi, and K. Iida, Phys. Rev. Research **4**, L012021 (2022).

Why does the sound velocity (compressibility) take maximum (minimum) near T^*?

➡ Rapid decrease of in-medium three-body binding energy E_B^M and development of Fermi sea

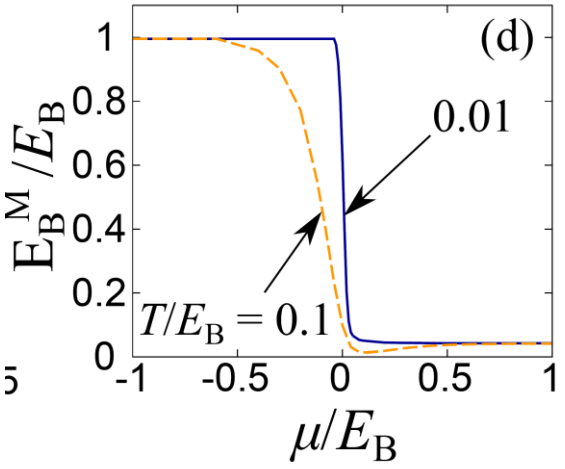

Mclerran-Reddy-like model

$$\frac{\kappa}{\kappa_0} = 1 + \sqrt{\frac{\mu}{3\mu + E_B^M}}\left(3 + \frac{\partial E_B^M}{\partial \mu}\right)$$

$$\kappa_{3D} = \frac{3(2m)^{\frac{3}{2}}}{4\pi^2\rho^2}\left[\sqrt{\mu} + \sqrt{3\mu + E_B^M}\left(3 + \frac{\partial E_B^M}{\partial \mu}\right)\right]$$

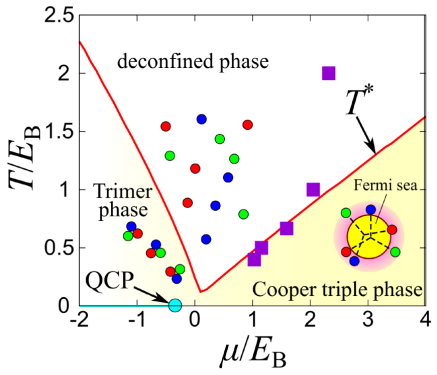

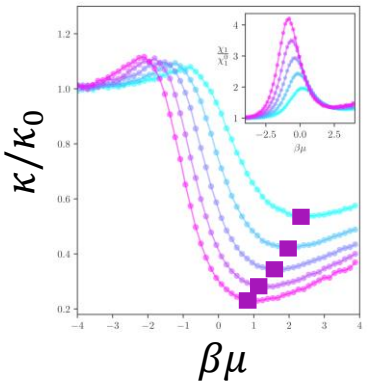

Possible “condensation” of Cooper triples

S. Akagami, HT, and K. Iida, PRA **104**, L041302 (2021).

Cooper triples can condense at the zero c.o.m. momentum regardless of its Fermi-Dirac statistics due to the internal degrees of freedom associated with relative momenta of constituent fermions.

Schematic phase diagram based on the Cooper problem

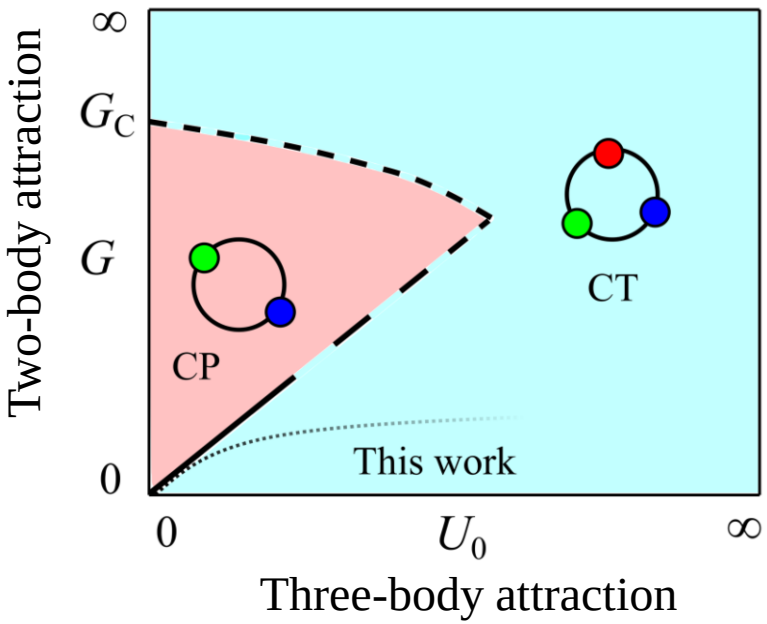

Creation/annihilation operator of triples

$$\hat{F}^\dagger_{\boldsymbol{k},\hat{R}} = \hat{c}^\dagger_{\boldsymbol{k},\mathrm{r}} \hat{c}^\dagger_{\hat{R}\boldsymbol{k},\mathrm{g}} \hat{c}^\dagger_{\hat{R}^2\boldsymbol{k},\mathrm{b}}, \quad \hat{F}_{\boldsymbol{k},\hat{R}} = \hat{c}_{\hat{R}^2\boldsymbol{k},\mathrm{b}} \hat{c}_{\hat{R}\boldsymbol{k},\mathrm{g}} \hat{c}_{\boldsymbol{k},\mathrm{r}},$$

$$\hat{F}^\dagger_{\boldsymbol{k},\hat{R}} \hat{F}^\dagger_{\boldsymbol{k}',\hat{R}'} |0\rangle \neq 0 \quad (\boldsymbol{k} \neq \boldsymbol{k}', \hat{R}\boldsymbol{k} \neq \hat{R}'\boldsymbol{k}', \hat{R}^2\boldsymbol{k} \neq \hat{R}'^2\boldsymbol{k}')$$

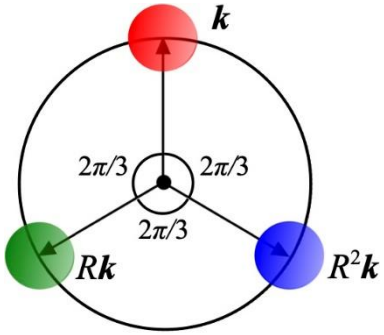

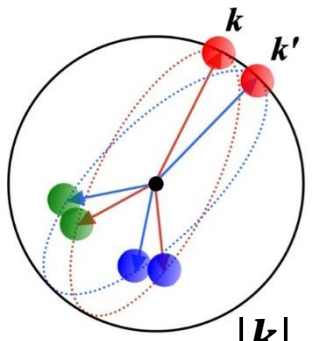

$$|\boldsymbol{k}|, |\boldsymbol{k}'| \simeq k_\mathrm{F}$$

BCS-type wave function for Cooper-triple condensation

$$|\psi_T\rangle = \prod_{\mathbf{k}} \left(u_{\mathbf{k}} + v_{\mathbf{k}} \hat{c}^\dagger_{\mathbf{k},\mathrm{r}} \hat{c}^\dagger_{\hat{R}\mathbf{k},\mathrm{g}} \hat{c}^\dagger_{\hat{R}^2\mathbf{k},\mathrm{b}} \right) |0\rangle$$

Quartet correlations

Y. Guo, HT, and H. Liang, PRC, **105**, 024317 (2022).
Y. Guo, HT, and H. Liang, PRResearch, **4**, 023152 (2022).

Alpha knockout reaction of Sn isotopes

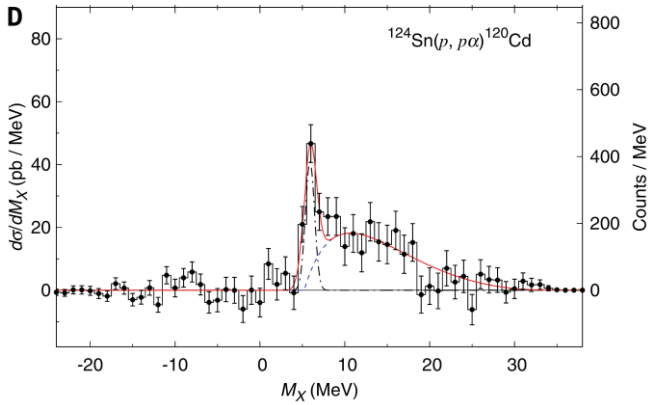

$$M_X = 392\text{MeV} - T_p - T_\alpha$$

J. Tanaka, et al., Science, **371**, 260 (2021).

Alpha particle

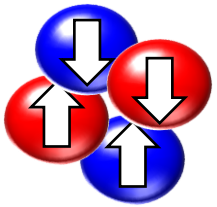

2 protons + 2 neutrons
bound state

$E_\alpha \simeq 28.39$ MeV

From alpha particles to Cooper quartets

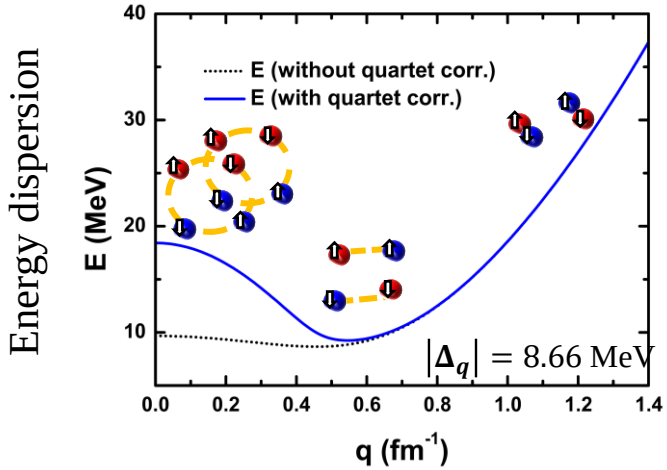

From biexcitons to Cooper quartets

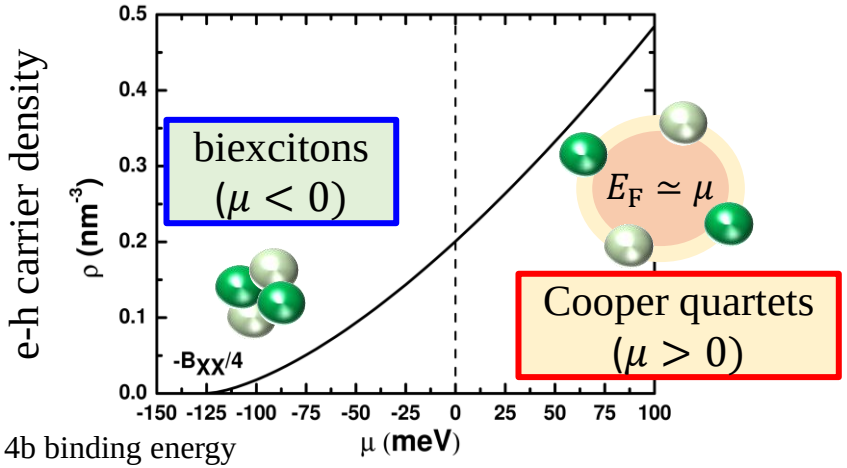

*B_{XX}: 4b binding energy

Outline

- Cold atoms and BCS-BEC crossover
- Strong pairing fluctuations
- Unitary Fermi gas and neutron matter
- Role of the multi-band configuration
- Beyond pairing effect
- Summary

Summary

The BCS-BEC crossovers in cold atomic gases, two-band superconductors, and nuclear systems have been discussed from the interdisciplinary viewpoint.

These show several similarities (universality) and differences (uniqueness) across highly different energy scales (10^{-9}K~10K~10^{10}K).

Review: Y. Ohashi, HT, and P. van Wyk, Prog. Part. Nucl. Phys. **111**, 103739 (2020).

Quantitative description

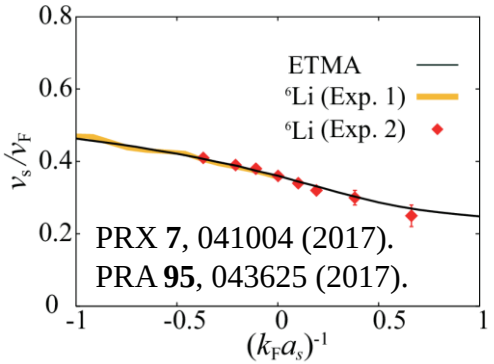

PRX **7**, 041004 (2017).
PRA **95**, 043625 (2017).

Multi-band BCS-BEC crossover

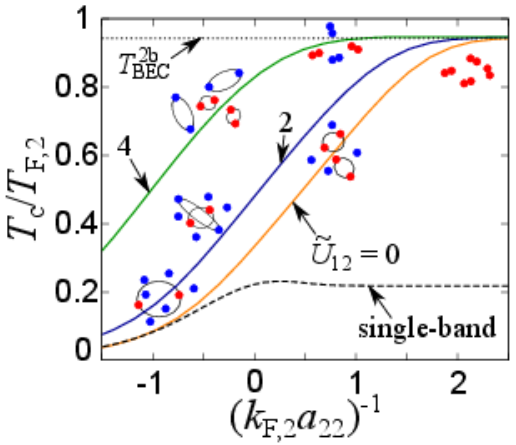

PRB **99**, 180503(R) (2019).
PRB **102**, 220504(R) (2020).
PRR **4**, 013032 (2022).

Three-body crossover

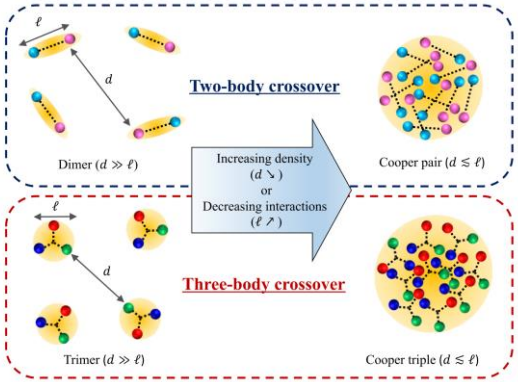

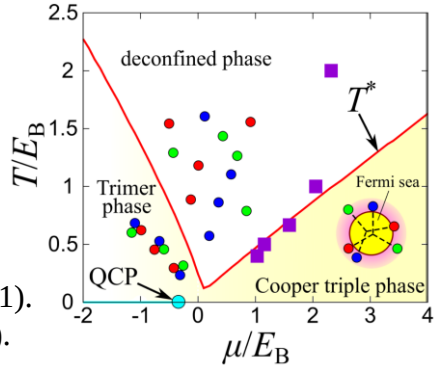

PRA, **104**, 053328 (2021).
PRR **4**, L012021 (2022).

Density-induced crossover

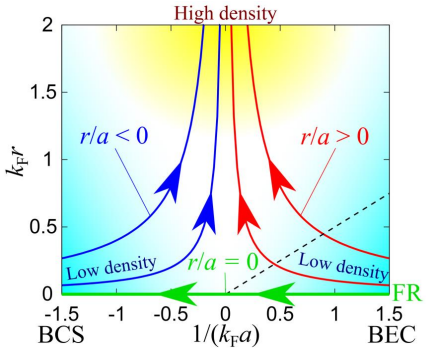

PRA **97**, 013601 (2018).
JPSJ **88**, 093001 (2019).
Sci. Rep. **9**, 18477 (2019).
PRA **104**, 043308 (2022).

Appendix

T-matrix approach (TMA)

- Successfully applied to the single-band BCS-BEC crossover and pairing pseudogap
- Applicable for lower dimensional and multi-band systems

Two-dimension

Exponent of pair correlations

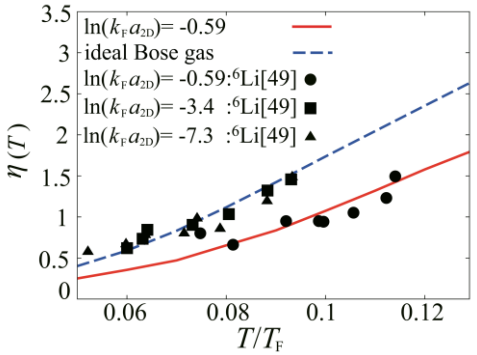

Radio-frequency spectra

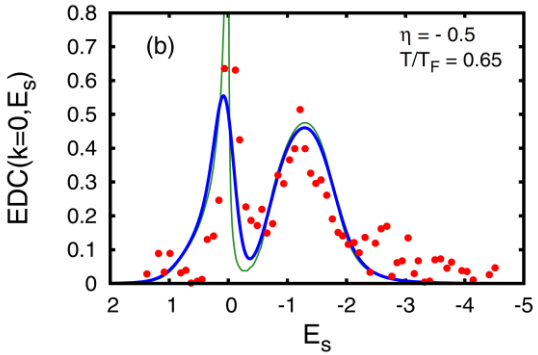

M. Matsumoto, *et al*, PRA **93**, 013619 (2016). F. Marsiglio, *et al*, PRB **91**, 054509 (2015).

Fermi gases near orbital Feshbach resonance

Density of states

S. Mondal, *et al*, JPSJ **87**, 084302 (2018).

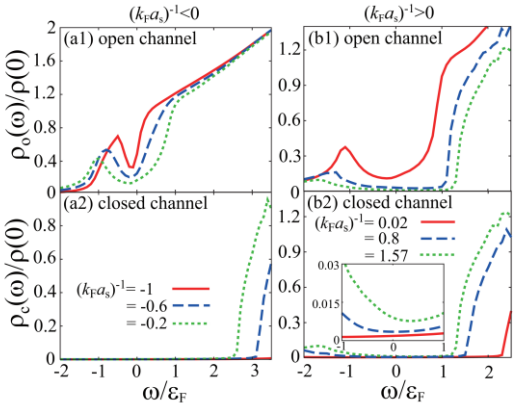

One-dimension

HT, *et al*, PRResearch **2**, 033441 (2020).
arXiv:2005.12124
arXiv:2105.11072

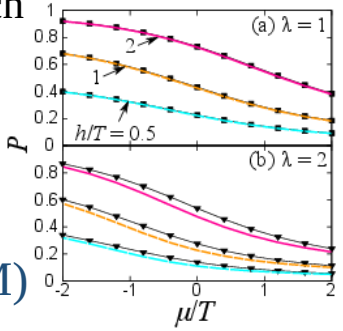

Polarization (TMA vs CLM)

Spectra

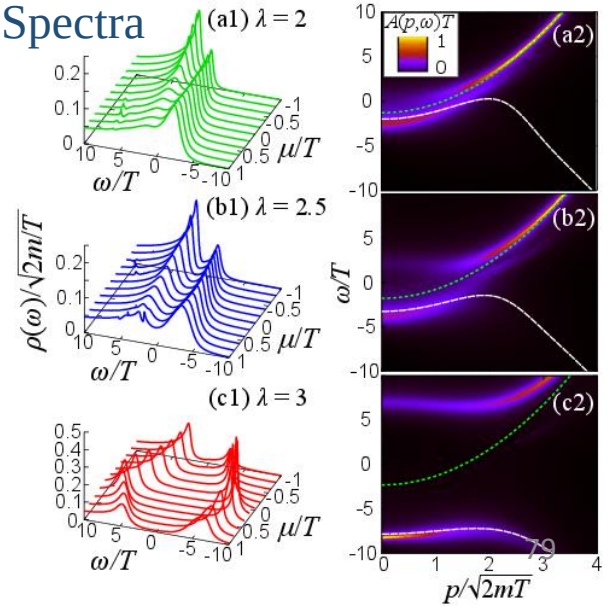

Effects of repulsive core

Phase shift of $^1S_0$ NN scattering

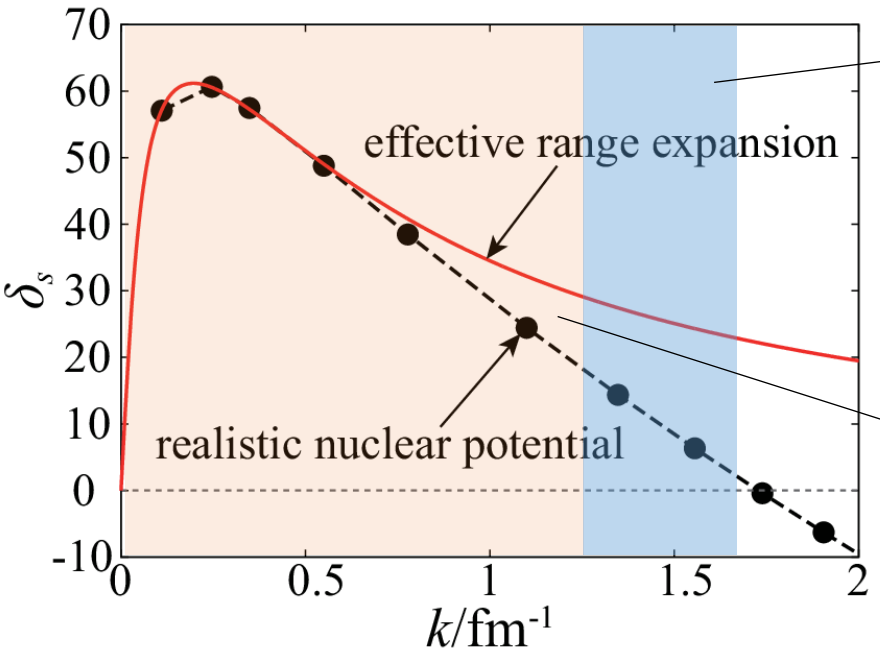

Realistic nuclear potential (AV18) : R. B. Wiringa, *et al.*, PRC **51**, 38 (1995).

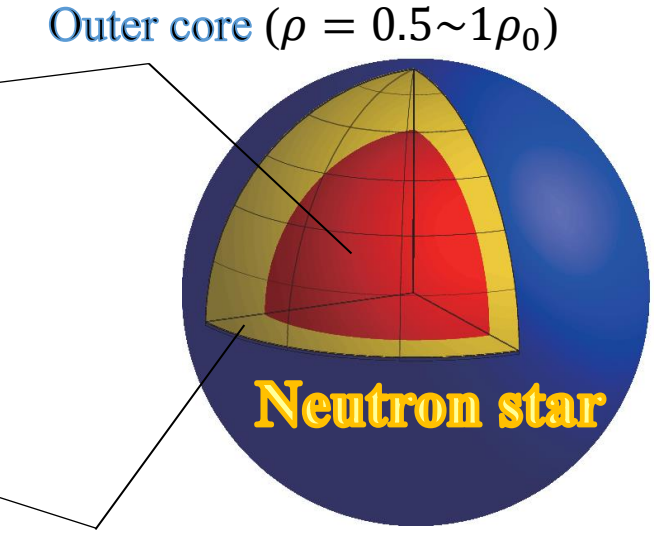

ρ_0: Nuclear saturation density

Effective range expansion

$$k\cot\delta_k = -\frac{1}{a_s} + \frac{1}{2}k^2 r_e$$

Effective range expansion breaks down in the relevant density region of neutron stars due to the high-energy repulsive force

Protons in “neutron star matter”

Proton fraction $Y_p = \dfrac{\rho_p}{\rho_n + \rho_p}$

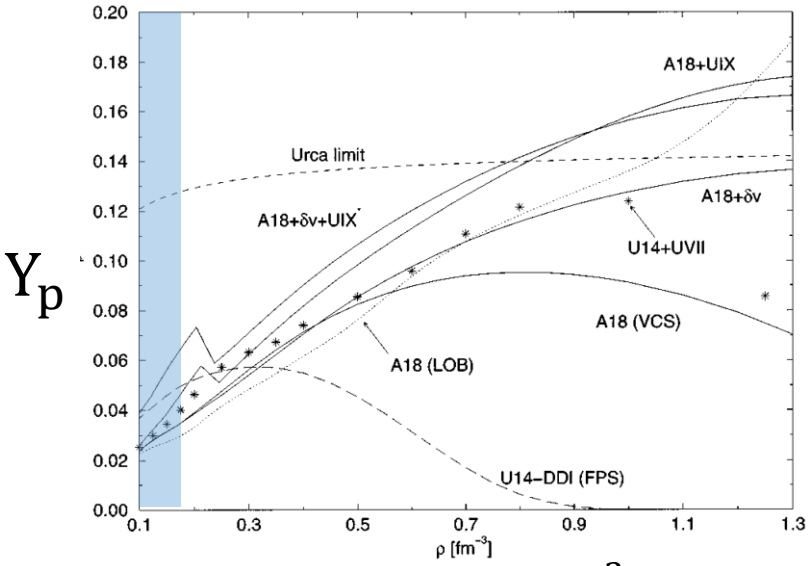

APR, PRC, **58**, 1804 (1998)

Typically $Y_p \simeq 0 \sim 0.1$

Dineutron correlation **V. S.** Deuteron formation

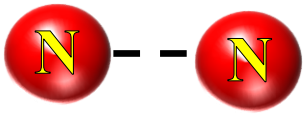

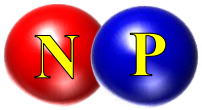

- Cooper pairing without the density imbalance
- No binding energy

- Large density imbalance due to small proton fraction
- Finite binding energy

How strong spin-triplet np pairing affects $^1S_0$ superfluidity?

フェルミ原子気体のハミルトニアン

$$H = \sum_{\sigma=\uparrow,\downarrow} \sum_{\boldsymbol{k}} \xi^{\mathrm{I}}_{\boldsymbol{k},\sigma} c^{\mathrm{I}\,\dagger}_{\boldsymbol{k},\sigma} c^{\mathrm{I}}_{\boldsymbol{k},\sigma}$$

S波相互作用

$$+ \sum_{\boldsymbol{k},\boldsymbol{k}',\boldsymbol{q}} V_{\mathrm{S}}(\boldsymbol{k},\boldsymbol{k}')\, c^{\mathrm{n}\,\dagger}_{\boldsymbol{k}+\frac{\boldsymbol{q}}{2},\uparrow} c^{\mathrm{n}\,\dagger}_{-\boldsymbol{k}+\frac{\boldsymbol{q}}{2},\downarrow} c^{\mathrm{n}}_{-\boldsymbol{k}'+\frac{\boldsymbol{q}}{2},\downarrow} c^{\mathrm{n}}_{\boldsymbol{k}'+\frac{\boldsymbol{q}}{2},\uparrow}$$

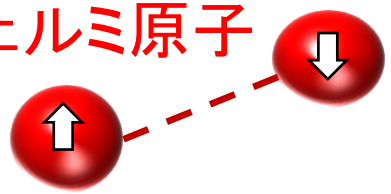

- 運動エネルギー: $\xi^{\mathrm{I}}_{\boldsymbol{k},\sigma} = \dfrac{k^2}{2m_{\mathrm{A}}} - \mu_{\mathrm{I}}$
- 擬スピン: $\sigma = \uparrow,\downarrow$
- 原子質量: m_{A}
- 化学ポテンシャル: μ_{I}
- 消滅演算子: $c^{\mathrm{I}}_{\boldsymbol{k},\sigma}$
- 相互作用ポテンシャル: $V_{\mathrm{S,T}}(\boldsymbol{k},\boldsymbol{k}')$

非対称核物質のハミルトニアン

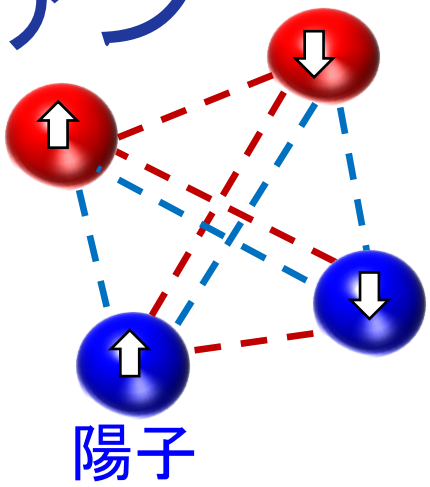

$$H = \sum_{\mathrm{I}=\mathrm{n,p}} \sum_{\sigma=\uparrow,\downarrow} \sum_{\boldsymbol{k}} \xi^{\mathrm{I}}_{\boldsymbol{k},\sigma} c^{\mathrm{I}\,\dagger}_{\boldsymbol{k},\sigma} c^{\mathrm{I}}_{\boldsymbol{k},\sigma}$$

$^1S_0$ spin-singlet 相互作用

$$+ \sum_{\mathrm{I}=\mathrm{n,p}} \sum_{\boldsymbol{k},\boldsymbol{k}',\boldsymbol{q}} V_{\mathrm{S}}(\boldsymbol{k},\boldsymbol{k}')\, c^{\mathrm{I}\,\dagger}_{\boldsymbol{k}+\frac{\boldsymbol{q}}{2},\uparrow} c^{\mathrm{I}\,\dagger}_{-\boldsymbol{k}+\frac{\boldsymbol{q}}{2},\downarrow} c^{\mathrm{I}}_{-\boldsymbol{k}'+\frac{\boldsymbol{q}}{2},\downarrow} c^{\mathrm{I}}_{\boldsymbol{k}'+\frac{\boldsymbol{q}}{2},\uparrow}$$

$$+ \sum_{\boldsymbol{k},\boldsymbol{k}',\boldsymbol{q}} \frac{V_{\mathrm{S}}(\boldsymbol{k},\boldsymbol{k}')}{2} \left(c^{\mathrm{n}\,\dagger}_{\boldsymbol{k}+\frac{\boldsymbol{q}}{2},\uparrow} c^{\mathrm{p}\,\dagger}_{-\boldsymbol{k}+\frac{\boldsymbol{q}}{2},\downarrow} + c^{\mathrm{p}\,\dagger}_{\boldsymbol{k}+\frac{\boldsymbol{q}}{2},\uparrow} c^{\mathrm{n}\,\dagger}_{-\boldsymbol{k}+\frac{\boldsymbol{q}}{2},\downarrow} \right) \left(c^{\mathrm{p}}_{-\boldsymbol{k}'+\frac{\boldsymbol{q}}{2},\downarrow} c^{\mathrm{n}}_{\boldsymbol{k}'+\frac{\boldsymbol{q}}{2},\uparrow} + c^{\mathrm{n}}_{-\boldsymbol{k}'+\frac{\boldsymbol{q}}{2},\downarrow} c^{\mathrm{p}}_{\boldsymbol{k}'+\frac{\boldsymbol{q}}{2},\uparrow} \right)$$

$^3S_1$ spin-triplet 相互作用

$$+ \sum_{\boldsymbol{k},\boldsymbol{k}',\boldsymbol{q}} \frac{V_{\mathrm{T}}(\boldsymbol{k},\boldsymbol{k}')}{2} \left(c^{\mathrm{n}\,\dagger}_{\boldsymbol{k}+\frac{\boldsymbol{q}}{2},\uparrow} c^{\mathrm{p}\,\dagger}_{-\boldsymbol{k}+\frac{\boldsymbol{q}}{2},\downarrow} - c^{\mathrm{p}\,\dagger}_{\boldsymbol{k}+\frac{\boldsymbol{q}}{2},\uparrow} c^{\mathrm{n}\,\dagger}_{-\boldsymbol{k}+\frac{\boldsymbol{q}}{2},\downarrow} \right) \left(c^{\mathrm{p}}_{-\boldsymbol{k}'+\frac{\boldsymbol{q}}{2},\downarrow} c^{\mathrm{n}}_{\boldsymbol{k}'+\frac{\boldsymbol{q}}{2},\uparrow} - c^{\mathrm{n}}_{-\boldsymbol{k}'+\frac{\boldsymbol{q}}{2},\downarrow} c^{\mathrm{p}}_{\boldsymbol{k}'+\frac{\boldsymbol{q}}{2},\uparrow} \right)$$

$$+ \sum_{\sigma=\uparrow,\downarrow} \sum_{\boldsymbol{k},\boldsymbol{k}',\boldsymbol{q}} V_{\mathrm{T}}(\boldsymbol{k},\boldsymbol{k}')\, c^{\mathrm{n}\,\dagger}_{\boldsymbol{k}+\frac{\boldsymbol{q}}{2},\sigma} c^{\mathrm{p}\,\dagger}_{-\boldsymbol{k}+\frac{\boldsymbol{q}}{2},\sigma} c^{\mathrm{p}}_{-\boldsymbol{k}'+\frac{\boldsymbol{q}}{2},\sigma} c^{\mathrm{n}}_{\boldsymbol{k}'+\frac{\boldsymbol{q}}{2},\sigma}$$

*I = n (neutron), p (proton)

- 運動エネルギー: $\xi^{\mathrm{I}}_{\boldsymbol{k},\sigma} = \dfrac{k^2}{2m_{\mathrm{N}}} - \mu_{\mathrm{I}}$
- 核子スピン: $\sigma = \uparrow,\downarrow$
- 核子質量: $m_{\mathrm{N}} = 939\mathrm{MeV}$
- 化学ポテンシャル: μ_{I}
- 消滅演算子: $c^{\mathrm{I}}_{\boldsymbol{k},\sigma}$
- 相互作用ポテンシャル: $V_{\mathrm{S,T}}(\boldsymbol{k},\boldsymbol{k}')$

相互作用ポテンシャル

- Separable multi-rank ポテンシャル (SEP n_{rank})

$$V(\boldsymbol{k},\boldsymbol{k}') = \sum_{n=1}^{n_{\mathrm{rank}}} \eta_n \gamma_n(\boldsymbol{k})\gamma_n(\boldsymbol{k}') = \boldsymbol{\gamma}^t(\boldsymbol{k})\hat{\eta}\boldsymbol{\gamma}(\boldsymbol{k}')$$

$\gamma_n(\boldsymbol{k}) = \frac{u_n}{k^2+\Lambda_n^2}$: form factor $\quad \boldsymbol{\gamma}(\boldsymbol{k}) = \begin{pmatrix}\gamma_1(\boldsymbol{k})\\ \gamma_2(\boldsymbol{k})\\ \vdots\end{pmatrix}$ $\quad \hat{\eta} = \mathrm{diag}(\eta_1,\eta_2,\dots)$ $\quad \eta_n = \pm 1$

- S波の位相シフト

AV18: PRC, **51** 38 (1995).

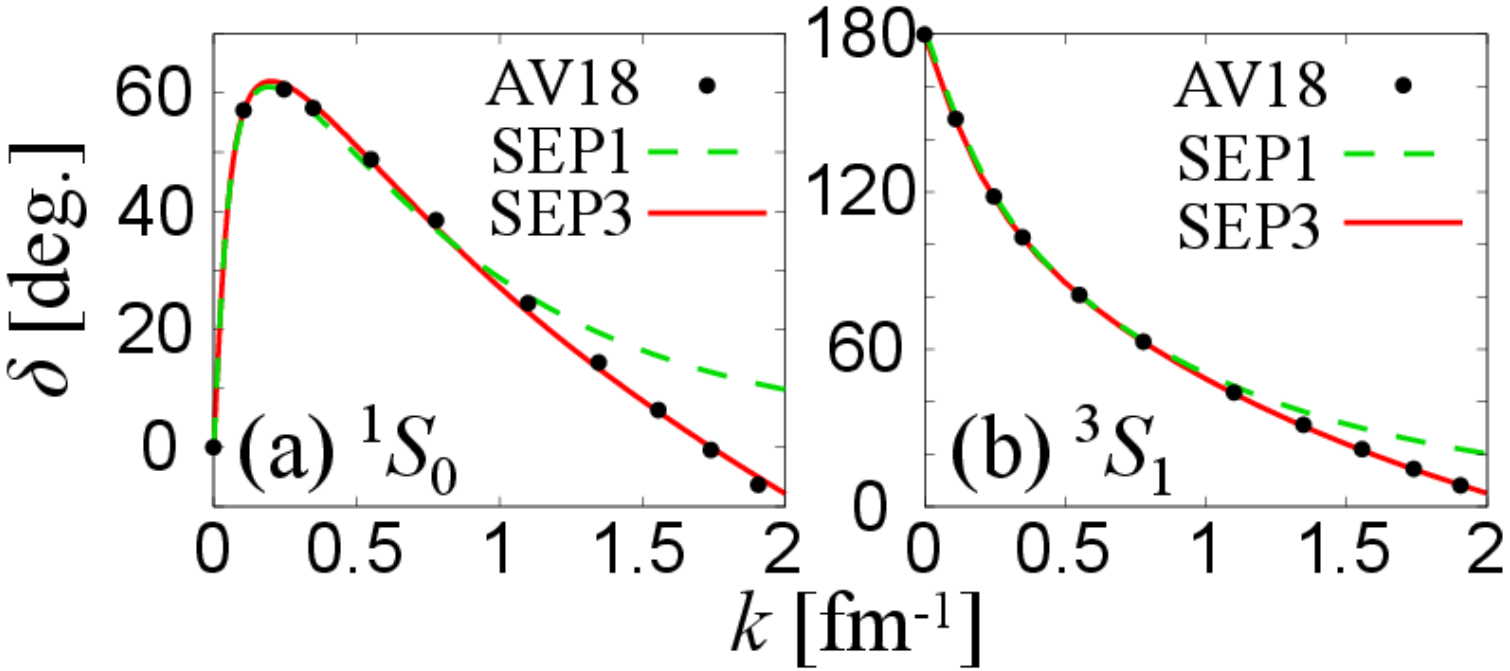

From pure neutron matter to neutron star matter

- T_c^{nn} of $^1S_0$ neutron superfluidity is shifted with changing the proton fraction
- $^1S_0$ Proton SC dominates over T_c^{nn} at high density due to the density imbalance

▶ Neutron SF/Proton SC in ANM

$$k_{F,p} = \left(3\pi^2 \rho_n \frac{Y_p}{1-Y_p}\right)^{\frac{1}{3}} \equiv \left(\frac{Y_p}{1-Y_p}\right)^{\frac{1}{3}} k_{F,n}$$

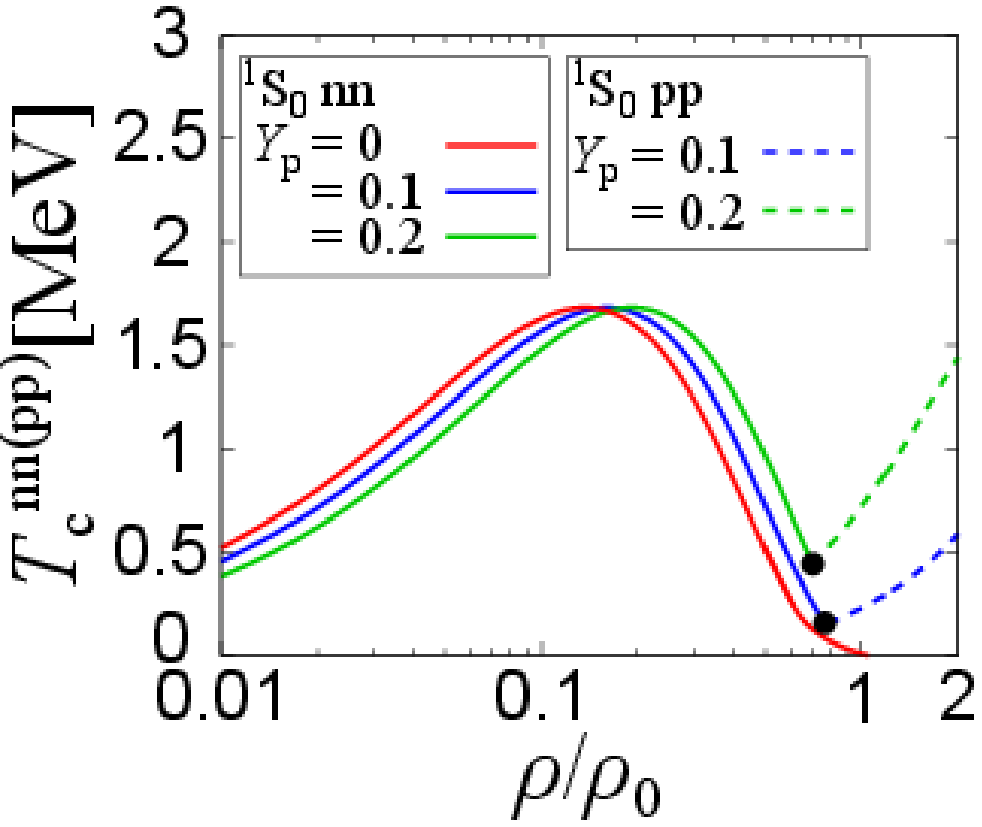

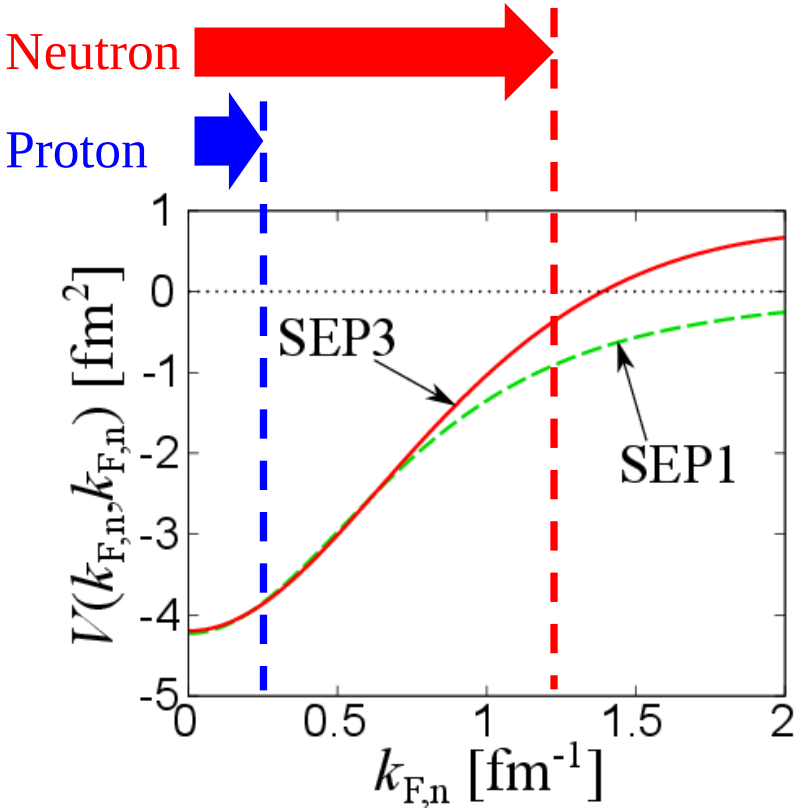

Strong neutron-proton pairing fluctuations

- Comparison between full calculation and the result without np pairng

◉Thermodynamic properties of protons are largely affected by np pairing fluctuations
◉ $^1S_0$ Proton SC is strongly suppressed by np pairing fluctuations (deuteron formation)

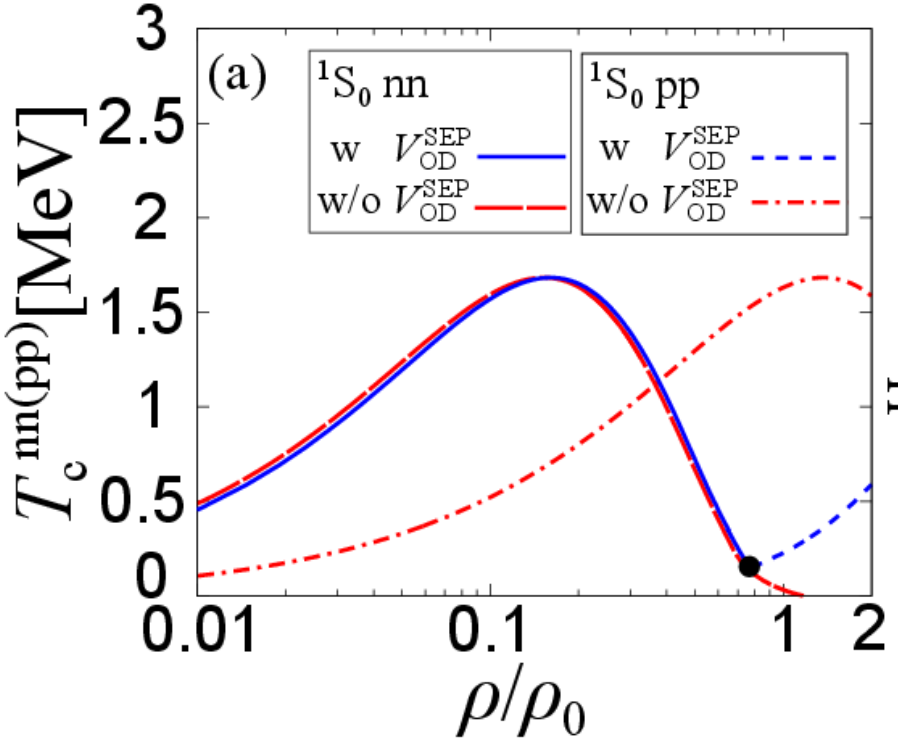

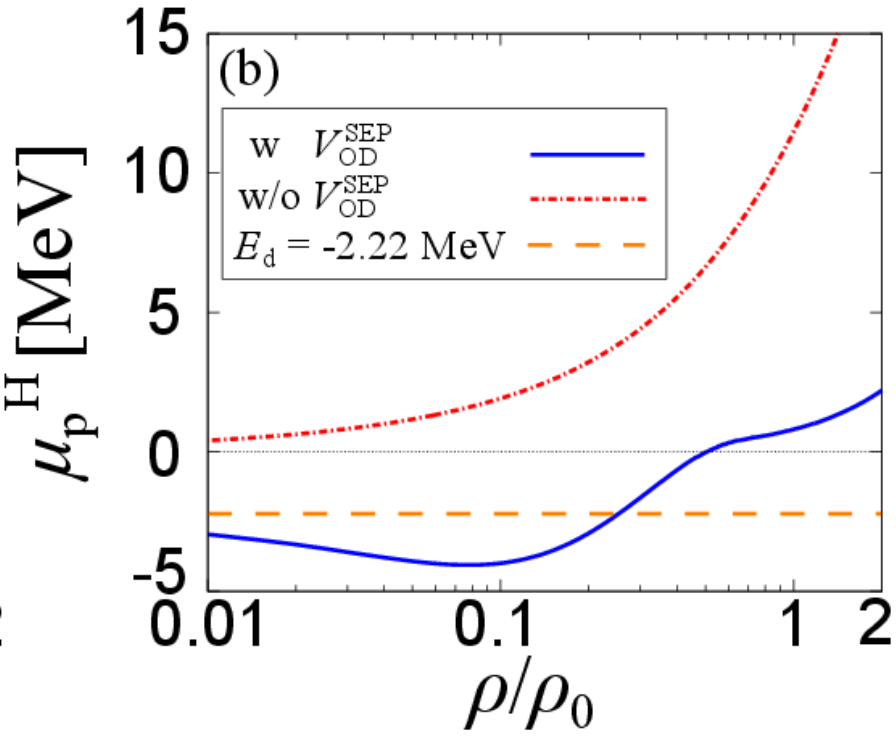

Strong neutron-proton pairing fluctuations

- Comparison between full calculation and the result without np pairng

◉Thermodynamic properties of protons are largely affected by np pairing fluctuations
◉ $^1S_0$ Proton SC is strongly suppressed by np pairing fluctuations (deuteron formation)

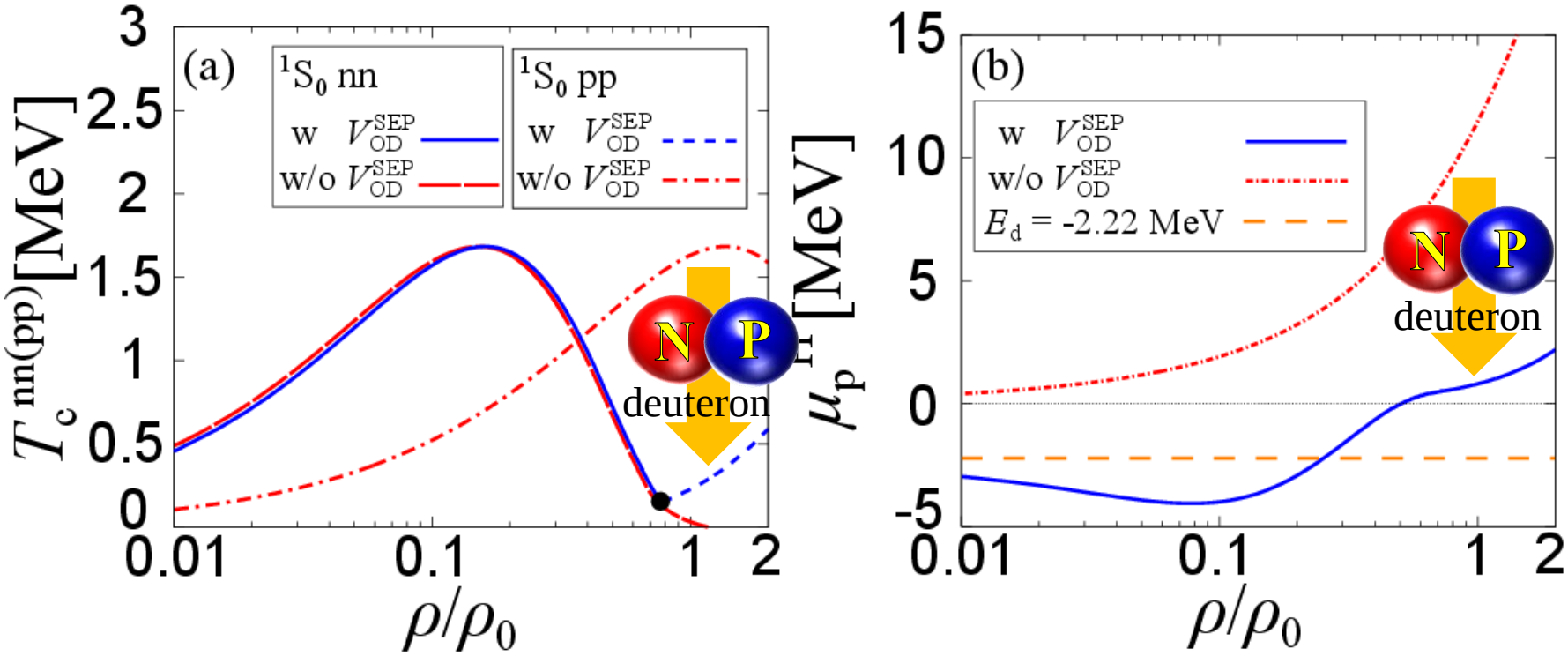

NG mode gap and FFLO-like correlations

- NG mode gap at critical temperatures

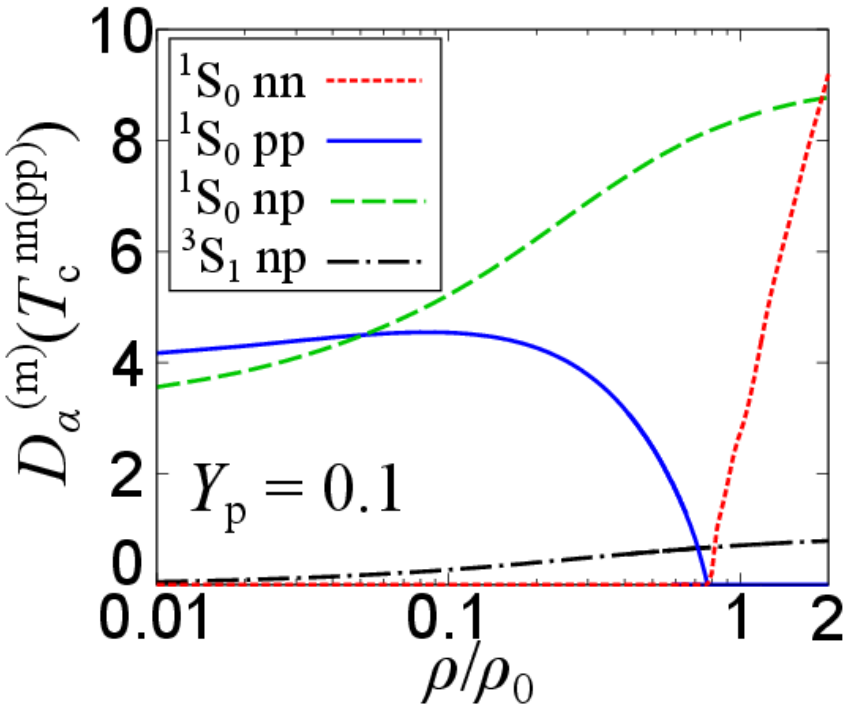

- FFLO-like correlations in ANM